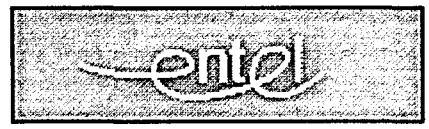

Toward All-IP Networks
IP and Wireless Networks Convergence

Ph.D. Thesis by

Xavier Pérez Costa

Thesis Advisor

Sebastià Sallent Ribes

Universitat Politècnica de Catalunya (UPC)
Department of Telematics Engineering

Campus Nord, Edifici C3
c/ Jordi Girona, 1-3
08034 Barcelona, Spain

February 16, 2005

Dedicat a la Rosa, la Rosa Maria i la Melanie.

Contents

Chapter 1

Motivation

Over the last decades there were two main drivers for the evolution of communications systems. On the one hand, the great popularity achieved by the Internet pushed the enhancement of its protocol stack and physical support to improve the reliability and speed of data transmissions. The development of new applications and services taking advantage of these advances further increased Internet's popularity becoming the de facto standard for transferring information.

On the other hand, the global deployment of second-generation cellular systems, e.g., Global System for Mobile Communications (GSM), allowed a user for the first time to be reachable and communicate almost all over the world thanks to roaming agreements between operators. This resulted in an enormous growth in the number of wireless users due to the the wide adoption of this technology by traditional fixed telephone customers.

Nowadays, the usage of the Internet to have access to diverse information is becoming a need in people's lives and recent trends show that the possibility of incorporating this capability in mobile devices is getting more and more important for the users. The evolution of second-generation cellular systems have already taken this into account by providing IP connectivity in the General Packet Radio Service (GPRS) system or including mobile Internet solutions in third-generation (3G) cellular networks, such as Universal Mobile Telecommunications System (UMTS) and cdma2000 (code-division multiple access).

In parallel with the evolution of cellular systems, emerging license-free wireless technologies as Wireless LAN (WLAN), which require minimum initial investment and operational cost, have captured a fast growing market. Such technologies can deliver high data rates to both private and enterprise users at a much lower cost than cellular technologies. Wireless LANs are currently extensively used in hot spot areas providing high bandwidth Internet access at offices, airports, hotels, conferences and university campuses. The high popularity achieved by wireless LAN in provisioning high speed Internet access has resulted in a com-

mon acceptance of its potential role in the future for providing services to 3G users in indoor environments.

Future communication networks should allow users to maintain service continuity while moving through different access networks and at the same time guarantee a certain level of service to ensure the quality needed by the applications. Currently there is no foreseeable alternative to IP as the best technology for functional integration of heterogeneous networks. However, the desired scenario presents a great complexity and generates a new set of requirements for the networks to adapt their technologies to IP and vice versa. The final result of this convergence process should end up in what is usually referred as *All-IP* networks.

The objective of this thesis is to contribute to three main working areas which have been identified as key in the way toward All-IP networks.

It is foreseen that 3G, as the chosen evolution for GSM networks, and wireless LAN, which brings a complementary technology towards cellular in hot spot environments, will be the predominant wireless access technologies in future All-IP networks. The extension of 3G to efficiently support QoS in an IP-based radio access network and of 802.11 to provide QoS guarantees is required to support the All-IP concept.

Mobility poses additional challenges in such heterogeneous networks since users will expect a service similar to the one experienced in wired networks even while moving through different access networks. Therefore, an IP-based mobility protocol capable to provide seamless handoffs across different access networks is necessary.

In addition to these three research areas, the derivation of the properties of the movement generated by mobility models is also subject of study given its importance to avoid the misinterpretation of performance results of mobility management schemes.

The rest of the document is organized as follows. In the next chapter the main IETF protocols to support IP-based mobility are described and analyzed including a comparison with a proposed enhancement. The influence of mobility models over performance studies results is analyzed in Chapter 3. In Chapter 4 solutions are proposed to mitigate the IP-based radio access networks overhead as compared to ATM and to provide QoS guarantees while making an efficient use of their scarce resources. Chapter 5 summarizes the different mechanisms proposed to provide absolute and relative bandwidth and delay guarantees in IEEE 802.11 wireless LANs. Additionally, the power saving issues expected to appear when wireless LAN capabilities are introduced in battery-limited mobile devices are analyzed and a solution proposed. The thesis concludes with a summary of the main results.

Chapter 2

IP-based Mobility Management

Mobile IP, as the current IETF proposal for mobility support at the IP layer, represents a key element for future All-IP wireless networks to provide service continuity while on the move within a multi-access environment, e.g., comprising 3G and WLAN. The IETF working group in Mobile IP defined Mobile IPv4 (MIPv4) [1] and Mobile IPv6 (MIPv6) [2] as the main protocols for supporting *IP-based mobility*. However, some enhancements have been already proposed since it is believed that in certain circumstances Mobile IP could result in poor performance.

Mobile IP introduces significant network overhead in terms of i) packet loss due to registration delays and ii) increased signaling due to frequent terminal registration. The network overhead is drastically increased if mobile hosts frequently change their point of attachment. Based on the assumption that the majority of frequent handovers take place between nodes of the same regional network, many IP micro-mobility protocols have been proposed [3] aimed to provide fast seamless local mobility. Hierarchical Mobile IPv6 [4] is the current IETF IPv6 micro-mobility proposal. Additionally, for applications that could suffer from a long interruption time due to a handoff, a fast handover mechanism has been introduced [5].

Previous work on Mobile IP almost exclusively dealt with IPv4 networks. Perkins and Wang [6] used *ns-1* to analyze the effects of route optimization and buffering ('smooth handoff'). Yokota et al. [7] proposed a link layer assisted Mobile IPv4 Fast Handoff method. Campbell et al. provided a comparison of IPv4 micro-mobility protocols in [3]. Because of the significant differences between Mobile IPv6 and Mobile IPv4, as outlined in Section 2.1, results obtained for MIPv4 do not take over for MIPv6. We have focused on IPv6 since we believe it will be the basis of the future *All-IP* networks as it can be seen for example with the 3GPP decision of adopting IPv6 as the only IP version for the IP-based multimedia subsystem (IMS).

Regarding Mobile IPv6, an analitycal study focusing on the HMIPv6 update

signaling messages frequency can be found in [8]. A protocol overview of Mobile IPv6, HMIPv6 and FMIPv6 is provided in [9] which provides handoff latency results for MIPv6, excluding HMIPv6 and FMIPv6 and considering only the interference of up to 4 static users. In [10] Mobile IPv6 and its enhancements is studied but the results are limited to TCP handoff latency and obtained bandwidth of a single user following a deterministic path without the interference of other users. Moreover, a key aspect of IPv6, the Neighbor Discovery protocol, was not considered.

Although the performance study of Mobile IPv6 enhancements has received significant attention from the research community, almost all studies have focused on analysing only the differences in handoff latency in very simple scenarios. In order to assess the performance that can be expected of the different mobility protocols in more realistic scenarios, a detailed study of the overall performance and associated overhead costs has been identified as our focus in this area. Our goal is not to determine which protocol performs 'best' but to help in the design decision of which is the best suited protocol for a specific scenario, broaden our knowledge of the reasons that influence the differences in the performance and check if the desired objectives are met or additional research is needed to solve detected drawbacks.

The rest of the chapter is structured as follows. First, a description of the above mentioned mobility protocols is provided followed by a description of our proposed enhancement, which combines Hierarchical Mobile IPv6 and Fast Handovers for Mobile IPv6, that aims to outperform both single approaches by adding the advantages of each other. Then, we present a study where we investigate the impact of various parameters on the overall performance as experienced by a single mobile node of a Mobile IPv6-based wireless access network and compare the performance obtained by the proposed enhancements, i.e., Hierarchical Mobile IPv6, Fast Handovers for Mobile IPv6, or our proposed combination of both (H+F MIPv6), with the performance of the MIPv6 base protocol. Finally, Section 2.5 summarizes our main results.

2.1 Mobile IPv6

Mobile IP supports mobility of IP hosts by allowing them to make use of (at least) two IP addresses: a home address that represents the fixed address of the node and a care-of address (CoA) that changes with the IP subnet the mobile node is currently attached to. Clearly, an entity is needed that maps a home address to the corresponding currently valid CoA.

In Mobile IPv4 [1] these mappings are exclusively handled by 'home agents'

(HA). A correspondent node (CN) that wants to send packets to a mobile node (MN) will send the packets to the MN's home address. In the MN's home network these packets will be 'intercepted' by the home agent and tunneled, e.g. by IP-in-IP encapsulation [11], either directly to the MN or to a foreign agent to which the MN has a direct link.

In MIPv6, home agents no longer exclusively deal with the address mapping, but each CN can have its own 'binding cache' where home address plus care-of address pairs are stored. This enables 'route optimization' compared to the triangle routing via the HA in MIPv4: a CN is able to send packets directly to a MN when the CN has a recent entry for the MN in its corresponding binding cache. When a CN sends a packet directly to a MN, it does not encapsulate the packet as the HA does when receiving a packet from the CN to be forwarded, but makes use of the IPv6 Routing Header Option. When the CN does not have a binding cache entry for the MN, it sends the packet to the MN's home address. The MN's home agent will then forward the packet. The MN, when receiving an encapsulated packet, will inform the corresponding CN about the current CoA.

In order to keep the home address to CoA mappings up-to-date, a mobile node has to signal corresponding changes to its home agent and/or correspondent nodes when performing a handoff to another IP subnet. Since in MIPv6 both, HA and CN, maintain binding caches, a common message format called 'binding updates' (BU) is used to inform HA and CNs about changes in the point of attachment. Additionally, since the BUs have associated a certain lifetime, even if the MN does not change its location a BU to its HA and CNs is necessary before the lifetime expires to keep alive the entry in the binding caches. In the rest of the document those BUs will be referred as periodic BUs. Binding updates can be acknowledged by BU Acks (BAck).

In contrast to MIPv4, where signaling is done using UDP, Mobile IPv6 signaling is done in extension headers that can also be piggybacked on 'regular' packets. To acquire a CoA in Mobile IPv6, a mobile node can build on IPv6 stateless and stateful auto-configuration methods. The stateless auto-configuration mechanism is not available in IPv4. In our work, we assume stateless auto-configuration for all tests since with this mechanism it is not necessary to contact any entity to obtain a new CoA, reducing the handoff process duration. For more details on Mobile IPv6 see [2]. In the following, we briefly look at the Neighbor Discovery [12] mechanism, one of the main differences when comparing IPv4 and IPv6.

2.1.1 Neighbor Discovery

Neighbor Discovery [12] is used by nodes to resolve link-layer addresses and keep track of the reachability of their neighbors. Hosts use it as well to locate routers on their link. The main difference is the IPv6 way of learning MAC addresses

and the Neighbor Cache, previously ARP Cache, which can be set in five different states: Incomplete, Reachable, Stale, Delay and Probe.

A MN, when performing a handover, has to learn the Access Router's (AR) MAC address before being able to inform about the new point of attachment via the BUs. In IPv4 a MN runs the ARP process and has to wait until its completion, delaying thus the BUs transmission. On the other hand, the IPv6 Neighbor Discovery protocol optimizes this process obtaining the AR's MAC address from the Router Advertisement. This results in the MN being able to send the BU without any delay after a handover and running the neighbor unreachability detection process in parallel. However, in IPv4, after the ARP process is completed, MAC addresses on both sides are obtained. This is not the case for IPv6 where the AR that has a packet to transmit to the MN must run the address resolution process to obtain the MN's MAC address. In fact, in the IPv6 case, when a MN learns a node's MAC address in a different way than the usual Request-Reply exchange or when it wants to send a packet after some time without using the entry, the neighbor unreachability detection has to be launched to resolve the MAC address, but this is a one way process (only one address is resolved). Note that in both cases, addresses will be resolved in parallel while sending packets, no delay is added. Additionally, some channel utilization can be saved if confirmation of reachability is received from upper layers.

2.1.2 Fast Handovers for Mobile IPv6

To reduce the service degradation that a mobile node could suffer due to a change in its point of attachment *Fast Handovers for Mobile IPv6* has been proposed [5]. During the IETF discussions regarding this proposal two different mechanisms have been described: anticipated and tunnel-based handover. Tunnel-based handover relies on link layer triggers to potentially obtain better results than Anticipated Handover, introducing though a link layer dependence that could make the solution unfeasible for some link layer technologies. In principle, a link layer independent solution would be a more desirable solution. Therefore, we have focused on the study of the *Anticipated Handover* proposal, which is solely based on network layer information.

Anticipated Handover proposes a 'make-before-break' approach. When a MN has information about the next point of attachment to which the MN will move, e.g., via reception of a Router Advertisement from a new AR (nAR), it sends a Router Solicitation for Proxy (RtSolPr) to the old AR (oAR) with an identifier of the point of attachment to which it wants to move. Once the oAR receives information that a MN wants to move to a nAR, it constructs a nCoA based on the MN's interface ID and the nAR's subnet prefix. It then sends a Proxy Router Advertisement (PrRtAdv) to the MN containing the proposed nCoA and the nAR's

IP address and link layer Address. At the same time, the oAR sends a Handover Initiate (HI) message to the nAR, indicating the MN's oCoA and the proposed nCoA.

Upon receipt of the HI message, the nAR first establishes whether there is already an active Neighbor Cache entry for the proposed nCoA. If the nCoA is accepted by the nAR, the nAR adds it to the Neighbor Cache for a short time period so it can defend it. The nAR then responds with a Handover Acknowledge (HAck), indicating that the proposed nCoA is valid. Upon receipt of the HAck the oAR is prepared to forward packets for the MN to the nCoA. As soon as the MN received confirmation of a pending network layer handover through the PrRtAdv and has a nCoA, it sends a Fast Binding Update (F-BU) to oAR, as the last message before the link layer handover is executed.

On receipt and validation of the F-BU, the oAR responds with a Fast Binding Acknowledgment (F-BAck), destined to the nCoA. The oAR waits for a F-BU from the MN before actually forwarding packets. On receipt of the F-BU, the oAR forms a temporary tunnel for the lifetime specified in the F-BAck, and the F-BAck is sent through the tunnel to the MN on the new link. When the MN arrives to the nAR and its link layer connection is ready for network layer traffic, it sends a Fast Neighbor Advertisement (F-NA) to initiate the flow of packets that may be waiting for it. The nAR will deliver packets to the MN as soon as it receives an indication that the MN is already attached to it, usually receiving a F-NA from the mobile node. The oAR is responsible for forwarding any packets that arrive for the MN under its oCoA after the MN has moved. Once the fast handoff process is completed, the MN will follow the MIPv6 normal procedure of informing the HA and correspondent nodes about its new location. For more details about Fast Handovers for Mobile IPv6 see [5].

2.1.3 Hierarchical Mobile IPv6

It is a well-known observation that MNs moving quickly as well as far away from their respective home domain or correspondent nodes produce significant BU signaling traffic and will suffer from handoff latency and packet losses when no extension to the baseline Mobile IP protocol is used. Hierarchical Mobile IPv6 (HMIPv6) is a localized mobility management proposal that aims to reduce the signaling load due to user mobility. The mobility management inside the local domain is handled by a Mobility Anchor Point (MAP). Mobility between separate MAP domains is handled by MIPv6.

The MAP basically acts as a local Home Agent. When a mobile node enters into a new MAP domain it registers with it obtaining a regional care-of address (RCoA). The RCoA is the address that the mobile node will use to inform its Home Agent and correspondent nodes about its current location. Then, the pack-

ets will be sent to and intercepted by the MAP, acting as a proxy, and routed inside the domain to the on-link care-of address (LCoA). When a mobile node then performs a handoff between two access points within the same MAP domain only the MAP has to be informed. Note, however that this does not imply any change to the periodic BUs a MN has to sent to HA, CNs and now additionally to the MAP.

HMIPv6 presents the following advantages: it includes a mechanism to reduce the signaling load in case of handoffs within the same domain and may improve handoff performance reducing handoff latency and packet losses since intra-domain handoffs are performed locally. However, since the periodic BUs are not reduced but the ones due to handoffs, the gain depends on the mobility of the mobile nodes. For more details on HMIPv6 the reader is referred to [4].

2.2 Hierarchical Mobile IPv6 plus Fast Handovers for Mobile IPv6

In [4] a sketch desription on how to combine FMIPv6 and HMIPv6 is provided. However, some issues are left open as for example when should the mobile node decide to perform the handoff. The main ideas of our approach and its differences with respect to a simple aggregation of the two proposals are as follows.

Our approach is based on two main observations that show that a simple aggregation of HMIPv6 and FMIPv6 would be inefficient. First, consider a MAP placed in an aggregation router above the ARs involved in a handover. The usual fast handover process of forwarding packets from the oAR to the nAR would be inefficient in terms of handover latency since packets would traverse the MAP-oAR link twice and could arrive disordered. On the other hand, if the entity responsible of establishing the redirection prior to the handoff would be the MAP, then this inefficiency would be removed. Therefore, in our approach, as suggested in [4], the entity performing the functionality of the Fast Handover process is the MAP instead of the mobility agent in the old access router.

Second, note that with FMIPv6 the traffic is redirected when the oAR receives the F-BU but in our case if the mobile node would perform the handoff right after sending the F-BU to the MAP, all the packets forwarded to the oCoA, during the period that the F-BU requires to arrive to the MAP, would be lost. Additionally, if the MN would perform the handoff right after sending the F-BU, it would not immediately receive any redirected packet for the same reason, increasing the handoff latency and packet losses. As a solution, we propose to wait as long as possible (until connectivity is lost) for the F-BAck at the old link to start the handover. In this case we assure that when we receive the F-BAck there are no packets lost sent to our oCoA and the ones redirected to our nCoA are buffered,

i.e., no packet losses. Additionally, assuming that the packets experience a similar delay in the path between the MAP and the ARs involved in the handoff, the reception of the F-BAck would act as a kind of synchronization packet telling us that new packets are already waiting or about to arrive to the new AR and therefore, the handover latency due to the wired part would be almost removed.

Our approach requires, as in the case of FMIPv6, that the MN has some time from the moment it realizes that a handover should be performed until it is necessary to perform it because of losing connectivity to the current AR. In the cases where this is not possible we apply the same recovery mechanisms as FMIPv6.

Addendum: During the preparation of this document a new internet-draft [13] appeared proposing a combination of HMIPv6 and FMIPv6 basically explaining in detail what was indicated in [4] but without the proposed optimization of waiting at the old access router for the F-BAck.

2.3 Simulation Scenario

The studied scenario was designed in order to be large enough to provide realistic results but to be small enough to be handled efficiently within *ns-2* [14]. The chosen scenario, depicted in Figure 2.1, is composed by the Home Agent and the Correspondent Nodes that are connected via the 'Internet' (modeled by adjusting the link delay *ld*) to a central router (CR). Four access routers (AR) –each one representing a different IP subnet– are connected via two intermediate routers (IR) to the central router. When Hierarchical MIPv6 is considered, the functionality of the Mobility Anchor Point is placed on the central router and the CR, IRs, and ARs form the micro-mobility domain. At the start of the simulation the mobile nodes are uniformly distributed over the system area.

The access routers have been positioned in a way to provide total coverage to an area of approximately 700×700 square meters considering a transmission range of 250 meters, see Figure 2.1. The mobile nodes move randomly within the coverage area following the random waypoint mobility model (RWP) [15]. As wireless medium the 2Mbps Wireless LAN 802.11 DCF [16] provided by *ns-2* is used.

Within the micro-mobility domain each wired connection is modeled as a 5Mbps duplex link with 2ms delay. The 'Internet' connecting the central router and the HA or CNs is modeled also as a 5Mbps duplex link with a default link delay (ld) of 10ms. In the simulations, the *ld* value has been varied to model various 'distances' between the MNs and the HA and CNs.

In our simulations we study the performance metrics as observed by one single mobile node but affected by other moving mobile nodes. In most of the simulations the observed mobile node follows a deterministic path while all other mo-

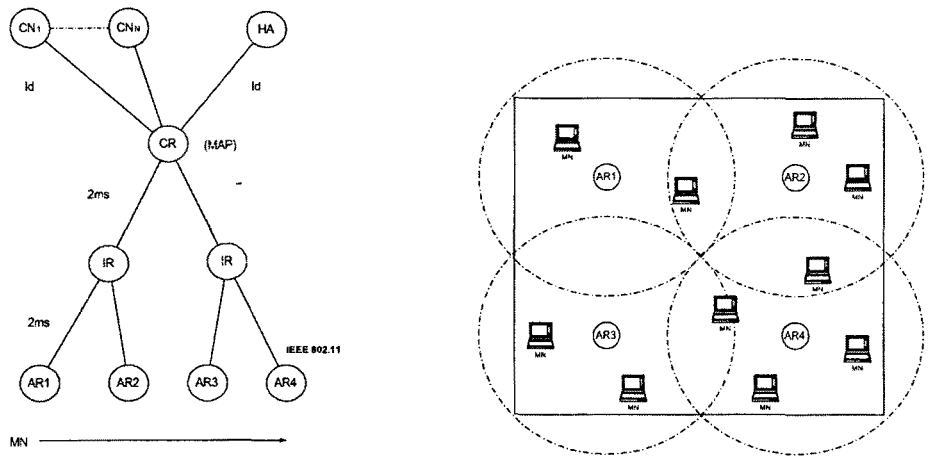

Figure 2.1: Simulation scenario and Access routers distribution

bile nodes move randomly. This case allows for full control of the mobility – and handoff rate – of the observed node while the interference of other nodes is still realistic due to their random movements. As a second case we allow the observed mobile node to move randomly, too. By doing this, mobility is less 'controllable' but random movement effects – like going back and forth between two ARs – can be analyzed. Thus, with both deterministic and random movements of the observed node studied separately, impact of the different parameters over the various protocols can be studied in a clear as well as realistic way.

The first type of sources used in our simulations will be UDP CBR sources. These sources provide constant traffic where no acknowledgments are required. This kind of traffic is usually generated by real-time applications and due to its deterministic characteristics, without recovery mechanisms, eases the protocols study and comparison. Unless otherwise noted, UDP CBR sources are used.

One of the applications expected to be used with MIPv6 is VoIP. We have implemented a VoIP model based on the one provided in [17]. The model assumes silence suppression and models each voice source as an on-off Markov process. The alternating active *on* and silence *off* periods are exponentially distributed with average durations of 1.004s and 1.587s. As recommended by the ITU-T specification for conversational speech [18], an average talk spurt of 38.57% and an average silence period of 61.47% is considered. A rate of 88 kbps[1] in *on* periods and 0 kbps in *off* periods is assumed for a voice source that generates CBR traffic.

As streaming application for real-time video traffic we have used a real H.263

[1]Assume 8KHz 8 bits/sample PCM codec was used with 20ms frame per packet. With 12 byte RTP header, 8 byte UDP header and 40 byte IPv6 header, the size of each voice packet is 220 bytes. The bandwidth required will be $(220 \times 8)/20 \times 10^{-3}$=88kbps

[19] video encoding provided by [20] (film: "Star Trek: First Contact") for a target bit rate of 64 kbps. The obtained frame sizes (in bytes) of the individual encoded video frames are used as input for the *ns-2* real-time video traffic application. Since these traces include only the raw packetized video, additional streaming protocol overhead has been added. As in the case of VoIP sources we consider a 12 byte RTP header plus 8 byte UDP header and plus 40 byte IPv6 header as the streaming protocol overhead.

TCP is the most widely used transport protocol. We simulate endless FTP sources to understand the impact of IP mobility on the congestion control mechanism of TCP.

The simulation code used for the experiments was designed on top of INRIA/Motorola MIPv6 [21] code for *ns-2* implementation. We have extended the code with four main modules: Neighbor Discovery, Hierarchical Mobile IPv6, Fast Handovers for Mobile IPv6 and their combination.

2.4 Performance Evaluation & Discussion

The degradation of the performance metrics from the point of view of a single mobile node that follows a *deterministic* path while all other mobile nodes in the system follow the random waypoint mobility (RWP) model is analyzed. The RWP model is well-suited to represent movements of mobile users in campus or 'hot spot' scenario at moderate complexity. When no other value is indicated, all the simulations have been performed with a maximum speed of 5m/s.

To obtain accurate results we have chosen a UDP probing traffic from the CN to our specific mobile node of 250 bytes transmitted at intervals of 10 ms. The other mobile nodes create background traffic sending or receiving data at a rate of 32 kbps.

All simulations have a duration of 125 seconds with a 5 seconds warm-up phase. Each point in the following graphs represent the average of at least 100 simulations. The sample size necessary to achieve a confidence interval of 99% with respect to the average value has been selected as indicated in [22]. This required in some cases to perform up to 1000 simulation runs, e.g., in the 50 mobile nodes or random movement case.

We assume a system where mobile nodes use the IPv6 stateless address autoconfiguration feature [23] performing Duplicate Address Detection (DAD) in parallel to avoid the introduction of an additional delay to the handoff process. Note that the delay introduced by DAD would be too time consuming resulting in a noticeable disruption of the service.

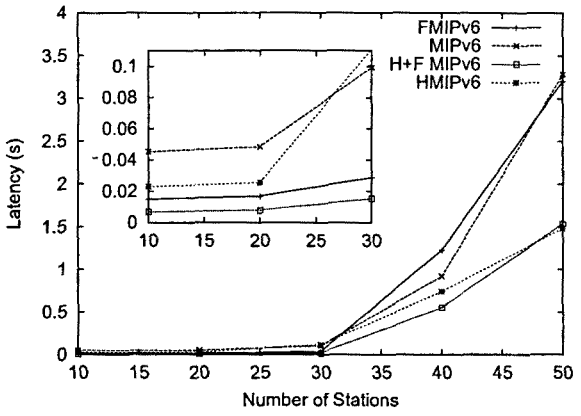

Figure 2.2: Impact of number of stations on handoff latency

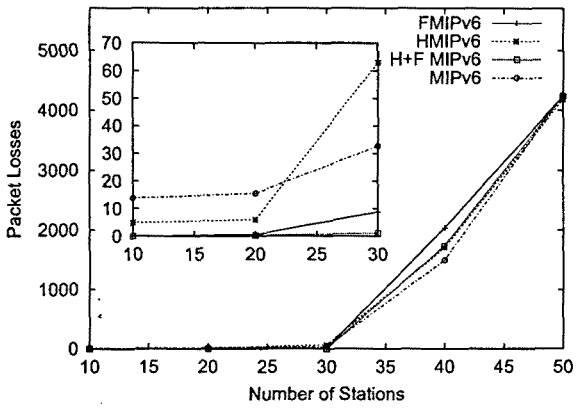

Figure 2.3: Impact of number of stations on packet losses

2.4.1 Impact of number of stations

We present here the results of the impact of the number of competing stations on the following parameters: handoff latency, packet loss, obtained bandwidth and the fast handoff process probability of success.

The studied MN performs 4 handoffs during a simulation run moving at 10 m/s from center to center of the ARs' coverage areas until it reaches again the starting point. The values represented in the graphs correspond to the analyzed MN.

Figures 2.2 and 2.3 show the increase in handoff latency and packet losses due to an increase in the number of MNs sharing the wireless channel. We can observe that up to 20 MNs the results are as expected considering that for a small number

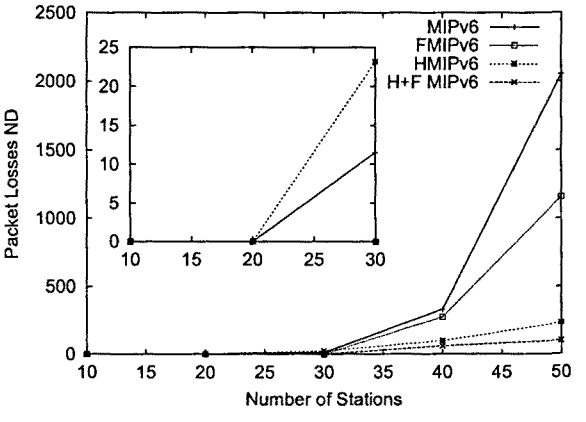

Figure 2.4: Impact of number of stations on packet losses in the Neighbor Discovery resolution queue

of mobile nodes, e.g. 20 or below, the dominating factor of the handoff latency is the wired delay. HMIPv6 latency outperforms standard MIPv6 one since the wired 'distance' in order to update the entity that forwards packets to the mobile node is always shorter. FMIPv6 outperforms standard HMIPv6, since the MN prepares the handoff in advance and thus, after a handoff, does not have to wait for the oAR to be updated to start receiving packets again. With FMIPv6 packets are redirected by the oAR to the nAR through the wired link and therefore only this delay is noticed. H+F MIPv6 performs better than all the other solutions since, as explained in Section 2.2, when the MN receives the F-BAck from the MAP indicating that the handoff should be performed, the re-directed packets are already waiting in the new AR.

An exceptional case can be observed for 30 MNs where MIPv6 shows a slight better performance than HMIPv6. Due to the encapsulation that HMIPv6 always does from the MAP to the current point of attachment we have a higher load on the channel, i.e., 40 additional bytes per packet, and thus HMIPv6 reaches earlier saturation conditions, increasing the wireless delay that now dominates over the wired one. This difference can not be noticed in the H+F MIPv6 case because although we have the same encapsulation problem, the higher load in the channel does not have a direct impact on the handoff performance due to the fast handover mechanism that prepares the handover in advance and re-tries up to three times. However, when the wireless delay becomes very high due to saturation in the channel, e.g., 40-50 stations case, we have again a better performance of HMIPv6 in comparison with MIPv6 due to two reasons. First, in the HMIPv6 case the BU to the MAP is sent right after attaching to the new link while MIPv6 sends a BU to the HA before the one to the CN, i.e., introducing an additional wireless

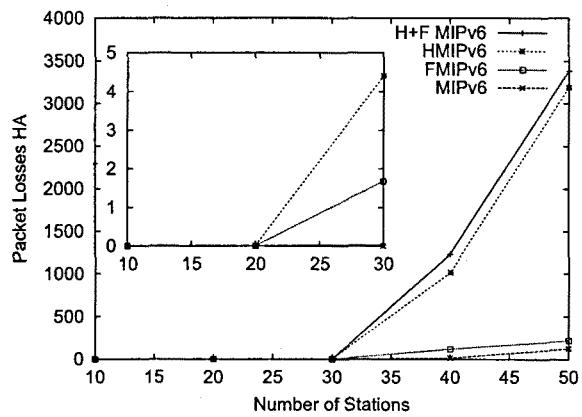

Figure 2.5: Impact of number of stations on packet losses at the HA

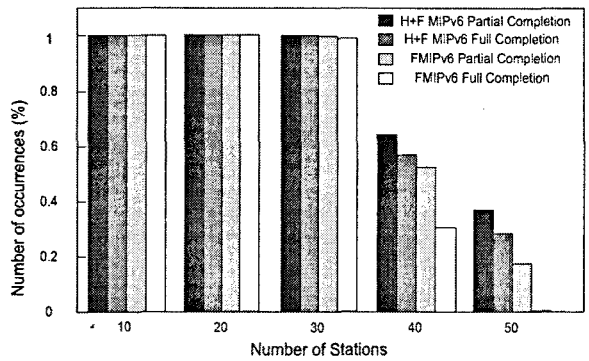

Figure 2.6: Fast Handover process success histogram

delay. This difference could be removed sending the BU first to the CN and then to the HA. Second, while the BAcks to HA and MAP are mandatory, the BAck to the CN is optional. In our implementation BAcks to CN BUs are not sent to avoid additional overhead and because in case of the BU being lost, the MN will re-send it again when receiving a data packet from the HA instead of directly from the CN. Under high saturation channel conditions the probability of a BU to be lost is higher, therefore, when using standard MIPv6 if a BU to the CN is lost[2], it is not retransmitted, increasing significantly the latency value. On the other hand, when the BAck from the MAP is not received, the BU will be retransmitted.

[2]Note that IEEE802.11 realizes when a packet was not correctly transmitted over the wireless medium due to the lack of a MAC layer acknowledgment and re-tries the transmission a certain number of times before discarding it (8 in our case)

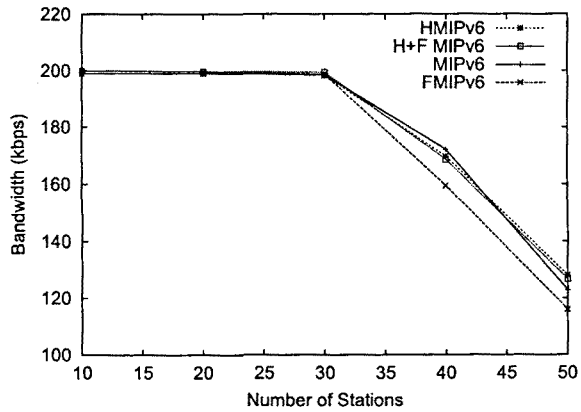

Figure 2.7: Impact of number of stations on bandwidth obtained by observed MN

Although the Fast Handover protocol is designed to minimize packet losses and latency during a handoff, we can observe a worse performance with respect to MIPv6 when saturation arises. To understand this behavior a few factors must be considered. In the scenarios with 40 or more MNs the load in the wireless channel is high, resulting in a channel with a long access time and high collision rate. If we take a look at the packets lost at the neighbor discovery resolution queue[3] (ND), Fig.2.4, we can see that they are higher when FMIPv6 is not used (they double with 50 MN). Those packets, that are dropped in the ND entry queue, are not sent through the wireless channel, which results in a lower channel saturation and, what is more important, a shorter access delay. In the FMIPv6 scenario though, the nAR learns the link layer address of the MN before having to send a packet to it (via the reception of the PrRtSol by the oAR which triggers the HI-HAck handshake) even if the FMIPv6 process has not been successfully performed. Therefore, the AR will send packets through the wireless medium without waiting for the address to be confirmed, once the F-NA has been received, introducing a higher load on the channel.

H+F MIPv6 and HMIPv6 present, under saturation conditions, similar packet losses results since the process to update the MAP and afterwards HA and CN about the new point-of-attachment is the same for both approaches (see Figure 2.5). They show the worst performance in packets lost at the HA, which is actually a good measure of whether the route updating mechanisms are working properly. Packet are lost at the HA only when the BU lifetime of both, CN and HA, has expired. As it can be seen in the figure, the higher load for 30 or more

[3]During the address resolution process only a small amount of packets are buffered for the same destination address, e.g., three in our implementation [12]

MNs produces a higher rate of packet losses at the HA. Which actually are most of the packet losses experienced in the H+F MIPv6 and HMIPv6 case. The reason is that the MN has to wait for the MAP's BAck to send the BUs to HA and CN, what can take a long time when the wireless channel is highly congested, resulting in the expiration of the BU lifetime (10s in our experiments) of the HA and CN. H+F MIPv6 obtains a slight higher HA packet loss rate due to its additional signaling load (see Section 2.4.2). These higher packet losses in the HA are compensated by lower packet losses due to Neighbor Discovery. Note that if the first signaling message of the fast handover procedure (PrRtSol) arrives at its destination, triggering the HI, the nAR will already have the link layer address before having to forward data packets to the MN, which explains the slight difference between H+F MIPv6 and HMIPv6. Another remarkable aspect of the ND packet losses graph is the big difference in saturation conditions between the protocols that use a hierarchical approach and the others. The ND procedure is triggered by the first packet received in the nAR, the BAck from the MAP. Using a hierarchical approach and under saturation conditions the BAck is not always immediately followed by data packets (because the HA and CN have not been updated on time and packets are being dropped in the HA) providing some additional time to the nAR to resolve the link layer address.

Although all the differences (either in ND or HA Packet Losses) described for the congestion case, we can observe that once the saturation level has been reached by all the protocols, if we increase the number of MNs the packet losses tend to converge, since for all cases the wireless channel presents a high collision rate and long channel áccess time reducing thus, the impact of the differences between the approaches. Figure 2.6 perfectly shows the saturation of the channel depending on the number of MNs. Up to 30 MNs the wireless channel conditions allows for a proper completion of the fast handoff process. However, for a higher number of MNs the probability of the process success decreases dramatically. We have differentiated between two cases: full completion of the fast handoff process and partial completion, i.e., the redirection of the traffic from the oAR to the nAR has been established. We believe that the latter case is a significant value since it means that the F-BAck packet has been lost but not the previous FMIPv6 corresponding messages, resulting in a smoother handoff compared to MIPv6. H+F MIPv6 presents a better performance than FMIPv6 since most of the packet are lost in the HA reducing the load introduced in the wireless channel compared to FMIPv6.

Figure 2.7 corresponds to the bandwidth obtained by our specific mobile node. As we can see, the bandwidth correlates almost perfectly the results shown for packet losses. The slight difference between both graphics (in the 40 and 50 MN case) is a consequence of the higher wireless load of the different enhancements. A higher number of data packets sent through the wireless channel and signal-

ing load yields a longer channel access delay and higher collision rate, resulting in a higher number of packets waiting to be sent in the current MN's AR interface queue at the end of the simulation and, therefore, lower bandwidth achieved. As commented above, H+F MIPv6 and HMIPv6 experience a lower load on the wireless channel since most of the packets are lost in the HA.

For the following studies we have focused on the case of 20 MNs since this represents the case with a highest number of MNs in the network where the cannel can still be accessed without experiencing a high degradation in the quality of service due to competing nodes.

2.4.2 Impact of handoff rate

In Section 2.4.1 we have shown some of the performance improvements obtained introducing the MIPv6 enhancements. However, as explained in Section 2.1 several additional signaling messages have been introduced to achieve those results. A trade-off between additional signaling load and performance improvement has to be considered. In Figure 2.8 we study the differences in signaling load between MIPv6 and the proposed enhancements for a handoff rate range varying from 0 to 10 handovers per minute for a simulation of 125 seconds.

H+F MIPv6 presents the higher signaling load within the local domain, as expected, since it introduces the HMIPv6 signaling load plus the FMIPv6 signaling load. The next highest signaling load within the local domain belongs to FMIPv6 since, in the event of a handoff, a higher number of signaling messages are required. One of the purposes of HMIPv6 is to keep constant the signaling load outside of the local domain. Figure 2.8 shows that this goal is achieved by HMIPv6 and H+F MIPv6. In the scenarios where a MAP is placed on the CR and when roaming within the local domain, HA and CNs do not realize any change in the point of attachment and receive only periodic BUs, therefore the signaling load is constant outside the local domain. However, with standard MIPv6 and FMIPv6, when a MN performs a handoff, it must inmediately inform its HA and CNs, and thus, although the periodic BUs are re-scheduled, the total signaling load is increased within and outside the local domain. Note though, that the introduction of a MAP in the system results in a quantitative increase of the signaling load in the local domain, i.e., additional MAP's BU-BAck plus the encapsulation for the BAcks originated by the HA.

As we can observe, MIPv6 and FMIPv6 introduce the same signaling load outside the local domain since all the additional FMIPv6 signaling is sent only within the local domain. The same case applies to H+F MIPv6 and HMIPv6 that only differ in the signaling behavior within the local domain obtaining thus, the same results outside the local domain.

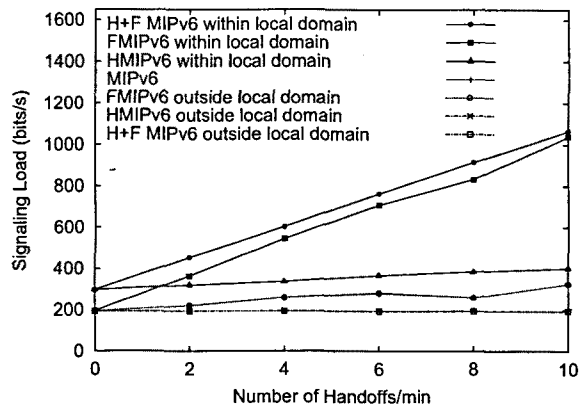

Figure 2.8: Impact of handoff rate on signaling load

The signaling load corresponding to standard MIPv6 presents, a priori, a strange behavior having a local minimum for the case of 8 handoffs/min. However, if we recall that for each handoff the MN re-schedules the periodic BUs to be sent we realize that if the timer of the periodic BUs is below the time between two consecutive handoffs we will observe the periodic BUs and afterwards the ones due to a handoff. On the other hand, if the time between two consecutive handoffs is below the timer of the periodic BUs, they will be always re-scheduled without being sent during the whole simulation. Thus, in the case of 8 handoffs/min, considering a timer of 10 seconds for the periodic BUs, they are always re-scheduled due to a handoff and never sent, resulting in a reduction of signaling load compared to the previous case.

2.4.3 Impact of number of correspondent nodes

One of the advantages of HMIPv6 is that when performing a local handoff the only entity that has to be informed via a BU is the MAP, which reduces the signaling load. This becomes specially important when the number of correspondent nodes increases, i.e., while the number of BUs to be sent increase linearly with MIPv6 and FMIPv6 remain constant for HMIPv6 and H+F MIPv6. However, HMIPv6 and H+F MIPv6 do not reduce the number of periodic BUs to be sent but increase it by the additional one sent to the MAP. Based on the above comments, a trade-off has to be considered between the number of handoffs performed within periodic BU periods and the number of correspondent nodes. This trade-off was already addressed in [8].

Figure 2.8 shows the impact of increasing the number of correspondent nodes over the signaling load for the different protocols in the case of a mobile node per-

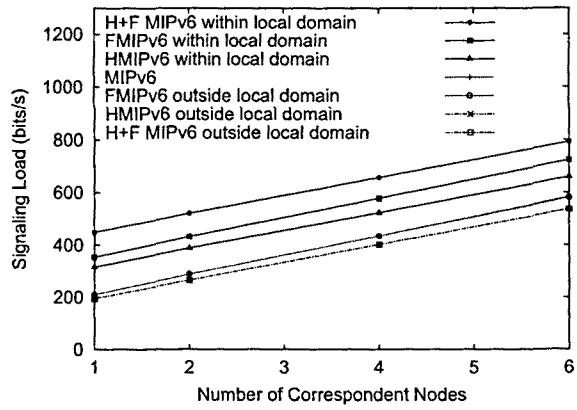

Figure 2.9: Impact of number of correspondent nodes on signaling load

forming 4 handoffs[4] in 120 seconds. FMIPv6 and H+F MIPv6 perform exactly as MIPv6 and HMIPv6, respectively, concerning to the signaling load sent outside of the local domain since there are no differences in the protocol behavior for the signaling messages sent outside of it. As we can observe, the usage of HMIPv6 or H+F MIPv6 reduces the signaling load outside of the local domain compared to MIPv6 and the difference tends to increase according to larger number of correspondent nodes. The difference though, is not very big since in our scenario the number of handoffs per periodic BU periods is small resulting in a small differentiation of HMIPv6. For a scenario with higher mobility or with larger BU periods the HMIPv6 signaling load reduction would be larger including also the local domain signaling.

2.4.4 Impact of wired link delay

We have measured the differences in handoff latency and packet losses between MIPv6 and its enhancements when the wired link delay *ld* from the CR to the HA and CN is increased. The different *ld* values model different 'distances' to the HA and CNs.

MIPv6's enhancements reduce the time that elapses between a MN change of point of attachment and the traffic redirection to its nCoA by introducing a new forwarding entity within the local domain, either oAR or MAP, responsible to redirect the traffic. Thus, the delay experienced by the re-directed traffic does not depend on 'how far' is the MN from its HA and CNs outside of the local domain.

[4]In [24] a twelve-week trace of a building-wide local-area wireless network was studied. The results presented there showed that 2 handoffs per minute is a high handoff rate for pedestrian mobile users

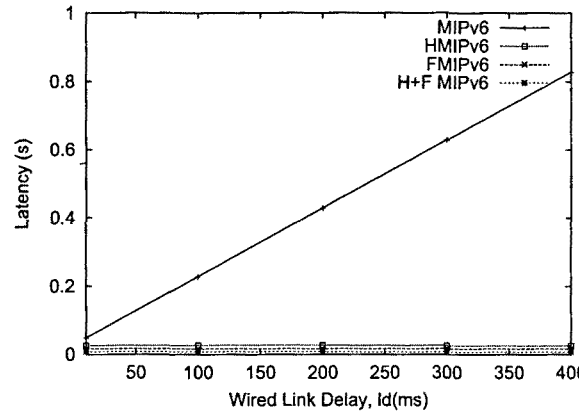

Figure 2.10: Impact of wired link delay on handoff latency

On the other hand, with MIPv6, the BUs sent after performing the handover, have to reach the HA and CNs (outside of the local domain) in order to send the traffic to the proper CoA resulting on a direct dependence with the *ld* value.

As we can see in Figure 2.10 the results are as expected: while an increase in the wired link delay implies an increase in the handoff latency for MIPv6, it does not affect the other proposals' handoff latency.

2.4.5 Impact of random movement

Mobile users are unaware of overlapping areas where handoff decisions are taken. This section studies whether the differences on the performance metrics observed in previous sections for a mobile node following a deterministic path still hold considering random movement. Note that unexpected movements can have a quite negative effect on the packet losses experienced due to back and forth movements around the overlapping areas. This effect could potentially prevail over the protocol enhancements.

Figure 2.11 shows the histogram of packet losses experienced by the studied mobile node moving randomly in the case of 20 mobile nodes for the four different protocols. The packet losses occurrences have been grouped in lower or equal than 1, 10, 100 and over 100. As we can observe from the figure, the results are consistent with the ones presented in Section 2.4.1. FMIPv6 and H+F MIPv6 show the better packet loss performance keeping for most of the cases values below or equal to 1. HMIPv6 outperforms MIPv6 but without reaching the level of the protocols that include the fast handover approach.

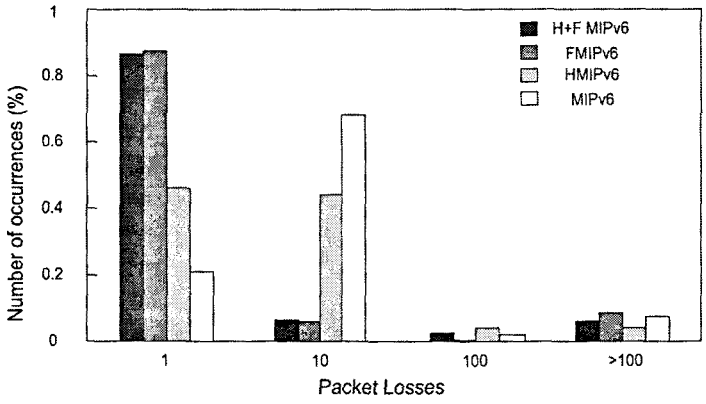

Figure 2.11: Packet losses histogram considering random movement

2.4.6 Impact of traffic sources

Until this section we have studied the impact of different parameters over a target station receiving a high constant traffic load (*probe*) in order to obtain results with a significant precision and without the interference of source burstiness (VoIP, Video) or recovery mechanisms (TCP). In this section we repeat the experiment of Section 2.4.1 but considering more realistic traffic sources and a simulation scenario where all the MNs send or receive the same type of traffic at the same rate. By doing this, we analyze whether the different performance improvements observed in previous sections are affected by the traffic source type, i.e., whether a user would realize a service improvement or the improvements are 'masked' by the traffic sources characteristics. Specifically, three different types of traffic are studied: VoIP, video and TCP transfers.

Markov process that results in a high variance between packet arrivals. Figure 2.12 shows the impact of the number of stations over the packet loss rate of VoIP traffic until the congestion level is reached. Since VoIP sources produce a relatively low traffic load ($\simeq$ 24kbps per source) no packet loss is observed for any of the protocols until the 20 MNs case. In this case, surprisingly, MIPv6 is the protocol that performs best in packet losses terms and HMIPv6 worst. The additional load introduced by the different enhancements in the wireless channel is the reason for this behavior. HMIPv6 is the worst one due to the encapsulation of all packets directed to the MNs performed by the MAP, FMIPv6 performs better since is 'better equipped' to avoid packet losses and H+F MIPv6 is in the middle since is the one producing more overhead but equipped as well with a mechanism to reduce packet losses. When the wireless channel is congested, i.e., 30 MNs

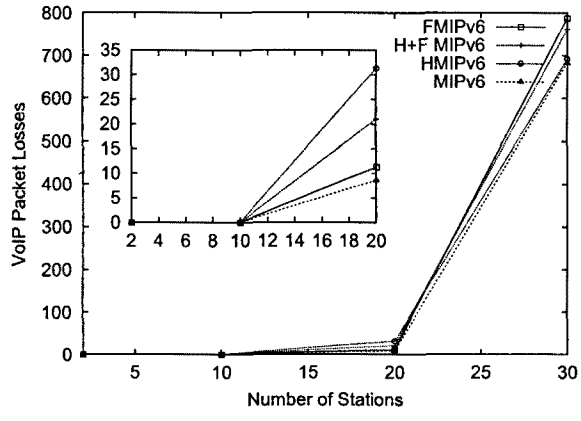

Figure 2.12: Impact of number of sources on VoIP packet losses by a receiving user

case, we observe the same behavior as the one already described in Section 2.4.1. We can conclude that, for a scenario with low rate traffic sources sending small packets (compared to the additional encapsulation header) and in no congestion conditions, the overhead introduced by the different enhancements would result in a worse performance in handoff latency an packet losses terms compared to the baseline Mobile IPv6.

64 kbps. We show the impact of the number of stations over the handoff latency. As we can observe in Figure 2.13, the results are similar to the ones already described in Section 2.4.1, i.e., H+F MIPv6 and FMIPv6 are the ones that perform best in handoff latency terms and MIPv6 is the worst. In this case, in contrast to the VoIP one, the implementation of the Mobile IPv6 enhancements results, as expected, in a better user experienced service since the additional signaling load is less relevant compared to the data traffic load.

in the received service by using one of the different proposals. For a user performing a download, handoff latency or packet loss rate are not relevant performance metrics but the experienced bandwidth during the TCP transfer is of major interest.

Figure 2.14 shows the differences on the available bandwidth for TCP users depending on the MIPv6 protocol enhancement used. In the figure we can observe the TCP sources adjustment of the sending rate to the available channel capacity when the number of mobile users increases. For a number of mobile nodes below 10, a lower packet loss rate obtained via the enhancements results in users achievement of larger bandwidth. H+F MIPv6 presents better packet losses results than FMIPv6; however, with the latter proposal a larger bandwidth value is obtained. In Section 2.4.1 we have shown that there is not a direct relationship

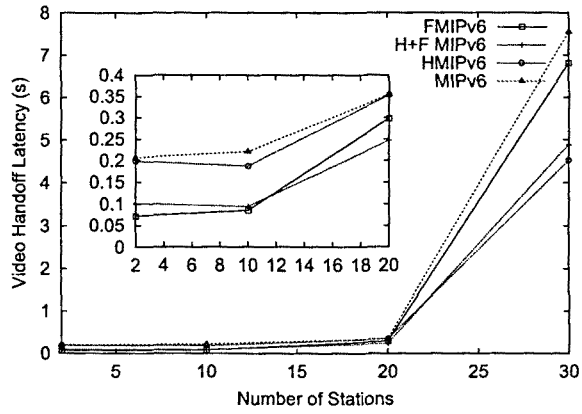

Figure 2.13: Impact of number of sources on Video handoff latency by a receiving user

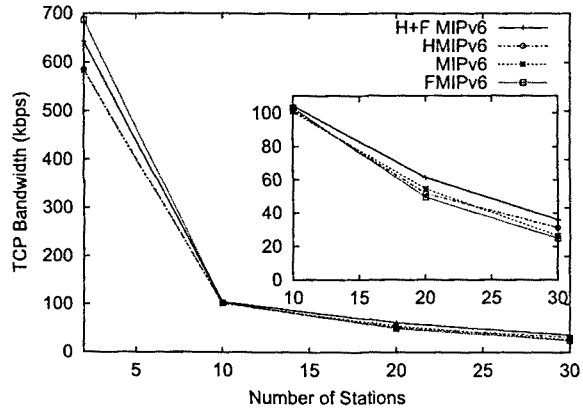

Figure 2.14: Impact of number of sources on TCP bandwidth obtained by a receiving user

between packet losses experienced and obtained bandwidth. The reason is that in the H+F MIPv6 case the MAP encapsulates all the data packets addressed to the mobile nodes, and this overhead reduces the available bandwidth in the wireless channel. The same explanation applies to HMIPv6, where the lower packet loss rate does not result in a significant higher bandwidth compared to MIPv6 because of the packet encapsulation within the local domain.

When the number of mobile nodes increases, the probability of experiencing a collision while trying to access the channel increases, too. This, in turn, triggers the TCP congestion avoidance mechanism more often reducing the packet losses experienced by the MNs and thus, decreasing the bandwidth differences between

the proposals. These differences would otherwise be much bigger, as it has been shown is Section 2.4.1, when the users try to get a larger bandwidth than the one actually available in the channel.

As a conclusion, TCP users would also benefit from the implementation of one of the MIPv6 protocol enhancements even though the improvement would be lower than for other types of traffic, e.g., CBR.

2.5 Summary of Main Results

Mobile IPv6 represents a key element of future *All-IP* wireless networks to allow a user to freely roam between different access networks. During the design process of a Mobile IPv6-based network the question of whether it is appropriate to implement any of the current IETF Mobile IPv6 proposed enhancements instead of pure Mobile IPv6 should be analyzed.

Between the several enhancement proposals for Mobile IPv6, Fast Handovers for Mobile IPv6 (FMIPv6) and Hierarchical Mobile IPv6 (HMIPv6) are the ones with a higher acceptation. In [25–30] we have studied the performance improvements obtained by implementing these proposals, including our proposed combination of FMIPv6 and HMIPv6, and their associated costs in order to support in the decision process of whether it is appropriate to implement any of them for a specific network. The results were used in the IST project *Moby Dick* [31] where such a decision was required.

With our work we have provided quantitative results on Mobile IPv6 performance as experienced by a mobile node and on the level of improvement that can be achieved by using the proposed Mobile IPv6 enhancements. The results were achieved through a study via simulation that required to implement Neighbor Discovery, HMIPv6, FMIPv6 and our combination of HMIPv6 and FMIPv6 for *ns-2*.

We performed a 'stress test' of the protocols where we studied how handoff latency, packet loss rate, obtained bandwidth and fast handoff process success probability are affected by the number of mobile nodes, i.e., by competition for the wireless medium, or by protocol interactions, e.g., with the Neighbor Discovery process of IPv6. The behavior of the protocols for a general case considering random movements and more realistic traffic sources, i.e., VoIP, video and TCP, were also studied. Finally, the signaling load costs associated to the different proposals compared to the performance improvements obtained were analyzed, considering a broad range of handoff rates and number of correspondent nodes. These factors were shown to have a significant influence over the performance metrics and we indicated the points to be taken into account in a real implementation.

Specifically, we have shown that while some simulation results corroborate the intention of the protocols specifications, other results give insights not easily gained without a thorough study. Some of the key results are that *i)* random movements of the observed mobile node do affect the experienced performance but the improvements with respect to the perceived quality of service when using one of the various protocol enhancements is still clearly noticeable, *ii)* in scenarios where the users produce a low rate with small packets, e.g, VoIP sources, the additional overhead introduced by the proposed enhancements can result in a worse performance than the baseline Mobile IPv6 one, and *iii)* Mobile IPv6 can eventually outperform its proposed enhancements in packet losses terms in saturation conditions due to the higher number of packets discarded directly that lower the load in the wireless channel.

Through this analysis a deep insight on the different overall performance of the various protocols and their causes was acquired. Therefore, the results of this study are twofold. First, we provided quantitative results for the different IETF proposals of the overall performance for a realistic 'hot spot' scenario. Second, we provided the reasoning behind the impact of the different parameters over the performance of the various protocols in saturation and no saturation conditions. This reasoning can applied when other scenarios are analyzed.

Chapter 3

Influence of Mobility Models over Performance Studies

The study of mobility protocols requires in most of the cases to use a mobility model to evaluate their resulting performance. Therefore, as part of our research, the impact of mobility models over the results obtained in performance evaluations has been studied.

Mobility models are important building blocks in simulation–based studies of wireless networks. Researchers in this area can choose from a variety of models that have been developed in the wireless communications and mobile computing community during the last decades [32–36]. Moreover, well–known motion models from physics and chemistry — such as random walk or Brownian motion — and models from transportation theory [37–39] are used in simulations of mobile networks. Surveys and classifications on this topic can be found in [34,36,37,40,41].

A very popular and commonly used mobility model is the *random waypoint (RWP) model.* It is implemented in the network simulation tools ns–2 [42] and GloMoSim [43] and used in several performance evaluations of ad hoc networking protocols [44–46]. This mobility model is a simple and straightforward stochastic model that describes the movement behavior of a mobile network node in a given system area as follows (see Fig. 3.1): A node randomly chooses a destination point ('waypoint') in the area and moves with constant speed on a straight line to this point. After waiting a certain pause time, it chooses a new destination and speed, moves with constant speed to this destination, and so on. The movement of a node from a starting position to its next destination is denoted as one *movement period* or *transition* in this document. The destination points are uniformly randomly distributed on the system area.

Related work by other authors on the analysis of the random waypoint model has been published in [47–51]. Blough, Resta, and Santi [47] performed a simulation–

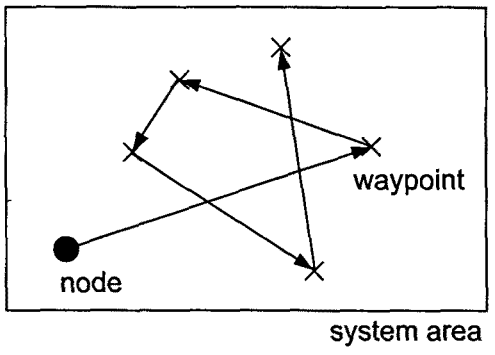

Figure 3.1: Illustration of random waypoint movement

based study in order to test for which parameters the spatial node distribution resulting from the RWP model and a Brownian motion–like model can be approximated by the uniform distribution. As mentioned above, the same group of authors investigated the impact of pause time on the node distribution [48].

Furthermore, Song and Miller [49] studied by means of OPNET simulations how the RWP parameters influence a node's 'mobility factor.' This factor is defined in that paper as the average change of distance of a node to all other nodes per unit time. Another paper that contains simulation results on various RWP issues is by Chu and Nikolaidis [51]. Finally, the paper [52], by Bettstetter, Resta, and Santi derives in an analytical manner an almost exact equation for the spatial node distribution of the RWP model in a square area.

In previous work [36], Bettstetter noted that a fundamental knowledge of the behavior of this model is important to interpret simulation results correctly. Although many researchers use the RWP model in their simulations, a basic understanding of its impact on the simulation results is still lacking. Our work addresses this issue. It presents a detailed investigation of some stochastic characteristics of the RWP model.

Our contributions are as follows: In Section 3.1 we define the RWP model in a formal manner as a discrete–time stochastic process. Based on this description, Section 3.2 derives typical stochastic parameters of a node's traveled distance and time during one movement transition by making use of some classical results of geometrical probability theory. In particular, we give equations for the expected value, variance, and probability density function of the transition length in a circular and rectangular system area. Next, we discuss the mapping from transition length to duration, where we consider scenarios with and without pause time at the destination waypoints. We are interested in this duration because it defines a 'mobility metric' that can be used to describe a certain simulation scenario. Section 3.3 discusses in detail the spatial distribution of nodes moving according to

the RWP model. It was already mentioned in previous papers that this distribution is non–uniform (see, e.g., [36,53]). This property has important consequences for all simulation–based studies in which the relative position of nodes is of relevance (e.g., studies of power control, medium access control protocols). Thus, knowing the spatial node distribution of the RWP model is an essential requirement for investigations in this field. In Section 3.4, we calculate the probability density function of the movement direction of a node at a given location. This direction distribution describes analytically the effect reported in [36, 53] that RWP nodes tend to move back from the border to the middle of the area. In Section 3.5, we employ the RWP model to study the movement of mobile stations in a cellular–structured network. Using a simple, rectangular cell layout, we investigate the expected number of cell changes per movement period and the expected number of cell changes per unit time, i.e., the cell change rate. Finally, Section 3.6 summarizes our main results.

3.1 Definition of the RWP Stochastic Process

Our analysis studies random waypoint movement in a one– or two–dimensional system space $\mathcal{A}$. In one dimension we consider a line segment; in two dimensions we consider a rectangular area of size $a \times b$ or a circular area with radius a. For proper nomenclature, several random variables must be defined. These variables are written in upper case letters, whereas specific outcomes are written in lower case. Multi–dimensional variables (e.g., random coordinates in an area) are written in bold face; scalar variables (e.g., random lengths) are in normal font. The parameter j identifies a particular node, and the discrete time parameter i denotes the movement period of this node.

The random variable representing the Cartesian coordinates of the waypoint that a node j chooses in its movement period i is denoted by the vector $\mathbf{P}_i^{(j)}$. With this definition, the movement trace of an RWP node j can be formally described as a discrete–time stochastic process, given by selecting a random waypoint $\mathbf{P}_i^{(j)}$ for each movement period i:

$$\left\{\mathbf{P}_i^{(j)}\right\}_{i\in\mathbb{N}_0} = \mathbf{P}_0^{(j)}, \mathbf{P}_1^{(j)}, \mathbf{P}_2^{(j)}, \mathbf{P}_3^{(j)}, \ldots \tag{3.1}$$

These waypoints are independently and identically distributed (i.i.d.) using a uniform random distribution over the system space $\mathcal{A}$. Since each node moves independently of other nodes, it is sufficient to study the movement process of a single node. Thus, we often omit the index j.

Let us now consider the case that a node randomly chooses a new speed V_i for movement from $\mathbf{P}_{i-1}$ to $\mathbf{P}_i$ and a pause time $T_{p,i}$ at waypoint $\mathbf{P}_i$. The complete

movement process of a node is then given by

$$\{(\mathbf{P}_i, V_i, T_{p,i})\}_{i\in\mathbb{N}} = (\mathbf{P}_1, V_1, T_{p,1}), (\mathbf{P}_2, V_2, T_{p,2}), (\mathbf{P}_3, V_3, T_{p,3}), \ldots, \quad (3.2)$$

where an additional waypoint $\mathbf{P}_0$ is needed for initialization. A sample of this process is denoted by $\{(\mathbf{p}_i, v_i, \tau_{p,i})\}_{i\in\mathbb{N}}$. A movement period i can be completely described by the vector $(\mathbf{p}_{i-1}, \mathbf{p}_i, v_i, \tau_{p,i})$. When we just refer to a single random variable of a process, we omit the index i and just write $\mathbf{P}$, V, or T_p. The values for the pause time are chosen from a bounded random distribution $f_{T_p}(\tau_p)$ in the interval $[0, \tau_{p,max}]$ with $\tau_{p,max} < \infty$ and a well–defined expected value $E\{T_p\}$. In general the speed is also chosen from a random distribution $f_V(v)$ within the interval $[v_{min}, v_{max}]$ with $v_{min} > 0$ and $v_{max} < \infty$.

3.2 Transition Length and Duration

In simulation–based research on wireless networks it is often desired to compare simulation results that have been obtained using different random mobility models. To do so, one should define a metric for the 'degree of mobility' of the simulated scenario. Due to the broad range of mobility models used in the literature and their various parameters, such a definition is not trivial. Nevertheless, we can state that two mobility parameters are of major interest in all models:

- Speed behavior: Is there a constant speed or a speed distribution? When and how does a node change its speed?
- Direction change behavior: What is the frequency of direction changes? How does a node change its direction?

For example, in the commonly used *random direction model* as described in [36], the time between two direction change events is taken from an exponential distribution. This time is independent of the speed of the node; and, if a wrap–around border behavior [54] is used, it is also independent of the size and shape of the area.

As opposed to this, the RWP model correlates the speed and the direction change behavior. The time between two direction change events is no longer an adjustable input parameter of the model, but it depends on the speed of the nodes and the size and shape of the area. For a given area, a higher speed results in a higher frequency of direction changes.

In this section, we thus investigate the time between two direction change events of the RWP model. We first regard the transition length, i.e., the Euclidian distance that a node travels during one movement period between two waypoints.

We define the sequence of these distances as a stochastic process and show its ergodic properties. Afterward, we give analytical expressions of its probability density function (pdf) and the first two moments. Hereby, we first investigate an RWP model in one dimension and then consider rectangular and circular areas. Finally, we explain the conversion from transition length to time and discuss the impact of the pause time. Among other results, we obtain equations for the average duration of an RWP period with uniform and discrete speed distribution of the nodes.

3.2.1 Stochastic Process of Transition Lengths

As defined above, the stochastic process representing the RWP movement of a node j is given by the sequence of random waypoints $\mathbf{P}_0^{(j)}, \mathbf{P}_1^{(j)}, \ldots$. The corresponding stochastic process of distances between two consecutive waypoints is given by

$$\left\{L_i^{(j)}\right\}_{i\in\mathbb{N}} = L_1^{(j)}, L_2^{(j)}, L_3^{(j)}, \ldots \quad \text{with } L_i^{(j)} = \left\| \mathbf{P}_i^{(j)} - \mathbf{P}_{i-1}^{(j)} \right\| \tag{3.3}$$

A sample of this process is written as $\{l_i^{(j)}\}$. While the random waypoints are i.i.d. per definition, the distances are not stochastically independent, essentially because the endpoint of one movement period i is the starting point of the successive movement period $i+1$.

We are now interested in the expected value of L. It can be interpreted in two ways:

$$E\{L\} = \underbrace{\lim_{m\to\infty} \frac{1}{m} \sum_{i=1}^{m} l_i^{(j)}}_{\text{time average of node } j} = \underbrace{\lim_{n\to\infty} \frac{1}{n} \sum_{j=1}^{n} l_i^{(j)}}_{\text{ensemble average at period } i} \tag{3.4}$$

In words, the *time average* of the transition lengths experienced by a single RWP node j over a long–run simulation ($m \to \infty$) is equal to the *ensemble average* of one period i in an RWP process with many nodes ($n \to \infty$). In the nomenclature of random processes, we thus have a mean–ergodic property of the RWP mobility model.

While this result is intuitively convincing, the proof is not trivial since the random variables $L_1, L_2, L_3, \ldots$ are not stochastically independent. But despite the fact that 'last endpoint equals next starting point,' the ergodic property holds as can be seen as follows. Assume we look at a random process given by

$$\{L_{2i-1}\}_{i\in\mathbb{N}} = L_1, L_3, L_5 \ldots, \tag{3.5}$$

i.e., we look only at every second variable of the original process of random distances. The length L_1 is a deterministic function of $\mathbf{P}_0$ and $\mathbf{P}_1$, the length L_3 a

deterministic function of P_2 and P_3, and so on. Since $\mathrm{P}_0, \mathrm{P}_1, \mathrm{P}_2, \ldots$ are i.i.d. random variables, it follows that $L_1, L_3, \ldots$ are also independent. The mean–ergodic property is obtained immediately in this sub–process because both the time and ensemble average is formed by mutually independent variables. The same is true for the sub–process

$$\{L_{2i}\}_{i\in\mathbb{N}} = L_2,\ L_4,\ L_6\ \ldots \tag{3.6}$$

Now, combining these two sub–processes does not change the asymptotic behavior of the time averages of the combined process, thus, Equation (3.4) holds. In the same manner one also obtains the distribution–ergodic property of the process.

With respect to our problem the above mentioned ergodic properties imply the following: in order to determine the distribution or expected value of the transition length and time observed by a single node following the RWP model, the analysis can be simplified by considering only the distribution of the distance between *two independent points* placed uniformly at random in the system area. This observation allows the transfer of results of geometrical probability theory to our problem. In the following, we make no difference in notation between the 'distance between two consecutive waypoints' and the 'distance between two independent random points sampled from a uniform distribution.' Both are represented by the random variable L.

3.2.2 Transition Length on One–Dimensional Line Segment

We first consider a one–dimensional line segment $[0, a]$. Two random points are uniformly placed on this segment, i.e., the pdf of a point's location $\mathrm{P} = P_x$ is

$$f_{P_x}(x) = \begin{cases} 1/a & \text{for } 0 \le x \le a \\ 0 & \text{else} \end{cases} \tag{3.7}$$

Since both points are independent from each other, their joint pdf is

$$f_{P_{x1}P_{x2}}(x_1, x_2) = f_{P_x}(x_1)\, f_{P_x}(x_2) = \begin{cases} 1/a^2 & \text{for } 0 \le x_1, x_2 \le a \\ 0 & \text{else} \end{cases} \tag{3.8}$$

The distance between two random points is defined by $L = |P_{x1} - P_{x2}|$. The probability that this distance is smaller than a given value l can be computed by the integral of the joint pdf over the area defined by $\mathcal{D} = |x_1 - x_2| \le l$ in the x_1–x_2–space, i.e.,

$$P(L \le l) = \iint_{\mathcal{D}} f_{P_{x1}P_{x2}}(x_1, x_2)\, dx_2\, dx_1\ , \tag{3.9}$$

for $0 \leq l \leq a$. Clearly, $P(L \leq l) = 1$ for $l > a$. Taking into account the bounds of both $\mathcal{D}$ and $f_{P_{x1}P_{x2}}(x_1, x_2)$, we obtain the cumulative distribution function (cdf)

$$P(L \leq l) = \frac{1}{a^2}\left(\int_0^l \int_0^{x_1+l} dx_2\, dx_1 + \int_l^{a-l} \int_{x_1-l}^{x_1+l} dx_2\, dx_1 + \right.$$
$$\left. + \int_{a-l}^{a} \int_{x_1-l}^{a} dx_2\, dx_1\right) = -\frac{1}{a^2} l^2 + \frac{2}{a} l\,. \tag{3.10}$$

The derivative of this function with respect to l yields by definition the desired pdf

$$f_L(l) = \frac{\partial}{\partial l} P(L \leq l) = -\frac{2}{a^2} l + \frac{2}{a} \tag{3.11}$$

for $0 \leq l \leq a$, and $f_L(l) = 0$ otherwise. The expected distance is

$$E\{L\} = \int_0^a l\, f_L(l)\, dl = \frac{1}{3} a, \tag{3.12}$$

and its variance yields

$$E\{L^2\} = \int_0^a l^2\, f_L(l)\, dl = \frac{1}{6} a^2 \tag{3.13}$$

With the above results on ergodicity, these stochastic properties of the distances between a pair of independently uniformly distributed points also represent the stochastic properties of the moved distance of an RWP node within one period.

3.2.3 Transition Length in Rectangular Area

Let us now consider RWP movement in a rectangular area of size $a \times b$ and again derive the distribution of the transition length L. Without loss of generality we assume $a \geq b$. The spatial distribution of the two–dimensional waypoints $\mathbf{P} = (P_x, P_y)$ is now given by the uniform distribution

$$f_{P_x P_y}(x, y) = \begin{cases} 1/(ab) & \text{for } 0 \leq x \leq a \text{ and } 0 \leq y \leq b \\ 0 & \text{else} \end{cases} \tag{3.14}$$

The distance between two points $\mathbf{P}_1 = (P_{x1}, P_{y1})$ and $\mathbf{P}_2 = (P_{x2}, P_{y2})$ is

$$L = \| \mathbf{P}_2 - \mathbf{P}_1 \| = \sqrt{|P_{x1} - P_{x2}|^2 + |P_{y1} - P_{y2}|^2} = \sqrt{L_x^2 + L_y^2} \tag{3.15}$$

Note that the random variable $L_x = |P_{x1} - P_{x2}|$ represents the random distance between two uniformly distributed coordinates P_{x1} and P_{x2} on a one–dimensional

line segment $[0, a]$. Thus, its pdf is given by Equation (3.11). The same holds for $L_y = |P_{y1} - P_{y2}|$ if we replace a by b. In addition, both random distances are independent of each other, and therefore the joint pdf of L_x and L_y is given by

$$f_{L_xL_y}(l_x, l_y) = f_L(l_x)\, f_L(l_y) = \frac{4}{a^2b^2}\big(-l_x + a\big)\big(-l_y + b\big) \tag{3.16}$$

for $0 \le l_x \le a$ and $0 \le l_y \le b$, and 0 otherwise. Knowing this expression, we can derive the cdf $P(L \le l)$ by integration of $f_{L_xL_y}(l_x, l_y)$ over the circle area $\mathcal{D} = l_x^2 + l_y^2 \le l$ in the l_x–l_y–space, i.e,

$$P(L \le l) = \iint_{\mathcal{D}} f_{L_xL_y}(l_x, l_y)\, dl_y\, dl_x \tag{3.17}$$

As in the one–dimensional case, we cannot compute this integral in a straightforward manner, namely by setting the right hand side of (3.16) in (3.17), but must take into account that $f_{L_xL_y}(l_x, l_y) = 0$ for $l_x > a$ or $l_y > b$. Thus, we distinguish between three cases:

$$P(L \le l) = \begin{cases} \int_0^l \int_0^{\sqrt{l^2-l_x^2}} f(l_x, l_y)\, dl_y\, dl_x & \text{for } 0 \le l \le b \\ \int_0^b \int_0^{\sqrt{l^2-b^2}} f(l_x, l_y)\, dl_y\, dl_x & \\ \quad + \int_0^{\sqrt{l^2-l_x^2}} \int_{\sqrt{l^2-b^2}}^l f(l_x, l_y)\, dl_y\, dl_x & \text{for } b < l < a \\ \int_0^b \int_0^{\sqrt{l^2-b^2}} f(l_x, l_y)\, dl_y\, dl_x & \\ \quad + \int_0^{\sqrt{l^2-l_x^2}} \int_{\sqrt{l^2-b^2}}^a f(l_x, l_y)\, dl_y\, dl_x & \text{for } a \le l \le \sqrt{a^2+b^2} \end{cases} \tag{3.18}$$

Solving these integrals, taking the derivate with respect to l, and performing some trigonometric simplifications, leads to the following result.

Result. The pdf of the transition length L of nodes moving according to the RWP model in a rectangular area of size $a \times b$, $a \ge b$, is

$$f_L(l) = \frac{4l}{a^2b^2} \cdot f_0(l) \tag{3.19}$$

with

$$f_0(l) = \begin{cases} \frac{\pi}{2}ab - al - bl + \frac{1}{2}l^2 & \text{for } 0 \le l \le b \\ ab \arcsin\frac{b}{l} + a\sqrt{l^2 - b^2} - \frac{1}{2}b^2 - al & \text{for } b < l < a \\ ab \arcsin\frac{b}{l} + a\sqrt{l^2 - b^2} - \frac{1}{2}b^2 - & \\ \quad ab \arccos\frac{a}{l} + b\sqrt{l^2 - a^2} - \frac{1}{2}a^2 - \frac{1}{2}l^2 & \text{for } a \le l \le \sqrt{a^2+b^2} \\ 0 & \text{otherwise} \end{cases} \tag{3.20}$$

The same result of the distance pdf between two random points was derived by Ghosh in 1951 [55] using a transformation to polar coordinates.

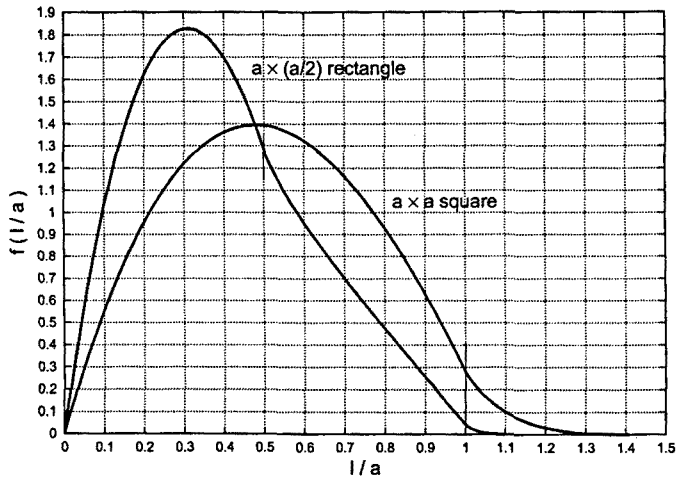

Figure 3.2: Pdf of transition length of RWP nodes in a rectangle

Introducing the normalized random length $\hat{L} = L/a$, Figure 3.2 shows $f_{\hat{L}}(\hat{l})$ for areas of size $a \times a$ and $a \times \frac{a}{2}$. For arbitrary a, the value of $f_L(l)$ is obtained by $f_L(l) = \frac{1}{a} f_{\hat{L}}(\hat{l})$. The expected value of L is [55]

$$E\{L\} = \frac{1}{15}\left[\frac{a^3}{b^2} + \frac{b^3}{a^2} + \sqrt{a^2+b^2}\left(3 - \frac{a^2}{b^2} - \frac{b^2}{a^2}\right)\right] + \frac{1}{6}\left[\frac{b^2}{a}\operatorname{arcosh}\frac{\sqrt{a^2+b^2}}{b} + \frac{a^2}{b}\operatorname{arcosh}\frac{\sqrt{a^2+b^2}}{a}\right] \tag{3.21}$$

with $\operatorname{arcosh}(x) = \ln\left(x + \sqrt{x^2-1}\right)$. Figure 3.3 shows the curve for $E\{L\}/a$ over b/a. For example, the expected length within a square of size $a \times a$ is $E\{L\} = 0.5214\,a$, and a rectangle of size of $a \times \frac{a}{2}$ yields $E\{L\} = 0.402\,a$. The variance of L is given by

$$E\{L^2\} = \frac{1}{6}\left(a^2 + b^2\right) \tag{3.22}$$

Note that for $b \to 0$ the moments for the one–dimensional case are obtained, i.e., $\lim_{b\to 0} E\{L\} = \frac{1}{3}\,a$ and $\lim_{b\to 0} E\{L^2\} = \frac{1}{6}\,a^2$.

3.2.4 Transition Length in Circular Area

On a circular system area of radius a, the distance pdf $f_L(l)$ can be derived, for example, as follows. We regard a node with a given starting waypoint $\mathbf{P} = \mathbf{p}$ and compute the conditional probability $P(L \le l \mid \mathbf{P} = \mathbf{p})$ using basic geometric

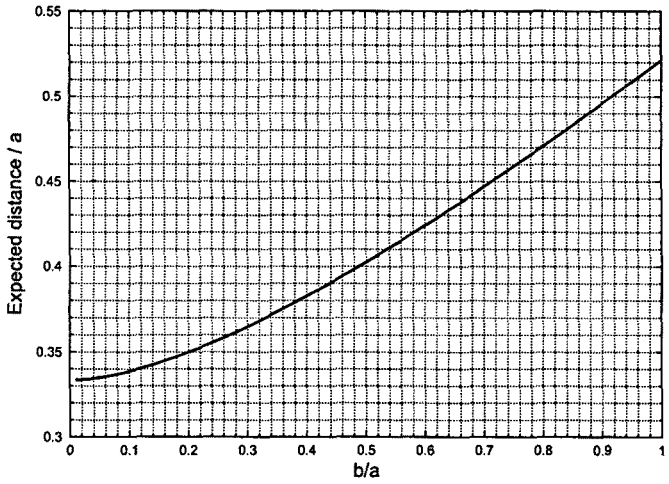

Figure 3.3: Expected transition length of RWP nodes within an $a \times b$ rectangle

equations on the intersection area of two circles. Hereby, we use polar coordinates. Straightforward integration over all possible starting waypoints in the area gives $P(L \leq l)$, whose derivate is $f_L(l)$. These operations lead to the following result, which is also reported in [56].

Result. The pdf of the transition length L of nodes moving according to the RWP model on a disk of radius a is given by

$$f_L(l) = \frac{8}{\pi a}\frac{l}{2a}\left(\arccos\frac{l}{2a} - \frac{l}{2a}\sqrt{1-\left(\frac{l}{2a}\right)^2}\right), \tag{3.23}$$

for $0 \leq l \leq 2a$ and 0 otherwise.

Again, we can introduce a normalized random variable $\hat{L} = L/2a$ for simplicity. Figure 3.4 shows the plot of $f_{\hat{L}}(\hat{l})$. The expected value of L is

$$E\{L\} = \int_0^{2a} l\, f_L(l)\, dl = \frac{128}{45\,\pi}\cdot a \;=\; 0.9054\, a\,, \tag{3.24}$$

and its variance is

$$E\{L^2\} = \int_0^{2a} l^2\, f_L(l)\, dl = a^2 \tag{3.25}$$

3.2.5 Transition Time

Let us now employ our results on the transition length to calculate the stochastic properties of the transition time, i.e., the time it takes a node to move from one

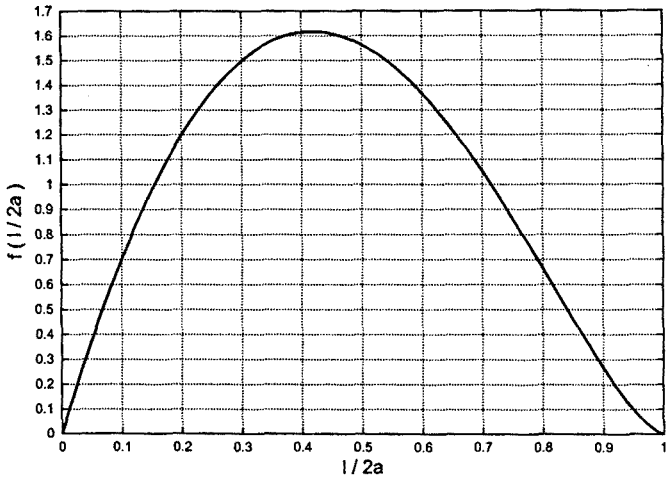

Figure 3.4: Pdf of transition length of RWP nodes on a disk of radius a

waypoint to the next waypoint. The corresponding random variable is denoted by T and an outcome is written as τ.

If the speed of a node is constant during the entire movement process, i.e., $V_i = v = const\ \forall i$ and $v > 0$, we have

$$T = \frac{1}{v} L \tag{3.26}$$

Hence, the expected transition time is

$$E\{T\} = \frac{1}{v} E\{L\}\ , \tag{3.27}$$

and its pdf can be computed by

$$f_T(\tau) = v\, f_L(v\tau)\ , \tag{3.28}$$

with $E\{L\}$ and f_L taken from (3.20–3.21) or (3.23–3.24), respectively.

We now consider the case in which the speed of a node is not constant but chosen from a random distribution $f_V(v)$ at each waypoint (and then stays constant during one transition). We require $v_{min} \leq V \leq v_{max}$ and $v_{min} > 0$ and can write

$$T = \frac{L}{V} \tag{3.29}$$

In this case, the random variable T is formed as a function $g(L, V) = L/V$ of two random variables L and V. In general, the expected value of a variable $g(L, V)$ can be expressed in terms of the joint pdf $f_{LV}(l, v)$ as [57]

$$E\{g(L,V)\} = \int_{-\infty}^{\infty} \int_{-\infty}^{\infty} g(l,v)\ f_{LV}(l,v)\, dl\, dv \tag{3.30}$$

In our case, L and V are independent, and thus their joint pdf is $f_{LV}(l,v) = f_L(l)\, f_V(v)$. The expected value can then be simplified to

$$E\{T\} = E\{L\} \int_{v_{min}}^{v_{max}} \frac{1}{v} f_V(v)\, dv \tag{3.31}$$

The pdf of $T = L/V$ can be computed by

$$f_T(\tau) = \int_{v_{min}}^{v_{max}} v\, f_L(v\tau)\, f_V(v)\, dv \tag{3.32}$$

for $0 \leq \tau \leq \tau_{max}$ with $\tau_{max} = l_{max}/v_{min}$, and $f_T(\tau) = 0$ otherwise. Let us explain these results in more detail by using three typical speed distributions: a continuous uniform distribution, a discrete distribution, and a continuous beta distribution.

Uniform Speed Distribution

If we employ a uniform speed distribution within $[v_{min}, v_{max}]$, the expected transition time is

$$E\{T\} = \frac{\ln(v_{max}) - \ln(v_{min})}{v_{max} - v_{min}} E\{L\} \tag{3.33}$$

Note that $\lim_{v_{max} \to v_{min}} E\{T\} = E\{L\}/v_{min}$ corresponds to the result (3.27) for constant speed $v = v_{min} = const$. Further note that the expected time for $v_{min} = 0$ is undefined. This is very reasonable because if a node chooses $V = 0$ the movement transition will take an infinite time. If the maximum speed can be expressed as a multiple of the minimum speed, i.e., $v_{max} = k \cdot v_{min}$, with $k > 1$, we obtain

$$E\{T\} = \frac{\ln k}{k-1} \frac{E\{L\}}{v_{min}} \tag{3.34}$$

Example. A mobile node moves according to the RWP model on a disk of radius a. It randomly chooses a new speed in each waypoint from a uniform distribution between $[\frac{v_0}{2}, v_0]$. The expected transition time is therefore given by $E\{T\} = 1.2552\, a/v_0$. The pdf can be computed by $f_T(\tau) = \int_{v_0/2}^{v_0} v\, f_L(v\tau)\, \frac{2}{v_0}\, dv$ for $0 < \tau \leq 4a/v_0$, with $f_L(v\tau)$ taken from (3.23). The resulting function for $a = 1$ m and $v_0 = 1$ m/s is illustrated in Fig. 3.5 and compared to a node that moves with deterministic speed $V = v_0$ for all periods. Clearly, the latter node has on average a much shorter transition time, namely $E\{T\} = 0.9054\, a/v_0$, since it always moves with the highest speed v_0. By proper scaling of both axes, we obtain the values for arbitrary a and v_0.

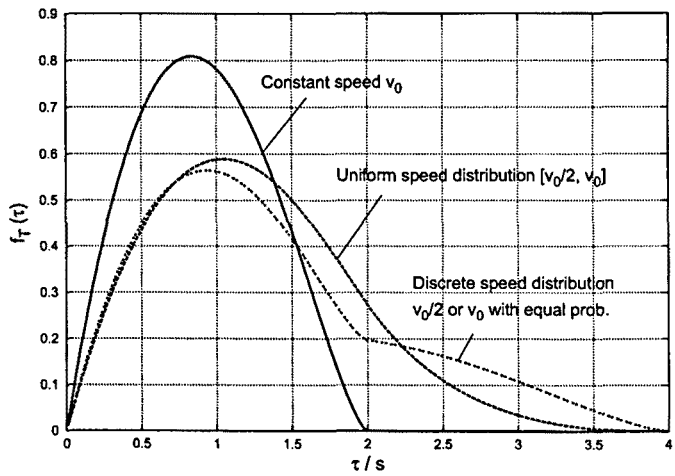

Figure 3.5: Pdf of transition time of RWP nodes on a disk ($a = 1\,\text{m}$, $v_0 = 1\,\text{m/s}$)

Discrete Speed Distribution

We now regard a node that chooses its speed from a set of J discrete values $\{v_1, \ldots, v_j, \ldots, v_J\}$, each value with a certain probability p_j. Clearly, $\sum_{j=1}^{J} p_j = 1$ must hold. Such a discrete speed distribution can be expressed by $f_V(v) = \sum_{j=1}^{J} p_j\, \delta(v - v_j)$, where the function $\delta(x)$ denotes the Dirac delta function. The latter has the properties $\delta(x) = 0$ for $x \neq 0$ and $\delta(0) = \infty$ and $\int_{-\infty}^{\infty} \delta(x)dx = 1$. The expected transition time is then given by

$$E\{T\} = E\{L\} \sum_{j=1}^{J} \frac{p_j}{v_j} \tag{3.35}$$

Example. An RWP node moving on a disk chooses in each waypoint either $V = v_1 = v_0/2$ or $v_2 = v_0$, both speed values with equal probability. We thus have $f_V(v) = \frac{1}{2}\left(\delta(v - v_0/2) + \delta(v - v_0)\right)$. The expected transition time of this node is $E\{T\} = 1.3581\, a/v_0$. The pdf of T can be computed with (3.32) and is shown in Fig. 3.5. If the speed value $v_0/2$ is chosen with a probability $p_1 = 0.9$ the average transition time is increased to $E\{T\} = 1.7203\, a/v_0$.

Beta Speed Distribution

A non–uniform, continuous speed distribution that is bounded by v_{min} and v_{max} can be expressed in terms of the beta distribution

$$f_V(v) = \frac{1}{B(\mu_1, \mu_2)} \cdot \frac{v_\star^{\mu_1 - 1}\,(1 - v_\star)^{\mu_2 - 1}}{v_{max} - v_{min}} \tag{3.36}$$

with $v_\star = \frac{v - v_{min}}{v_{max} - v_{min}}$. The beta function $B(\mu_1, \mu_2)$ is defined by $\int_0^1 z^{\mu_1 - 1} (1-z)^{\mu_2 - 1}\, dz$. Depending on the non–zero parameters μ_1 and μ_2, the function $f_V(v)$ takes a variety of shapes. For example, if $\mu_1 > 1$ and $\mu_2 > 1$, it has a concave down shape with $f_V(v) \to 0$ for both $V = v_{min}$ and v_{max}. If $\mu_1 = \mu_2$, the curve is symmetric around $\frac{1}{2}(v_{max} - v_{min})$, otherwise the maximum or minimum is shifted closer to v_{max} or v_{min}. For $\mu_1 = \mu_2 = 1$, a uniform distribution is obtained. The average speed is always given by $E\{V\} = \frac{1}{\mu_1 + \mu_2}(\mu_1 v_{max} + \mu_2 v_{min})$. Example plots of the beta distribution can be found, for instance, in [57, 58]. Using this large class of speed distributions, the integral in (3.31) is again solvable, and we can calculate $E\{T\}$ for a given system area in a straightforward manner.

Example. An RWP node in a square area of side a chooses its speed from a beta distribution with parameters $\mu_1 = 4$ and $\mu_2 = 1$ in an interval between $v_{min} =$ 1 m/s and $v_{max} = 10$ m/s. The expected transition time is $E\{T\} = 0.0665\, a$ s/m. For $\mu_1 = 2$ and $\mu_2 = 6$ we obtain $E\{T\} = 0.1892\, a$ s/m.

3.2.6 Time Between Two Direction Changes

We now extend our study to the case in which a node rests a certain pause time in each waypoint. The total time T' of an RWP period is then composed of a movement transition time T and a pause time T_p, i.e,

$$T' = T + T_p \tag{3.37}$$

This linear combination of two independent random variables yields an expected value

$$E\{T'\} = E\{T\} + E\{T_p\} \tag{3.38}$$

and the pdf

$$f_{T'}(\tau') = \int_0^{\tau'} f_T(\tau)\, f_{T_p}(\tau' - \tau)\, d\tau \quad \text{for } \tau' \geq 0 \tag{3.39}$$

The value of $E\{T'\}$ represents the average time between two direction changes. Thus, the direction change frequency is given by $1/E\{T'\}$ in unit 1/s.

Example. We consider a $1000 \times 500\,\text{m}^2$ simulation area. The nodes move according to the RWP model with constant speed $v = 10$ m/s and a pause time taken from an exponential distribution $f_{T_p}(\tau_p) = \mu e^{-\mu \tau_p}$ with a mean pause time $\mu = 10$ s. The expected epoch length is $E\{L\} = 402$ m. The expected epoch time is $E\{T'\} = 40.2\,\text{s} + 10\,\text{s} = 50.2\,\text{s}$. If we increase the speed to $v = 20$ m/s, we obtain $E\{T'\} = 20.1\,\text{s} + 10\,\text{s} = 30.1$ s, i.e., a node is expected to change its direction more frequently. Increasing the area to $1000 \times 1000\,\text{m}^2$ reduces the frequency of direction changes. We then have $E\{T'\} = 62.1$ s (with $v = 10$ m/s) and $E\{T\}' = 36.05$ s (with $v = 20$ m/s).

This example illustrates that, in the RWP model, the mobility metric 'speed' and the size and shape of the area directly influence the mobility metric 'direction change.' In other words, the two metrics 'speed' and 'direction change' cannot be treated as independent input parameters in this model.

3.3 Spatial Node Distribution

In the previous section, we investigated the distance and time between two consecutive waypoints in the RWP model. These waypoints, which represent the starting and ending points of a node's movement period, are uniformly distributed per definition. In this section, we also take into account the locations that a node visits while moving in a straight line between its waypoints: we study the spatial distribution of nodes resulting from their RWP movement in a rectangular or circular system area $\mathcal{A}$. Again, it is sufficient to regard a single node, because each node moves independently.

Let the random variable $\mathbf{X} = (X, Y)$ denote the Cartesian location of a mobile node in $\mathcal{A}$ at an arbitrary time instant t. A particular outcome of this variable is denoted by $\mathbf{x}$. With this definition, we can express the spatial distribution of a node in terms of the probability density function

$$\begin{aligned} f_{\mathbf{X}}(\mathbf{x}) &= f_{XY}(x,y) \\ &= \lim_{\delta \to 0} \frac{P\left((x-\frac{\delta}{2} < X \leq x+\frac{\delta}{2}) \wedge (y-\frac{\delta}{2} < Y \leq y+\frac{\delta}{2})\right)}{\delta^2} . \end{aligned} \tag{3.40}$$

Note that, in general, a conversion to polar coordinates $R = \sqrt{X^2 + Y^2}$ and $\Phi = \arctan(Y/X)$ yields the joint distribution $f_{R\Phi}(r,\phi) = r \cdot f_{XY}(r\cos\phi, r\sin\phi)$.

The probability that a given node is located in a certain subarea $\mathcal{A}' \subset \mathcal{A}$ can be computed by integrating $f_{\mathbf{X}}(\mathbf{x})$ over this subarea, i.e.,

$$P(\text{node in } \mathcal{A}') = P(\mathbf{X} \in \mathcal{A}') = \iint_{\mathcal{A}'} f_{XY}(x,y)\, dA \tag{3.41}$$

The differential area element dA is given by $dA = dx\,dy$ in Cartesian coordinates. The resulting probability $P(\mathbf{X} \in \mathcal{A}')$ can be interpreted as the percentage of time that a given mobile RWP node is located in the subarea $\mathcal{A}'$ during a long–run movement process with many transitions. But it can also be interpreted as the ensemble average if we regard a simulation with many mobile RWP nodes ($n \gg 1$). Then, $E\{n'\} = n\,P(\text{node in } \mathcal{A}')$ denotes the expected number of nodes located in $\mathcal{A}'$ at an arbitrarily chosen time instant.

At the beginning of a simulation, all nodes are typically uniformly distributed, so $f_{\mathbf{X}}(\mathbf{x})$ is given by a uniform distribution over $\mathcal{A}$ at time $t = 0$. However, as it

has been observed in [36, 47, 53], this distribution changes as the nodes start to move. This is because the nodes' movement paths tend to go through the center of the system area. For example, a node starting at a waypoint close to the border of the system area clearly finds more destination waypoints in directions toward the center of the area than toward the border. Most likely, it chooses a destination point that requires the node to pass the central area during its next movement period. As time goes on and the nodes perform a number of movement periods, the node distribution becomes more and more non–uniform, with a maximum in the middle of the area and a probability density of $f_{\mathbf{X}}(\mathbf{x}) = 0$ at the borderline. Finally, for a long running time of the movement process, a *stationary distribution* is achieved [54]. In the following, we show this stationary distribution for RWP movement with and without pause time.

3.3.1 Spatial Distribution without Pause Time

We first regard random waypoint mobility without pause time at the waypoints, i.e., the nodes are continuously moving. Figure 3.6 shows the spatial node distribution $f_{\mathbf{X}}(\mathbf{x})$ of such an RWP movement process obtained through a long–running simulation in a square system area of size $1000 \times 1000\,\mathrm{m}^2$ as well as on a disk of radius $a = 500\,\mathrm{m}$ [54, 59]. In both cases $f_{\mathbf{X}}(\mathbf{x})$ has its maximum at the center of the system area, while the probability of finding a given node close to the border goes to zero. The circular distribution is rotational–symmetric around the center and also the distribution of the square area shows a symmetry. Another important observation is that the distribution is independent of the speed of the nodes.

As suggested in [59], we can use the analytical expression

$$f_{\mathbf{X}}(\mathbf{x}) = f_{XY}(x, y) \approx \frac{36}{a^6}\left(x^2 - \frac{a^2}{4}\right)\left(y^2 - \frac{a^2}{4}\right) \tag{3.42}$$

to approximate the distribution in a square area of size $a \times a$ defined by $-a/2 \leq x \leq a/2$ and $-a/2 \leq y \leq a/2$. As usual, $\iint_A f_{\mathbf{X}}(\mathbf{x})\, dA = 1$ holds. The quality of this approximation is evaluated in detail by Santi and Resta in [48]. In fact, it was shown that (3.42) approaches very closely the distribution obtained by high–confident simulations. An almost exact equation for the spatial distribution in a square has been derived in [52], and [59] gives an approximation for the circular case. The asymptotic density function on a line segment $[0, a]$ is given by

$$f_X(x) = -\frac{6}{a^3}x^2 + \frac{6}{a^2}x \tag{3.43}$$

for $0 < x < a$, and 0 otherwise [52, 59].

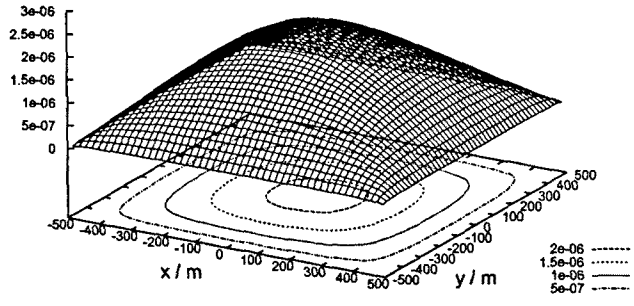

a. Square system area

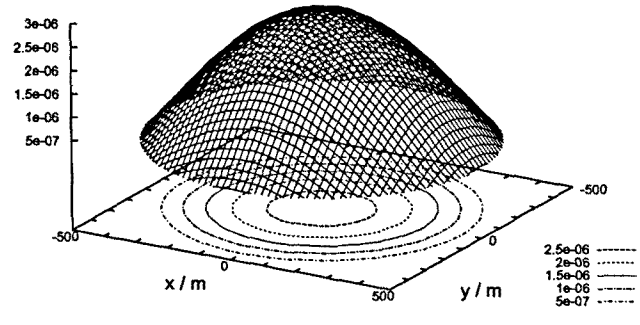

b. Circular system area

Figure 3.6: Spatial node distribution resulting from the RWP model (simulation results)

3.3.2 Spatial Distribution with Pause Time

Let us now move on to study RWP nodes that are also allowed to pause a certain amount of time τ_p at their destination points. The resulting spatial node distribution $f_{\mathbf{X}}(\mathbf{x})$ is then given by the superposition of two distinct components, namely a pause component and mobility component. Both components are probability density functions weighted by the probability that a node pauses or moves, respectively [48]. Let p_p denote the probability that a given node pauses at a randomly chosen time. We can then set up:

$$f_{\mathbf{X}}(\mathbf{x}) = \underbrace{p_p \, f_{\mathbf{X},p}(\mathbf{x})}_{\text{pause component}} + \underbrace{(1-p_p) \, f_{\mathbf{X},m}(\mathbf{x})}_{\text{mobility component}} . \tag{3.44}$$

Table 3.1: Mapping between pause probability and expected pause time (square area)

p_p	0	0.1	0.161	0.2	0.5	0.658	0.9	0.951	1.0
$\frac{v}{a}E\{T_p\}$	0	0.058	0.1	0.130	0.521	1.0	4.689	10	∞

The pdf $f_{\mathbf{X},p}(\mathbf{x})$ represents the spatial distribution of all nodes that are currently pausing at a destination point. Since the destination points are chosen from a uniform distribution, $f_{\mathbf{X},p}(\mathbf{x})$ is also uniform. Thus,

$$f_{\mathbf{X},p}(\mathbf{x}) = \begin{cases} \frac{1}{\|\mathcal{A}\|} & \mathbf{x} \in \mathcal{A} \\ 0 & \text{else} \end{cases} \tag{3.45}$$

The pdf $f_{\mathbf{X},m}(\mathbf{x})$ of the mobility component represents the spatial distribution of all moving nodes. It is thus given by the results of Section 3.3.1, i.e., the right hand side of (3.42) for a square.

Recall that τ_i and $\tau_{p,i}$ denote the time that a node moves or pauses, respectively, during an RWP period i. The pause probability p_p is given by the percentage of time that a node pauses during a long–running process. Assuming that each node pauses a fixed time period τ_p at each waypoint i (i.e., $T_{p,i} = \tau_p \; \forall i$) we have [48]

$$p_p = \lim_{m\to\infty} \frac{\sum_{i=1}^{m} \tau_{p,i}}{\sum_{i=1}^{m} (\tau_{p,i} + \tau_i)} = \frac{\tau_p}{\tau_p + E\{T\}} \tag{3.46}$$

with the expected transition time $E\{T\} = \lim_{m\to\infty} \frac{1}{m} \sum_{i=1}^{m} \tau_i$ given in Section 3.2.5. If we regard a generalization in which the pause time is taken from a pdf $f_{T_p}(\tau_p)$ with an expected value $E\{T_p\}$, the pause probability can be calculated by

$$p_p = \frac{E\{T_p\}}{E\{T_p\} + E\{T\}} \tag{3.47}$$

Applying the values of p_p in (3.44) allows for the computation of the node distribution in a variety of scenarios. Table 3.1 shows some mappings between the pause probability p_p and expected pause time $E\{T_p\} = \frac{p_p}{1-p_p} \cdot \frac{E\{L\}}{v}$ in a square system area of size $a \times a$.

3.4 Movement Direction

One of the major reasons why the spatial node distribution resulting from the RWP model is non–uniform is the fact that nodes take a non–uniformly distributed

direction angle at the beginning of each movement period i.[1] The probability density function of this angle is determined by the shape of the system area and the starting waypoint $\mathbf{p}$ of the node. Let us investigate this issue in more detail for a one–dimensional line segment and a circular system area. All angles are defined in radian notation.

3.4.1 One–Dimensional Line

We first consider a one–dimensional line segment $[0, a]$. The random variable representing the direction of a node is denoted by Γ and a specific value is γ. A node located at a given waypoint $\mathbf{P} = x$, with $0 \leq x \leq a$, chooses a new destination point and then moves either to the right (direction $\Gamma = 0$) or to the left (direction $\Gamma = \pi$).

It is straightforward to observe that a certain direction is chosen with high probability, if many potential destination points lie in this direction. Since the destination points are taken from a uniform distribution, we obtain $P(\Gamma = 0 \,|\, \mathbf{P} = x) = \frac{a-x}{a}$ and $P(\Gamma = \pi \,|\, \mathbf{P} = x) = \frac{x}{a}$, and therefore

$$f_\Gamma(\gamma \mid \mathbf{P} = x) = \frac{a-x}{a}\,\delta(\gamma) + \frac{x}{a}\,\delta(\gamma - \pi)\,, \tag{3.48}$$

where $\delta(\cdot)$ again denotes the Dirac delta function.

3.4.2 Circular Area

In a circular area it is useful to employ polar coordinates for the location of the starting waypoint. We use P_r and P_ϕ as random variables, and r and ϕ for particular values of theses variables. The definition of a node's movement direction γ (random variable Γ) in a two–dimensional system space is shown in Figure 3.7. It denotes the angle between a horizontal line and the current movement vector of the node, where $0 \leq \gamma < 2\pi$. In each waypoint a node 'chooses' such a direction angle whose value remains constant during one movement period. Unfortunately, the outcome of this angle depends on both polar coordinates of the starting waypoint. Thus, as shown in Fig. 3.7, we introduce in each waypoint a second, alternative direction angle denoted as θ (random variable Θ). This angle is defined in a way that $\Theta = 0$ for movement transitions going through the center of the circular system area. Again we have $0 \leq \Theta < 2\pi$. A major advantage of this definition is that the outcome of Θ is independent of the polar angle ϕ of

[1] Note that other stochastic mobility models which directly choose a destination direction rather than a destination point and allow a bounce back or wrap–around behavior at the border of the system area are able to achieve a uniform spatial distribution (see, e.g., [54]).

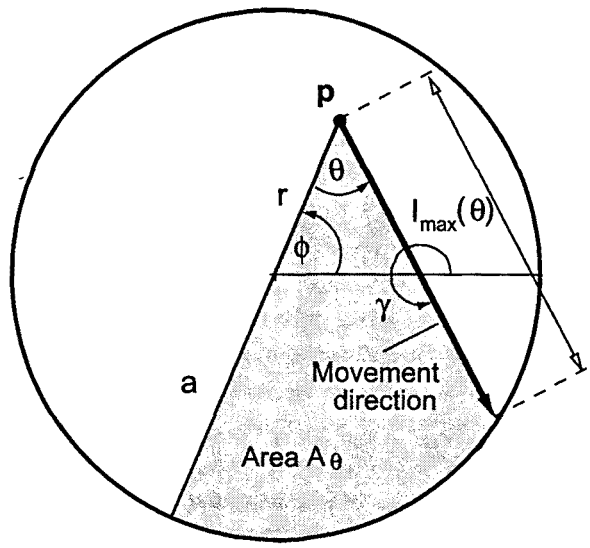

Figure 3.7: Definition of direction angles

the starting waypoint. On the other hand, it is only convenient to use θ in the waypoints. It can then be directly mapped to γ for given ϕ. If we define that counterclockwise angles count positive, we have

$$\gamma = \theta + \phi + \pi \tag{3.49}$$

Our aim is now to derive first the distribution of Θ for a given starting waypoint $\mathbf{P} = \mathbf{p}$. This conditional distribution is denoted by $f_\Theta(\theta \mid \mathbf{P} = \mathbf{p})$. Later, we transform this distribution to $f_\Gamma(\gamma \mid \mathbf{P} = \mathbf{p})$. Both probability density functions give us information about the direction that a node takes when it starts at a waypoint with known location $\mathbf{p}$. Finally, we integrate over all possible starting points in the circle to obtain the unconditional pdf $f_\Theta(\theta)$.

Without any calculation, we can already make the following four statements about the pdf of the direction Θ in a given waypoint. First, it is independent of the polar angle ϕ of the starting waypoint, i.e., $f_\Theta(\theta \mid \mathbf{P} = \mathbf{p}) = f_\Theta(\theta \mid P_r = r)$. Thus, in the following, we just write $f_\Theta(\theta \mid r)$ for simplicity of notation. Second, the direction is uniformly distributed for nodes starting at $P_r = 0$, i.e.,

$$f_\Theta(\theta \mid 0) = \frac{1}{2\pi} \quad \text{for } 0 \leq \theta < 2\pi\,.$$

Third, for all $P_r \neq 0$, the highest value in the pdf is achieved for $\Theta = 0$, the lowest for $\Theta = \pi$:

$$\begin{aligned} \max\left(f_\Theta(\theta \mid r)\right) &= f_\Theta(0 \mid r) \quad \text{for } 0 < r < a \\ \min\left(f_\Theta(\theta \mid r)\right) &= f_\Theta(\pi \mid r) \quad \text{for } 0 < r < a. \end{aligned}$$

Last but not least, the pdf shows the symmetry

$$f_\Theta(\theta - \Delta\theta \mid r) = f_\Theta(\theta + \Delta\theta \mid r) \quad \forall \Delta\theta, \forall r\,.$$

In the following we derive $f_\Theta(\theta \mid r)$. Let $P(\Theta \leq \theta \mid r)$ denote the probability that a node at a given waypoint (r, ϕ) takes a movement angle Θ that is lower than a certain value θ. Clearly, a node takes such a direction, if it chooses a destination point within the area spanned by $0 \leq \Theta < \theta$ (see Fig. 3.7). Let us denote this subarea by $\mathcal{A}_\theta$. The probability that a destination point is chosen in $\mathcal{A}_\theta$ is given by the area integral of the spatial pdf $f_{P_x P_y}(x, y)$ over this subarea. Since the destination waypoints are chosen from a uniform spatial distribution, we can set up

$$P(\Theta \leq \theta \mid r) = \iint_{\mathcal{A}_\theta} \frac{1}{a^2\pi}\, dA = \frac{\|\mathcal{A}_\theta\|}{a^2\pi}\,, \tag{3.50}$$

with the area element given by $dA = dx\,dy = r\,dr\,d\phi$. For given r, we define the length $l_{max}(\theta')$ as the maximum possible transition length of a node at r in the direction θ' (see Fig. 3.7). Note that this length is independent of the polar angle ϕ. Using the law of cosines for θ' in the triangle with sides $\{l_{max}(\theta'), a, \text{and } r\}$, we obtain a quadratic equation for $l_{max}(\theta')$, whose solution is

$$l_{max}(\theta') = r\cos\theta' + \sqrt{a^2 - r^2\sin^2\theta'} \tag{3.51}$$

The area size $\|\mathcal{A}_\theta\|$ can now be computed by

$$\|A_\theta\| = \int_{\theta'=0}^{\theta} \int_{r'=0}^{l_{max}(\theta')} r'\,dr'\,d\theta' = \int_{\theta'=0}^{\theta} \frac{1}{2} l_{max}^2(\theta')\,d\theta'\,, \tag{3.52}$$

The desired pdf $f_\Theta(\theta \mid r)$ is given by the derivate of $P(\Theta \leq \theta \mid r)$ with respect to θ, which gives

$$f_\Theta(\theta \mid r) = \frac{\partial}{\partial\theta} P(\Theta \leq \theta \mid r) = \frac{1}{a^2\pi}\,\frac{1}{2}\, l_{max}^2(\theta) \tag{3.53}$$

We can conclude with the following result.

Result. A node moves in a circular area of radius a according to the RWP model. At the beginning of each movement period, it chooses a new destination waypoint. The pdf of the direction Θ from the old waypoint (r, ϕ) toward the new waypoint is

$$f_\Theta(\theta \mid r) = \frac{1}{2\pi}\left(\frac{r}{a}\cos\theta + \sqrt{1 - \frac{r^2}{a^2}\sin^2\theta}\right)^2 \tag{3.54}$$

The plot of this pdf is shown in Figures 3.8 and 3.9 for various r. Let us briefly discuss this distribution. We can say that the above statements on the symmetry

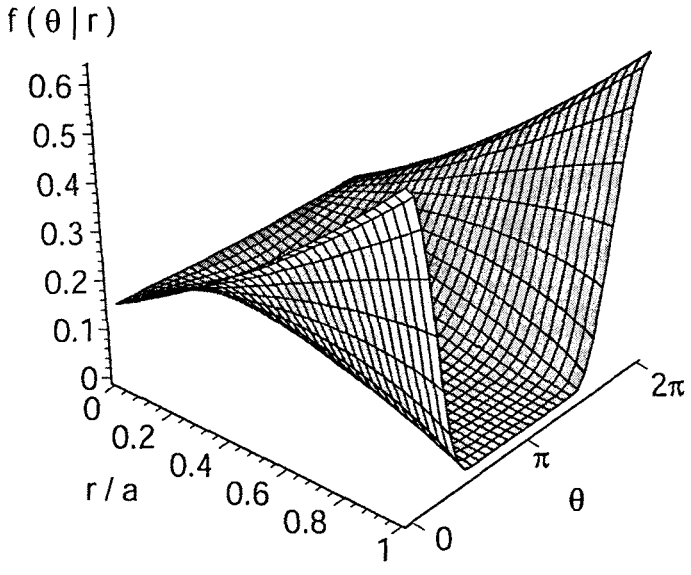

Figure 3.8: Distribution of movement direction

and maxima/minima hold. Furthermore, we observe that the function just depends on the ratio r/a. Nodes located at the border of the area, i.e., r close to a, have a high probability of taking θ around 0, i.e., they tend to move toward the center of the disk. In the extreme case $r \to a$, we have $f_\Theta(\theta \mid r) = 0$ for $\frac{\pi}{2} < \theta < \frac{3}{2}\pi$. This effect decreases as a node starts closer to the center of the disk, until a uniform direction distribution is achieved for $r = 0$.

As mentioned above, we now convert our result to the random variable Γ. This yields

$$f_\Gamma(\gamma \mid (r, \phi)) = f_\Theta(\gamma - \phi - \pi \mid r) \tag{3.55}$$

and

$$E\{\Gamma\} = \phi + \pi \tag{3.56}$$

Finally, we calculate from the conditional pdf $f_\Theta(\theta \mid r)$ the unconditional pdf $f_\Theta(\theta)$. This distribution informs us about the direction θ that a node chooses at an arbitrary waypoint, if we do not know the location of this waypoint. Weighting $f_\Theta(\theta \mid r)$ with the (uniform) spatial distribution of the waypoints and integrating

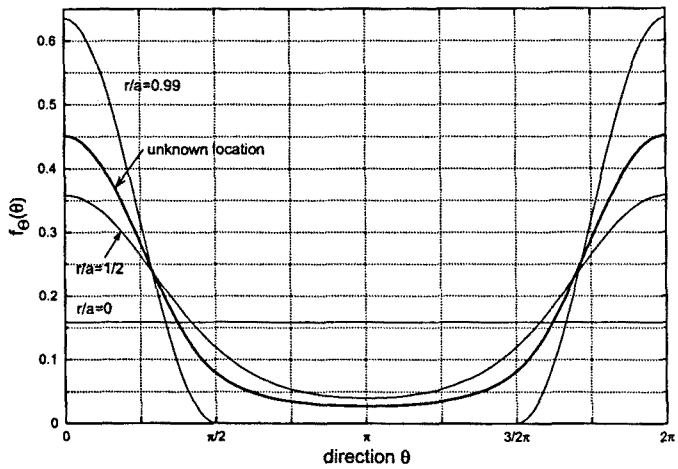

Figure 3.9: Distribution of movement direction

over all possible locations yields

$$f_\Theta(\theta) = \int_0^{2\pi} \int_0^a f_\Theta(\theta \,|\, r) \, \frac{1}{a^2\pi} \, r \, dr \, d\phi \tag{3.57}$$

$$= \frac{1}{4\pi \, |\sin^3 \theta|} \Big[|\sin\theta| \Big(-2\cos^4\theta - 2\cos^3\theta \, |\cos\theta| + \cos^2\theta + \cos\theta \, |\cos\theta| + 1 \Big) + \arcsin\left(|\sin\theta|\right) \cos\theta \Big]$$

The plot of $f_\Theta(\theta)$ is also shown in Figure 3.9. Clearly, the most frequent direction is $\Theta = 0$ while $\Theta = \pi$ is very unlikely. In fact, the probability that a node takes its direction within the interval $\left[\frac{\pi}{2}, \frac{3\pi}{2}\right]$ is only 12.5 %, whereas in 61.4 % of all movement transitions a node moves toward the central region of the area with $-\frac{\pi}{4} \leq \Theta \leq \frac{\pi}{4}$.

3.5 Cell Change Rate

We now regard RWP movements on a system area that is structured by a grid into a set of cells. We are then interested in the corresponding cell change rate of an RWP node, defined as the number of cell changes per unit time. There are two reasons for studying the cell change rate: first, our major motivation is that some network services in a mobile ad hoc network, like the Grid Location Service [60], assume that the system area shows a grid structure and nodes have to send some

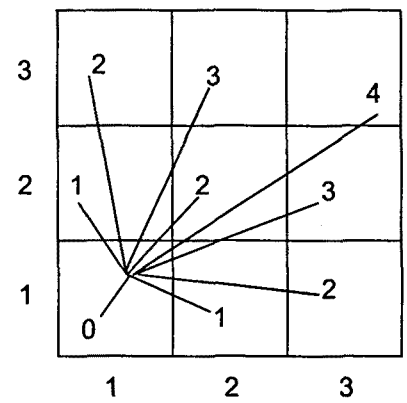

Figure 3.10: Cell changes per transition

signaling messages whenever they move from one cell to another one. A second reason is that the RWP model can also be applied to model a node's mobility behavior in a cellular network, e.g., in a wireless LAN system, where the cells represent the radio coverage of the base stations. In both scenarios, the amount of signaling traffic is related to the cell change rate.

For this analysis we consider a rectangular system area of size $a \times b$. This area is divided into $\alpha \times \beta$ rectangular cells of equal size. Figure 3.10 gives an example with $a = b$ and $\alpha = \beta = 3$. A cell change event occurs if a node crosses the boundary line between two cells. Clearly, the assumption of rectangular non–overlapping cells is an idealization for the second scenario described above. Real radio cells have various shapes and are overlapping. Moreover, the cell change rate depends, for example, on the handover decision and location update algorithm. However, since stating an expression that covers all the particular cases is not feasible, we study the simplest but most general case, the grid scenario.

3.5.1 Cell Changes per Transition

Our first aim is to analyze how many cell boundaries a node crosses on average during one movement transition. The corresponding random variable is denoted by C. By denoting c_i the outcome of this random variable in transition i, we can write

$$E\{C\} = \lim_{m\to\infty} \frac{1}{m} \sum_{i=1}^{m} c_i \tag{3.58}$$

The outcome of C is a deterministic function of the random starting waypoint $\mathbf{P}_1 = (P_{x1}, P_{y1})$ of a node and its next destination waypoint $\mathbf{P}_2 = (P_{x2}, P_{y2})$. In fact, in our grid structure, the number of cell changes depends only on the cell

positions of these two independent waypoints. In the following, the horizontal position of a cell is indexed by $\xi = 1, 2, \ldots, \alpha$ and its vertical position by $\psi = 1, 2, \ldots, \beta$. The cell position of a point can thus be written as (ξ, ψ). A point at (x, y) has cell position $\xi = \lceil \frac{x\alpha}{a} \rceil$ and $\psi = \lceil \frac{y\beta}{b} \rceil$, where $\lceil x \rceil$ denotes the ceiling function giving the smallest integer that is larger then or equal to x. If a node moves from a waypoint in cell (ξ_1, ψ_1) to a waypoint in cell (ξ_2, ψ_2), the number of cell changes is given by the Manhattan distance (l_1 norm) between the cells, i.e.,

$$c(\xi_1, \psi_1, \xi_2, \psi_2) = |\xi_1 - \xi_2| + |\psi_1 - \psi_2| \tag{3.59}$$

The expected value of C can then be computed by the average of $c(\xi_1, \psi_1, \xi_2, \psi_2)$ over all possible cell pairs:

$$E\{C\} = \frac{1}{\alpha^2\beta^2} \sum_{\xi_1=1}^{\alpha} \sum_{\psi_1=1}^{\beta} \sum_{\xi_2=1}^{\alpha} \sum_{\psi_2=1}^{\beta} c(\xi_1, \psi_1, \xi_2, \psi_2) \tag{3.60}$$

Example. We give a simple example for a scenario with 3×3 cells (see Fig. 3.10). A movement transition from cell $(1, 1)$ to $(1, 1)$ yields no cell change, a transition from $(1, 2)$ to $(1, 1)$ or vice versa yields $c = 1$ cell change, between $(2, 2)$ to $(1, 1)$ we obtain $c = 2$, and so on. Using Equation (3.59) in (3.60) with $\alpha = \beta = 3$ yields $E\{C\} = 1.778$ cell changes per transition.

Let us make some more comments on the above result. We observe that if we use the Manhattan distance $|\xi_1 - \xi_2| + |\psi_1 - \psi_2|$, the expected number of changes can be expressed as a sum $E\{C\} = E\{C_\xi\} + E\{C_\psi\}$, where $C_\xi = |\xi_1 - \xi_2|$ and $C_\psi = |\psi_1 - \psi_2|$ represent the number of horizontal or vertical cell changes, respectively. Moreover we note that an upper bound for $E\{C\}$ is given by $\frac{1}{3}(\alpha + \beta)$. For many cells, i.e., high α and β, this bound can be used as a good approximation for $E\{C\}$. In other words,

$$E\{C\} = \frac{1}{3}(\alpha + \beta) - \epsilon\,, \text{ with small } \epsilon > 0 \tag{3.61}$$

The relative error of this approximation, $\epsilon / E\{C\}$, is lower than $+1\,\%$ if $\alpha > 10 \wedge \beta > 10$, and it decreases for increasing α and β. In the asymptotic case, we have $\lim_{\alpha,\beta\to\infty} \epsilon = 0$.

Using the Manhattan distance metric, the movement of a node to a diagonally adjacent cell is always counted as two cell changes. We do this because the probability that such a movement transition goes directly through a single grid point goes to zero. Thus, the set of all transitions crossing a single grid point is a 'null set.'

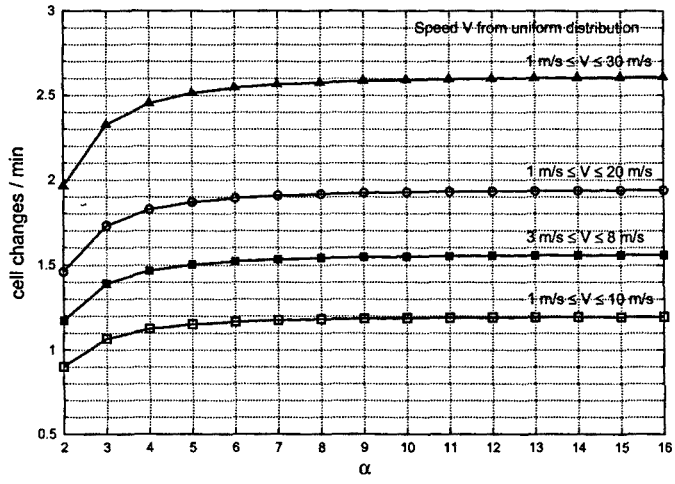

Figure 3.11: Expected cell change rate $E\{C_t\}$ on a square area of size $\|\mathcal{A}\| = 62500\,\alpha^2\,\mathrm{m}^2$. The number of cells is α^2. The length of one square cell is always 250 m.

3.5.2 Cell Change Rate

We are now interested in the average number of cell changes of an RWP node per unit time, denoted by $E\{C_t\}$. This value can be interpreted as the 'cell change rate' or 'cell change frequency' and serves as a good measure for the degree of mobility of a node or a certain scenario.

The expected number of cell changes per unit time is given by the sum of all cell changes that occur in a long run simulation divided by the entire simulation time. We can therefore apply our results from the number of cell changes per movement transition and the transition time (Section 3.2). We write:

$$E\{C_t\} = \lim_{m\to\infty} \frac{\sum_i^m C_i}{\sum_i^m T_i} = \frac{E\{C\}}{E\{T\}} \tag{3.62}$$

Example. An RWP node moves on a square system area $\mathcal{A}$ consisting of $\alpha \times \alpha$ cells, each cell with a side length of 250 m. In each waypoint it chooses a new speed V from a uniform distribution between v_{min} and v_{max}. There is no pause time in the destination points. We now investigate the cell change rate as the number of cells α^2 increases. Using $\alpha \times \alpha$ cells of fixed side length 250 m, the size of the system area is given by $\|\mathcal{A}\| = 62500\,\alpha^2\,\mathrm{m}^2$. Using $E\{C_t\} = E\{C\}/E\{T\}$ with (3.59,3.60) and (3.33), we computed the number of cell changes per minute for four different pairs of v_{min} and v_{max}. The result is shown in Figure 3.11.

For each speed distribution we obtain a different cell change rate. The dependency on the number of cells shows an asymptotic behavior for an increasing

system area: if α is small the cell change rate increases significantly, but if α is large enough it is almost independent on α and converges smoothly toward an asymptotic value. This is because for a large system area, the maximum number of cell crossings per transition is limited only by the speed of the node. The asymptotic cell change rate can be computed using (3.61) with $\epsilon = 0$. It represents a metric for the node mobility of a given scenario. For example, a node with a uniform speed distribution within $3 \ldots 8$ m/s has a higher cell change rate than a node with a uniform speed within $1 \ldots 10$ m/s, although both node types have the same average speed $E\{V\} = 5.5$ m/s.

3.6 Summary of Main Results

The random waypoint model is a commonly used mobility model for simulations of wireless communication networks. After giving a formal description of this model in terms of a discrete–time stochastic process, we investigated (a) the length and duration of a movement between two waypoints, (b) the resulting spatial node distribution and its dependence on the pause time, (c) the chosen direction angle at the beginning of a movement transition, and (d) the number of cell changes for an RWP model used in a cellular–structured network. These results give a deeper understanding on how this model behaves in simulation–based analysis of mobile wireless networks.

The results of our work (see [15,61–63]) are of practical value for performance analysis of mobile networks and give a deeper understanding of the behavior of this mobility model. Such understanding is necessary to avoid misinterpretation of simulation results. The movement duration and the cell change rate enable us to make a statement about the 'degree of mobility' of a certain simulation scenario. Knowledge of the spatial node distribution is essential for all investigations in which the relative location of the mobile nodes is important. Finally, the direction distribution explains in an analytical manner the effect that nodes tend to move back to the middle of the system area. Such a mobility metric is needed if we want to compare simulation results made with the RWP model and a different model and to identify the influence of mobility on simulation results. The knowledge of the spatial node distribution is essential for simulation–based investigations on interference between nodes, medium access control, and connectivity issues, to name a few.

The methods employed in our work can also be applied to other models, in order to derive appropriate measures describing stochastic mobility in a precise and meaningful manner.

Chapter 4

IP-based UMTS Radio Access Networks

The Universal Mobile Telephony System (UMTS), which has been specifically thought to support mobile multimedia communications, is being slowly introduced in parallel to the available second generation cellular networks to become, in the near future, the replacement of current cellular systems. UMTS has been standardized and developed with the main objectives of improving the multimedia transmission quality while guaranteeing broadband communications and allowing users ubiquitous access.

The UMTS architecture is composed of a set of logical components, each with its specific functionalities, that are divided in the following way: Core Network (CN), which is responsible for connection switching and routing toward external systems; UMTS Terrestrial Radio Access Network (UTRAN), which manages the functionality related to the handling of the air interface; and User Equipment (UE), which is a logical component in charge of interfacing the multimedia user to the UTRAN. The UTRAN is composed of a set of radio network subsystems (RNSs) which in turn are composed of a controller element, the Radio Network Controller (RNC), and many radio base stations (Node-Bs). The Node-Bs are in charge of physical layer functions across the air interface (channel coding, interleaving, spreading, etc.) as well as basic functions of radio resource control, such as the closed-loop power control functionality. The RNC is the element responsible for UTRAN radio resource management and is interfaced to the switching infrastructure on one side and to many Node-Bs on the other.

At the end of 1999, 3GPP (Third Generation Partnership Project) started working toward an All-IP architecture. The architecture evolution was driven by two main objectives: independence of the transport and control layer to ease the implementation of new applications up to the mobile terminal and operation and maintenance optimization for the access network. During the transition from 3G

to All-IP systems, the UTRAN and CN should evolve toward the IP transport solution as an alternative to the original asynchronous transfer mode (ATM) transport. The substitution of the ATM transport in the UTRAN by IP (IP-RAN) has already been proposed and specified by 3GPP for Release 5 [64], Figure 4.1 depicts the IP-RAN architecture. However, this substitution raises several issues in order to make an efficient use of the network that have not been solved yet by 3GPP:

1. The protocol overhead increases significantly when IP transport is considered as compared to ATM. Mechanisms to improve the IP transport efficiency have to be engineered to guarantee the feasibility of UMTS IP-based radio access networks.

2. Due to the 'best effort' nature of IP, the actual level of QoS the network is able to guarantee to applications is uncertain. Methods to guarantee QoS differentiation are required to fulfill applications' requirements

Even though the problem of properly supporting IP in the RAN is a recent topic, it has already received some attention in the literature. 3GPP standardization has started discussions on the convenience of adopting IP-RAN as can be observed for instance in the technical report [65]. A study comparing the efficiency of ATM and IP transport was done by the MWIF (Mobile Wireless Internet Forum) and can be found in [66]. Venken et al. [67, 68] have identified the need for admission control for voice traffic in IP-RAN. Finally, Kasera et al. [69] have proposed an admission control scheme for IP-RAN.

In the following sections we describe our proposed solutions to alleviate the aforementioned unefficiencies. We present first a solution to reduce the protocol overhead introduced in the air interface due to VoIP. Then, a multiplexing scheme that improves the efficiency of the transport between the RNC and the Node-Bs is described and evaluated. In Section 4.3 we propose a scheduling mechanism adapted to the UMTS radio access network transport requirements and application needs. Finally, a summary of the main results is provided.

4.1 Configuration of a VoIP Radio Acess Bearer

3GPP has defined the concept of Radio Access Bearer (RAB) as a user plane connection provided by the UMTS Terrestrial Radio Access Network (UTRAN) between a User Equipment (UE) and the Core Network. The general characteristics of a RAB (data rates, QoS, etc.) are normally set by the Core Network (CN) based on subscription and/or requirements of the media or set of medias using the RAB. The actual configuration for a RAB is decided by UTRAN based on the RAB information received from the CN.

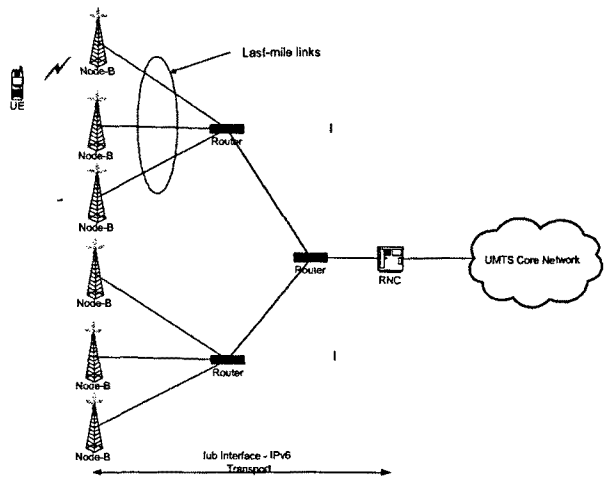

Figure 4.1: IP-RAN architecure

The RAB configuration has a direct impact on network resource usage. The more suited the RAB configuration is to the actual pattern of the data being transferred, the more efficient the RAB is in terms of usage of network resources. Choosing proper RAB configurations is key to UTRAN, given the high cost of last-mile transport (Iub interface) and the rather limited radio resources.

Between the RNC and the UE data is always transferred inside frames which length is within a set of allowed frame sizes. The set of allowed frame sizes is configured when the RAB is setup but, for complexity reasons, the size of the set has to be small. In general, no packet switched reference RAB has a set size larger than three. This is, the RAB has three allowed sizes (e.g. 200 bits, 400 bits and 600 bits). In simplified terms, when data is to be transferred, an appropriate frame size is selected and padding bits are added, if needed, to fill the remaining bits of the frame.

The RAB bandwidth determines the QoS received by the application, and the set of allowed frame sizes for the RAB determines the amount of bandwidth wasted for padding. Given a certain application, it is crucial to define its RAB well adjusted to its requirements; too small bandwidth will result in a bad quality, while too large bandwidth or improper frame sizes will result in a waste of resources.

From the above it follows that a RAB design optimized for VoIP is an important issue in UMTS networks. The fact that VoIP traffic sends at a variable bit rate, may include control traffic like e.g. RTCP and, if Robust Header Compression (RoHC) is used, headers have a variable size, makes the definition of the optimal RAB a challenging task. While 3GPP has already defined a reference

RAB for VoIP support [70], this RAB provides no optimized handling of VoIP traffic.

In our work we focused on the search for an optimized RAB for VoIP as one of the main RABs that will determine the efficiency of IP-based UTRANs.

4.1.1 Radio Access Bearer Description

The transmission of data within a RAB in UMTS works as follows. Data (namely IP packets) generated by an application at the UE is stored in an internal buffer. This buffer is emptied periodically, every Transmission Time Interval (TTI), when a radio frame is created with the data stored at the buffer up to a certain maximum frame size (MFS). The RAB bandwidth corresponds to MFS/TTI. In this document we take TTI equal to 20 ms which is a commonly used value in current implementations.

In case the amount of data in the buffer is less than MFS, a frame of size smaller than MFS may be created. However, only a few frame sizes are allowed, so that we need to fill the frame with padding up to the next frame size allowed.

Once the frame has been created as described above, it is transported through the air interface to the Node B, where an IP packet containing the frame is created[1]. The IP packet is then transported through the Radio Access Network (RAN) to the RNC. The last-mile link in the RAN is commonly E1 on leased lines or microwave links.

The RNC terminates the radio protocol; it extracts the radio frames from the IP transport packets, and the data from these frames, discarding the padding, and transmits the resulting data (which are IP packets) further into the Core Network (CN). The UMTS architecture and protocol stack are illustrated in Fig. 4.2.

A reference RAB for VoIP is defined by 3GPP in [70], which defines a RAB bandwidth of 46 Kbps and frame sizes of 920, 304 and 96 bits. As we will see later on with our simulation results, the proposed RAB is not optimized for VoIP with or without RoHC but rather tries to cover both cases.

4.1.2 Simulator Description

In order to evaluate performance of VoIP depending on the RAB configuration we have developed our own simulator. Ours is an event-driven simulator, written in the C++ programming language, that closely simulates the frame creation, buffering and transmission at the UE, and all the aspects involved with it, that have an

[1]According to 3GPP specifications, the Radio Access Network (RAN) may be based on IP or ATM transport [65]; throughout this document we focus in IP transport since we argue that it is better suited for supporting a mix of traffic types, allows for economy of scale and that having an All-IP network saves management and operational costs.

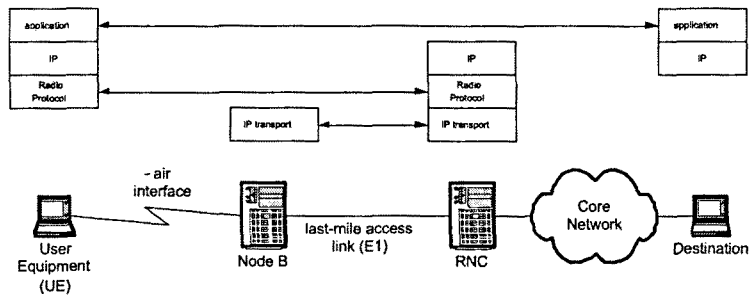

Figure 4.2: UMTS Architecture (air interface and radio access network)

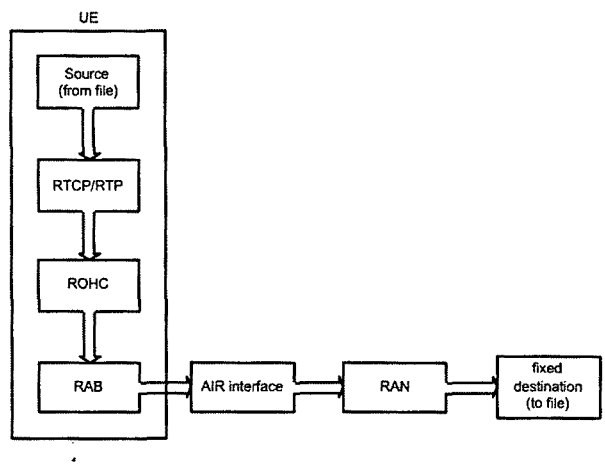

Figure 4.3: Simulator modules

impact on the appropriate RAB configuration. We focus in the upstream part because it is where the packets to be transmitted over the RAB are created. The configuration for the upstream case will also apply to the downstream case since the packets to be sent over the RAB are the ones received from the upstream part. Fig. 4.3 depicts the modules of which the simulator consists; in the following we describe them in detail.

Source Model

Voice sources are modeled according to real-life audio clips obtained from the 3GPP web site [71]. We extract the frame arrival times and sizes from these clips, which are written into a file and then used as input into our simulator. The specific audio clip that we have used in this experiment corresponds to a 12.2 Kbps AMR codec audio clip of about 20 seconds with active and idle periods. Each speech frame is encapsulated into an RTP/UDP/IPv6 packet. Overhead includes the IPv6

header (40 bytes), the UDP header (8 bytes), the RTP header (12 bytes), the profile (1 byte) and the PDCP (1 byte).

RTCP Model

In addition to the speech frames, Real-Time Control Protocol (RTCP) packets are also sent periodically by the UE. In the simulation results we present in this document, we have considered two different scenarios for RTCP, average and worst-case, depending on the size and inter-arrival times of RTCP packets.

Average RTCP

With average RTCP we consider a payload size of 60 bytes, which roughly matches the size of an RTCP packet with a useful CNAME tag and a Receiver Report[2].

[73] specifies that the maximum rate at which RTCP packets may be sent is of one packet every 5 seconds. This is the RTCP inter-arrival time that we have taken in our average RTCP scenario.

Worst-case RTCP

From [73] we have that the bandwidth used by RTCP should be limited to 2.5% of the total bandwidth. Assuming an AMR RTP payload of 32 bytes [74], which produces a total sending rate of 36900 bps, and an RTCP inter-arrival time of 5 seconds, this gives the following RTCP packet size:

$$S_{RTCP} = 5 \cdot 0.025 \cdot 36900 \approx 4600 \text{ bits} \tag{4.1}$$

We have taken the above in our worst-case RTCP scenario[3].

RoHC Model

In our simulator we assume the Birectional Optimistic mode of RoHC [76] and emulate its behavior by means of a simplified state machine. We consider the compressed header sizes shown in Table 4.1 for a large CID of one byte; optional ACKs are not sent, in order to avoid additional overhead. Fig. 4.4 illustrates the compressor and decompressor state-machine, which we detail in the following.

[2]For example, in [72] (section 3.4), it is mentioned that a typical RTCP packet size is 90 bytes, which taking out the IPv4/UDP header leaves us with this 60 byte payload, approximately.

[3]Note that [75] gives as maximum payload size 130 bytes, but states that this may change with the RTCP packet size.

Header Name	Header Function	Header Size [bytes]
IR	Initialization/Refresh	60
IR_DYN	Partial context update	21
UOR2-ID	Compressed header	6
UO1-ID	Compressed header	5
UO0	Compressed header	4

Table 4.1: RoHC header sizes

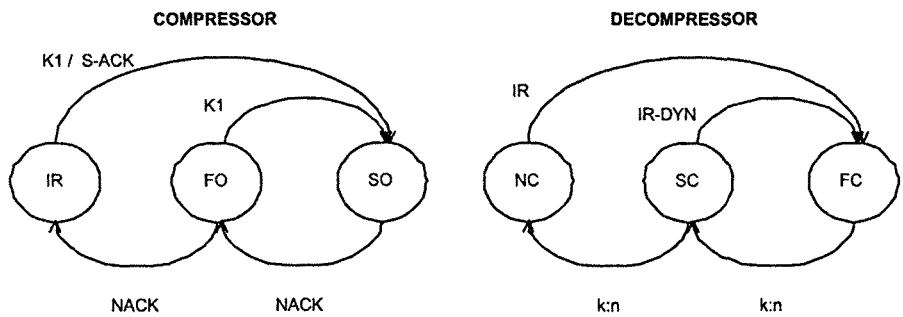

Figure 4.4: Compressor and decompressor state-machine

Compressor

The compressor adds the IR header size to the payload while in the IR (Initialization/Refresh) state, the IR-DYN size while in the FO (First Order) state and the average size of the UOR2-ID, UO1-ID and UO0 while in the SO (Second Order) state.

The transition from the IR to the SO state is performed when a fixed amount of IR headers, K1 (which we take equal to 3), has been sent, such that we can safely assume that the decompressor is in the FC (Full Context) state or when a S-ACK has been received.

The transition from the FO to the SO state is performed when a fixed amount of IR-DYN headers, also K1, has been sent, such that we can safely assume that the decompressor is in the FC.

The transition from the SO to the FO state or from the FO to the IR state is performed when a NACK from the decompressor is received.

Decompressor

The transition from the NC (No Context) to the FC state is performed when an IR header is received and produces a S-ACK feedback message to the compressor.

The transition from the SC (Static Context) to the FC state is performed when an IR-DYN header is received; no feedback message is sent.

The transition from the FC to the SC state or from the SC to the NC state is performed when k packets out of n (we take 3:6) are received with errors, resulting in a NACK feedback message.

We do not consider the impact of packet drops onto the state machine in our model, since the probability of a burst of drops large enough to cause a sequence number wraparound is negligible.

Errors introduced by the air interface into the (possibly compressed) header result, considering a 3 bits CRC, in a detected error with probability 7/8, which leads to an increase in the k counter, and in an undetected error with probability 1/8. As explained above, after 3 detected errors, a NACK is sent.

When errors are detected we assume that RoHC will be able to repair k out of n, i.e., the audio quality will not be harmed. On the other hand, when the errors are not detected they will not be repaired resulting in a packet drop, since a packet with an incorrect header will not reach its destination.

Feedback

The RoHC feedback messages experience the same delay as the data packets from the UE to the UPS, i.e., no immediate feedback is assumed. A medium free of errors is assumed for the feedback path.

Radio Access Bearer (RAB)

The RAB module in our simulator works according to the explanation given in Section 5.5. The various RAB parameters are configurable in the simulator, so that we can sweep along the parameter space in the search for the optimal configuration.

Air interface

The ARROWS IST project [77] shows that there is no correlation between errors in different TTI's [78], as

- For vehicle speeds above 13 km/h the coherence time is lower than 10 ms, so there is no correlation between consecutive TTI's.
- Below 13 km/h the power control, updated 1500 times/s, will cancel fast fading and shadowing fading, so the Eb/N0 will remain approximately constant.

The above leads to independence among errors at different TTI's. Based on [79], we consider packet error rates of 10^{-2} and 10^{-3}. We consider that an erroneous packet with header of size H and payload of size S has its error in the header with probability $\frac{H}{S+H}$ and in the payload with probability $\frac{S}{S+H}$. In the former case, the error impacts the RoHC, while in the latter it impacts the resulting audio quality.

Radio Access Network (RAN)

In order to model the RAN behavior, we have used the OPNET simulator [80], which includes a UMTS module, to simulate two scenarios where the RNC is connected to a Node B through an E1 link. The first scenario consists of a few UEs and therefore no congestion, while the second one increases the number of UEs to create congestion. From each simulation we have taken the delays and drops suffered by a sequence of packets. Then, we have treated the packets in our simulator according to this sequence, i.e., we drop or introduce a certain delay to packet i in our simulator according to the behavior experienced by packet i of the recorded sequence. The average drop rate for the congested sequence is of about 4%; for the uncongested sequence there are no drops.

Destination Playback time

We assume audio and video playback applications, which are intolerant to packets arriving later than their playback time [81]. Therefore, we drop packets that arrive later than this time. The playback time represents the maximum delay that can be supported between the creation of a frame in its source and the moment when it is played in the destination, and is a configurable value.

4.1.3 Performance Evaluation & Discussion

In order to identify the optimal RAB configuration, we conducted a series of simulation experiments sweeping along the configuration parameters. In this section we describe the results obtained for the no RoHC and RoHC cases. In each case, we consider the scenarios shown in Table 4.7.

No RoHC

Fig. 4.5 shows the drop rate experienced by the VoIP application in the no RoHC case as a function of the RAB bandwidth for the five scenarios described above. By drop rate we count the frames dropped at the IP-RAN, the frames resulting

Scenario	frame error rate at the air interface	congestion at the RAN	RTCP	playback time
Ideal conditions	10^{-3}	no	no	100 ms
Ideal conditions + average RTCP	10^{-3}	no	average	100 ms
Bad conditions + average RTCP	10^{-2}	yes	average	100 ms
Bad conditions + worst-case RTCP	10^{-2}	yes	worst-case	100 ms
Bad conditions + worst-case RTCP + PB = 50 ms	10^{-2}	yes	worst-case	50 ms

Table 4.2: Simulation scenarios

with errors in the air interface and the frames that arrive at the destination later than the playback time.

From the figure it can be seen how the drop rate decreases with an increase in the RAB bandwidth. As long as RTCP is not worst-case, the smallest possible drop rate is already achieved with a RAB of 40.000 bps, and a larger bandwidth does not further decrease the resulting drop rate.

Based on the above, we propose a RAB of 45.000 bps, i.e., the 40.000 bps plus some additional safeguard. We argue that provisioning the RAB bandwidth taking into account the worst-case RTCP would require a very large bandwidth and lead to an inefficient use of this bandwidth in most cases.

One additional recommendation from our results is that special care must be taken by the application developers in the design of RTCP. In fact, our results show that the worst-case RTCP allowed by the standards produces a quite large additional packet drops with our recommended bandwidth. This drop rate is specially harmful for the perceived QoS, as drops occur in bursts at the instants when long RTCP messages are sent.

The remaining configurable parameters are the allowed frame sizes. Frame sizes adjusted to the payloads will result in smaller frames, and therefore smaller IP packets in the RAN, so that less bandwidth will be used by them in the expensive last-mile links.

In order to understand the payload distribution resulting from the different scenarios, we study the histogram of payloads in the no RTCP, average RTCP and worst-case RTCP cases[4], when the RAB bandwidth is of 40.000 bps. This is illustrated by Fig. 4.6 (even though not appreciated in the graph due to scale

[4]In our scenarios, the payload size distribution turned out to be mainly dependent of RTCP.

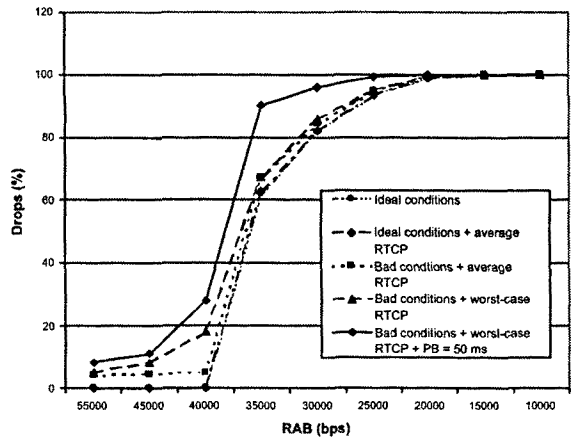

Figure 4.5: No RoHC: Packet drops vs. bandwidth

problems, all sizes that appear in the y-axiscontain at least one frame for one of the cases).

From the figure, it can be seen that the most frequent payloads are 900, 760 and 552, the last two corresponding to the size of an active and an idle frame, respectively. The maximum payload size (900) is used when the data to be transmitted does not fit into one frame, due to some additional load caused e.g., by an RTCP. In such case one, or more maximum payload frames may occur, plus possibly one transition frame of intermediate size.

In Fig. 4.7 we study the bandwidth consumed in the RAN as a result of using one frame size (900), two (900, 760), three (900, 760 and 552) and four (900, 760, 552 and 880). It can be observed that significant savings are achieved when using up to three frame sizes, and that using a fourth one produces no further gain. As a consequence, our proposal for the allowed frame sizes in the optimal RAB for RoHC is of 900, 760 and 552 bits.

RoHC

We repeated the above experiments when RoHC is used. Fig. 4.8 illustrates the drop rate as a function of the bandwidth; following the same reasoning as in the previous case, we propose a RAB bandwidth of 25.000 bps for the RoHC case.

Fig. 4.9 depicts the payload size histogram when the RAB bandwidth is set equal to 25.000 bps. It can be observed from the distribution that the more frequent payload sizes are 500, 304 and 96 bits.

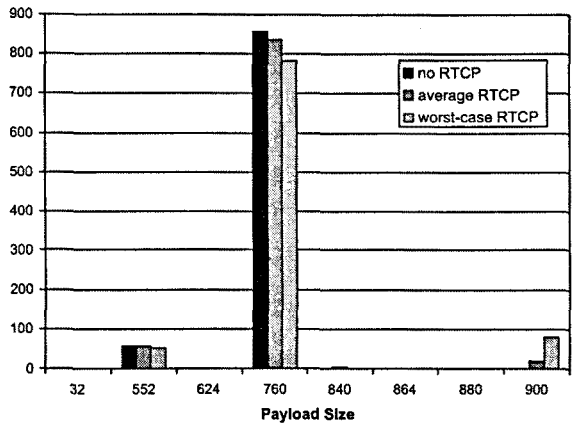

Figure 4.6: No RoHC: Packet distribution

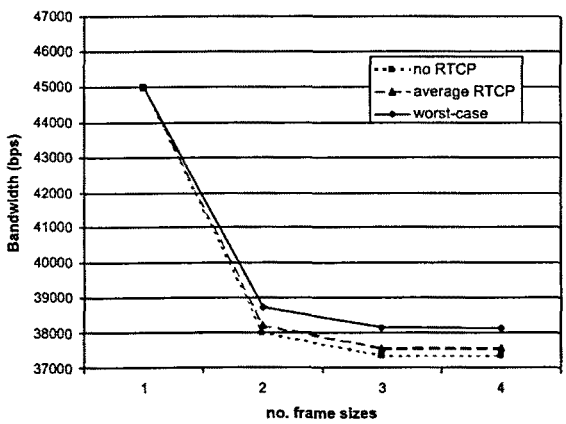

Figure 4.7: No RoHC: RAN bandwidth consumption

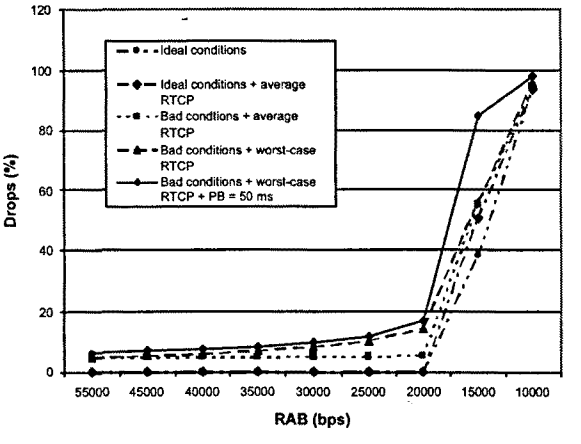

Figure 4.8: RoHC: Packet drops vs. bandwidth

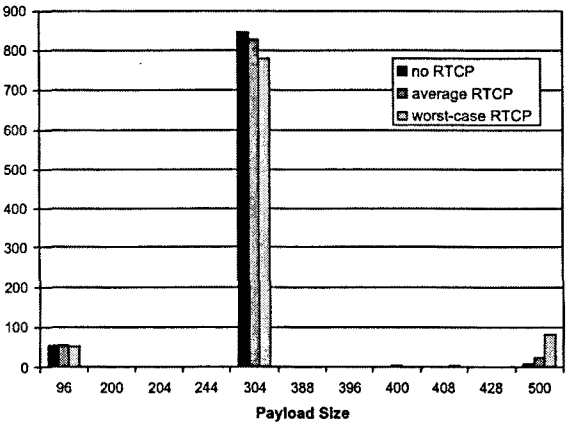

Figure 4.9: RoHC: Packet distribution

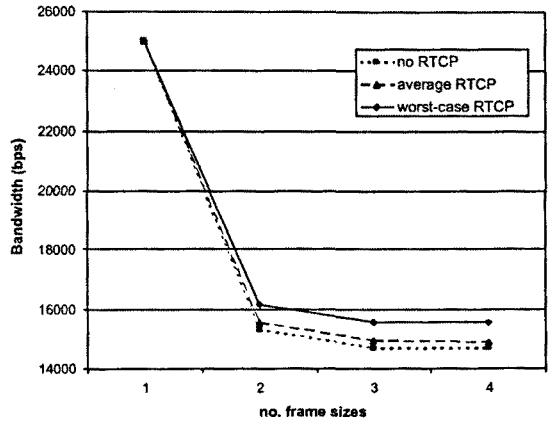

Figure 4.10: RoHC: RAN bandwidth consumption

Fig. 4.10 illustrates the bandwidth consumption at the RAN when one frame size is allowed (500 bits), two (500 and 304), three (500, 304 and 96) and four (500, 304, 96 and 428). Results show that there is no gain when using more than three frame sizes; therefore, our proposal for the allowed frame sizes is 500, 304 and 96 bits.

Finally, we note that the RAN bandwidth consumption in the RoHC case is of about half of the bandwidth consumption when no RoHC is used. We conclude that the bandwidth savings when using RoHC is of about 50%, both in the air interface and in the RAN.

4.1.4 Summary

VoIP is targeted as one of the key applications for future UMTS cellular networks. To efficiently support this type of traffic, the bandwidth consumption at the air interface and last-mile links, which commonly are the most expensive parts of the network for operators, have to be minimized while ensuring a sufficient QoS.

In order to achieve the above goal, it is fundamental to define optimized RABs for VoIP support. In our work we studied this issue: we developed a simulator and simulated a range of RAB configurations; as a result, we propose two RAB configurations for VoIP (one with RoHC and one without).

For the case without RoHC, we propose a RAB bandwidth of 45.000 bps and frame sizes of 900, 760 and 552 bits. For the case with RoHC, we propose a RAB bandwidth of 25.000 bps and frame sizes of 500, 304 and 96 bits. The resulting bandwidth consumption at the RAN is of about 30.000 and 15.000 bps,

respectively.

It follows from the above that the gain of using RoHC is of about 50%, both in the air interface and the RAN. The gain of our proposed RAB adapted for RoHC is also about 50% with respect to the reference VoIP RAB defined by 3GPP, which recommends a RAB bandwidth of 46.000 bps.

4.2 IP Overhead in the Radio Access Network

In this section we study the protocol overhead introduced in the Radio Access Network (RAN) when IP transport is used and evaluate possible optimizations for its reduction.

Nowadays, the predominant traffic in current cellular networks is voice traffic. The evolution of UMTS networks toward IP transport introduces the possibility of migrating current circuit-switched voice calls to the packet-switched domain using Voice over IP (VoIP). However, in an IP-based UTRAN, the overhead required to transmit each single VoIP packet largely exceeds the actual information carried per packet resulting in an unefficient use of the scarce networks resources specially in the wireless medimum and in the last-mile links. Table 4.3 shows the amount of payload generated by an AMR codec at the data rate 12.2 kbps and the required overhead to transmit this payload in the UTRAN. Note that link layer and physical layer overhead has been omitted.

Full header case	bits
AMR Payload	244
AMR Frame Overhead	19
RTP AMR profile	10
RTP	96
UDP	64
IPv6	320
UDP	64
IPv6	320

Table 4.3: VoIP payload versus overhead in the full header case.

To reduce part of this overhead, as we have seen in the previous section, header compression schemes can be considered. Robust Header Compression (RoHC), which has been specially designed for the case of wireless links, can compress the RTP, UDP and IPv6 headers together. In [82] a performance study of the header reduction achieved by RoHC was done reporting an average size for the

compressed header of 6 bytes. Table 4.4 shows the resulting overhead when RoHC is considered.

RoHC header case	bits
AMR Payload	244
AMR Frame Overhead	19
RoHC(RTP/UDP/IPv6)	48
UDP	64
IPv6	320

Table 4.4: VoIP payload versus overhead in the RoHC header case.

The RoHC solution solves the first part of the problem corresponding to the reduction of the overhead in the air interface. Unfortunately, since we can not assume neither direct links from the Node-Bs to the RNC nor RoHC-capable IP routers in the path, we can not apply the same mechanism to reduce the overhead introduced by the IP transport in the UTRAN. This problem has already been studied in the literature resulting in similar solutions [64,66,83,84]. The proposed solutions reduce the IP transport overhead by multiplexing several packets from different connections into a single packet. A multiplexed packet, in contrast to a packet with a compressed header, is an ordinary IP packet and can be transparently routed through the Internet.

The Mobile Wireless Internet Forum studied this issue in [66] were different parties proposed several multiplexing schemes and evaluated their performance. The results of this study have been introduced in a 3GPP technical report as possible solution [64] but no recommendation is given. As a result, it can not be guaranteed that UTRAN equipment from different vendors will be compatible when a multiplexing scheme is used if different mechanisms are chosen. A multiplexing scheme based in PPP multiplexing is presented in [83]. The advantage of this scheme as compared to the ones proposed in [66] is that it is based in a standardized solution [84].

Figure 4.11 depicts the protocol stack proposed to be used for the multiplexing case which is like the one presented in [83] with the difference that no compression is considered for L2TP and UDP since no standard solution is available and no multiclass multiplexing is used due to their different QoS requirements. The overheads required by this solution for the AMR VoIP case are detailed in table 4.5 where N refers to the number of voice packets being multiplexed.

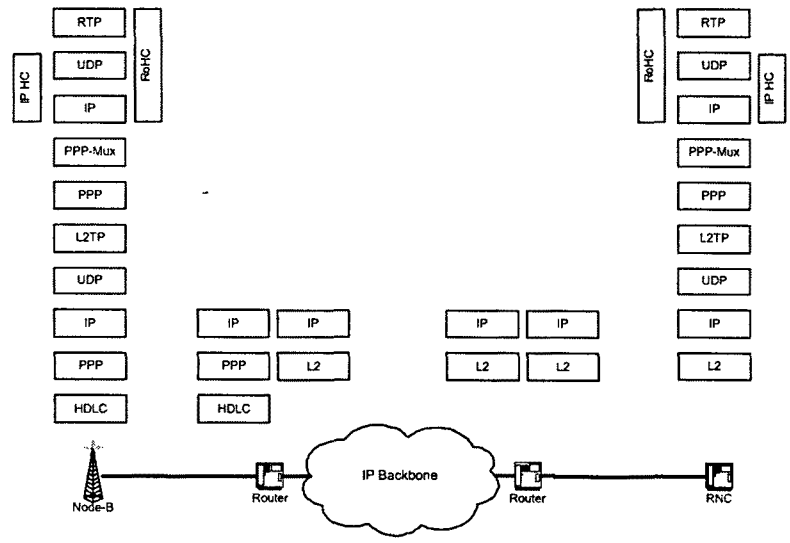

Figure 4.11: Protocol stack for the multiplexing scheme

4.2.1 Simulation Scenario

The scenario chosen for the analysis of the overhead gains is similar to the one depicted in figure 4.1. It consists of a variable number of UEs uniformly distributed along the coverage area of 5 NodeBs and of an RNC connected to the Node-Bs through a bottleneck link. The bottleneck link is emulated as one E1 link (2048 kbps capacity).

Since voice is currently the predominant application in wireless networks and is supposed to be the main application generating traffic in 3G networks in the near future, we consider three different scenarios were the mix of VoIP traffic with other multimedia traffic increases progressively. The first scenario considers VoIP traffic only representing 'current' cellular networks were almost all traffic is voice. Then, a 'Mid-term' scenario is considered where multimedia users represent 20% of the total number of users and the other 80% are VoIP users. Finally, a 'Long-term' scenario is studied where the number of VoIP users and of other multimedia traffic are equal, i.e., 50% each group.

Since UMTS defines four different types of classes depending on their QoS requirements [85], see Table 4.6, we divided the multimedia users generating traffic different than VoIP as shown in Table 4.7. Background traffic was selected as the most significant after Conversational (VoIP) because of the wide spread e-mail usage.

In the following we describe the characteristics of the traffic generated by each different class:

PPP multiplexing case	bits
N × AMR Payload	244
N × AMR Frame Overhead	19
N × RoHC(RTP/UDP/IPv6)	48
PPPmux	32
PPP	16
L2TP	96
UDP	64
IPv6	320

Table 4.5: VoIP payload versus overhead in the PPP multiplexing case.

Traffic Class	Conversational	Streaming	Interactive	Background
Error tolerant	Voice and Video	Video and Audio	E-commerce	Fax
Error intolerant	Telnet, Games	Still Image	Web Browsing	E-mail

Table 4.6: UMTS Traffic Classes.

- *Conversational* AMR [74] is the chosen voice codec for VoIP for future IP-based UMTS networks [64]. We modeled the AMR VoIP traffic generated by a UE as a Markov chain where a VoIP source during a call session can be in the ON or OFF state, generating a rate of 12.2 kbps or 1.8 kbps, respectively. The permanence time in the ON and OFF state is 3 seconds.
- *Streaming* MPEG-4 streaming of the movie Jurassic Park (average rate 35 kbps, frames generated every 40ms [20]).
- *Interactive* Web traffic, page interarrival time exponentially distributed with mean 60 seconds and an average page size of 7250 bytes.
- *Background* Short FTP downloads, inter-request time exponentially distributed with a mean of 10s, file size exponentially distributed with a mean of 10 kbytes.

The performance metric of interest to determine the gain achieved by using RoHC or the multiplexing mechanism is the maximum throughput observed in the bottleneck link of 2048 Kbits capacity. Additionally, since the multiplexing scheme increases the delay for transmitting a packet we computed the average increase in the delay experienced by VoIP packets which are the ones with the most stringent delay requirements as an indication of the 'cost' of this mechanism. In our study we have focused in the downlink direction (RNC to UEs) as the most relevant case for studying the achievable gain in the number of users since, except

Traffic Class	Conversational	Streaming	Interactive	Background
Current	100%	0%	0%	0%
Mid-term	80%	5%	5%	10%
Long-term	50%	10%	10%	30%

Table 4.7: Distribution of the number of users of each QoS class used on each scenario.

for the case of VoIP only, usually users tend to 'download' more information from the network than to 'upload' it.

The multiplexing is performed at the RNC as depicted in Figure 4.12. When data packets arrive to the multiplexing module, they are classified depending on their traffic class and inserted in their corresponding multiplexing buffer. Then containers of each traffic class are filled and sent with the corresponding data when either the maximum size threshold or the timeout threshold is triggered. For this experiment we have set the maximum size threshold for all classes to 12000 bits and the timeout threshold to 10ms. These values have been chosen considering the maximum ethernet MTU size (12000 bits) and the usual timing requirements (20ms) for the transmission between the RNC and the Node-Bs (Iub interface). The Iub interface requirements will be explained in Section 4.3.1. The proper selection of the values of these two thresholds determine the maximum achievable multiplexing gain and also the delay introduced by the multiplexing module. We did not evaluate the performance differences when considering different threshold values since the aim of our work was to determine whether such a mechanism would be useful to reduce the overhead using 'reasonable' threshold configurations rather than finding the 'optimal' configuration parameters which would depend on the scenario considered.

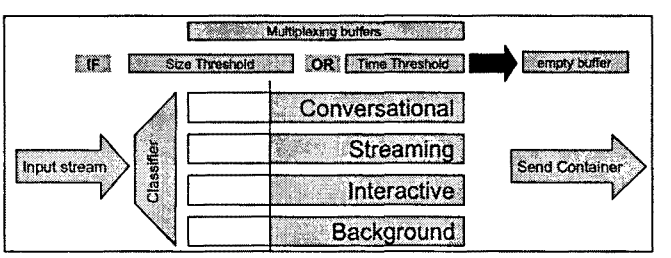

Figure 4.12: Multiplexing scheme applied at the RNC (downlink) or Node-Bs (uplink)

4.2.2 Performance Evaluation & Discussion

In this section, we evaluate via simulation the performance improvement that results from implementing the described RoHC and multiplexing scheme. The results have been obtained using the OPNET [80] simulator in the scenario already described. The simulations required to modify the UMTS R'99 elements provided by OPNET in order to emulate the IP-RAN architecture previously described, e.g., substitution of ATM transport by IP, and to include the RoHC[5] and multiplexing mechanisms.

VoIP users only scenario

Figure 4.13 depicts the results with respect to the maximum observed throughput in the bottleneck link for the case of VoIP users only for each of the three cases: full header, RoHC and RoHC plus multiplexing. As expected, when the number of UEs increases, the usage of RoHC and of the multiplexing scheme plus RoHC allows for a much larger number of UEs using the bottleneck link before it gets congested. The gain in the number of UEs that can be accepted with respect to the full header case considering the bottleneck link capacity is around 80% for RoHC and about 260% for the multiplexing plus RoHC case.

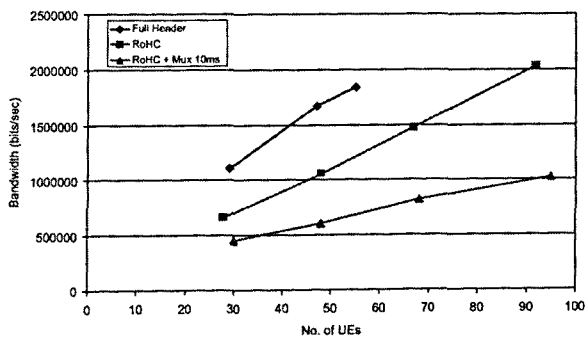

Figure 4.13: VoIP only case, Maximum downlink bandwidth

On the other hand, Figure 4.14 shows that the significant overhead gain of the multiplexing comes at the cost of additional delay at the Iub interface. RoHC represents an intermediate case where the overhead reduction is not as significant as when using multiplexing but it does not introduce additional delay and actually presents better results than the full header case due to the smaller size of the packets. Note that in the RoHC plus multiplexing case even though the average delay

[5]In the RoHC case the model considers the resulting average header size.

value starts from a large value due to the multiplexing time, the slope increases slower according to an increasing number of UEs.

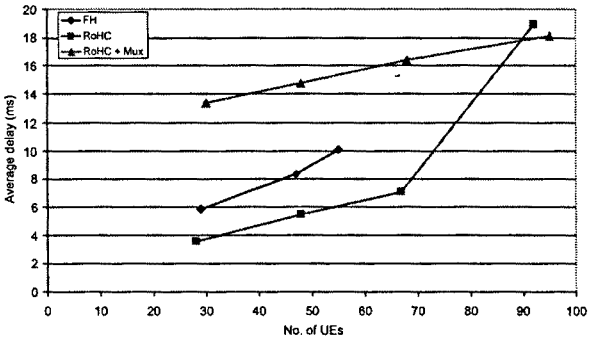

Figure 4.14: VoIP only case, Average downlink delay

Mid-term scenario

For the mid-term scenario, Figure 4.15, results similar to the ones obtained for the VoIP only case are observed, i.e., 80% gain in bandwidth utilization as compared to the full header case. However, the gain for the RoHC plus multiplexing scheme presents worse results as compared to the previous scenario, 140% gain instead of 260%. The reason for this worse performance is that now the traffic is not all of the same class and therefore the probability of sending multiplexed packets with a smaller payload is higher resulting in a larger overhead.

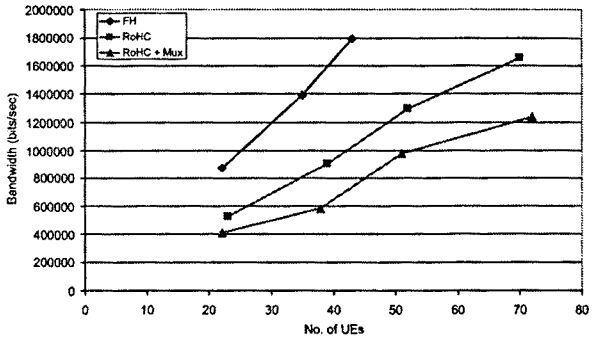

Figure 4.15: 80%-20% case, Maximum downlink bandwidth

The results for the average downlink delay match the bandwidth ones as can

be observed in Figure 4.16. The reasons for the differences in the delay values are the same as the ones of the previous scenario.

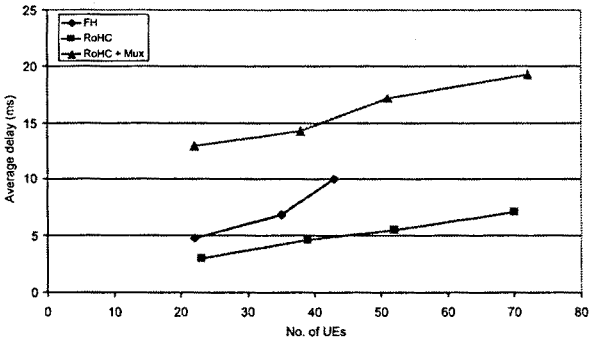

Figure 4.16: 80%-20% case, Average downlink delay

Long-term scenario

In the long-term scenario the gains get further reduced with respect to the bandwidth utilization, see Figure 4.17. RoHC advantages diminish (50% instead of 80%) because the payload of the packets of classes different than conversational are larger yielding a better ratio payload/overhead. The RoHC plus multiplexing scheme benefits are lower also because of the higher probability of sending multiplexed packets of a smaller payload, around 100% gain instead of 140%.

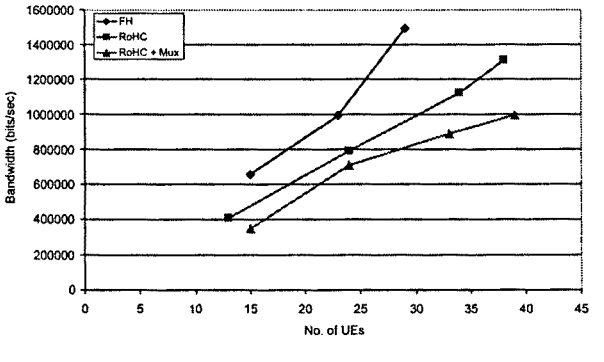

Figure 4.17: 50%-50% case, Maximum downlink bandwidth

Figure 4.18 shows similar results for the delay as the ones already described in the previous scenarios. The same reasoning for the differences applies here.

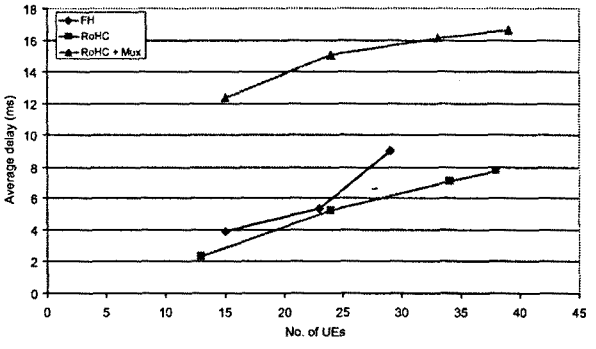

Figure 4.18: 50%-50% case, Average downlink delay

4.2.3 Summary

The results presented in this section clearly show the efficiency gains with respect to the overhead reduction when RoHC is used and specially when multiplexing is added to RoHC. RoHC improvement of the bandwidth utilization with respect to the full header case ranged from 50% to 80% depending on the scenario considered, the larger the payload the smaller the gain. The RoHC plus multiplexing scheme outperformed RoHC in all cases obtaining improvements ranging from 100% to 260%. The best results were obtained, as expected, in the scenarios where more packets could be multiplexed into a single packet and the payload was smaller, e.g., VoIP only case.

The cost of the significant gains in the efficiency of the bottleneck bandwidth utilization of the RoHC plus multiplexing scheme is the additional delay introduced by the multiplexing module.

Based on the results obtained, RoHC and specially the ROHC plus multiplexing scheme are remarkable solutions to be taken into account when an increase in the efficiency of the Iub interface capacity utilization is required. In the latter case, however, attention has to be paid to the configuration of the multiplexing module to avoid outweighting the capacity utilization gains with the additional delay introduced.

4.3 QoS for IP-based UTRAN

As pointed out in the beginning of this chapter, the possibility of substituting in future UMTS networks the ATM transport in the UTRAN by IP introduces several challenges regarding the QoS provided to the applications and the efficient use

of the UTRAN scarce resources that require to be addressed. In this section the specific requirements of the communication between the RNC and the Node-Bs are explained followed by a description and evaluation of our proposed scheduling method which aims to take into account both the UTRAN synchronization requirements and the QoS application needs.

4.3.1 Iub Interface Specific Requirements

The communication between the RNC and the Node-Bs (Iub interface) has specific synchronization requirements for packets sent through a dedicated channel (DCH) as described in [86]. These requirements, which are different depending on whether the downlink[6] or uplink case is considered, have to be fulfilled in order to ensure that the UTRAN resources are not wasted. In the following the different synchronization requirements that apply to the downlink and uplink communication are described.

Downlink

In the downlink case two different synchronization requirements apply:

- First, the fact that the RNC already creates the radio frames that are going to be sent by the Node-B over the air interface, i.e., assigns to each particular radio frame a transmission time, results in a synchronization requirement which specifies that packets have to arrive at the Node-Bs at a certain instant with a maximum deviation corresponding to a specific *receiving window* value [86]. Packets arriving at an instant of time above or below this maximum deviation trigger a timing adjustment process that is used to keep the synchronization of the DCH data stream in the downlink direction (see Figure 4.19). If packets arrive at an instant of time above a fixed maximum deviation they are discarded since the reserved resources are not available anymore. As a result, the Iub interface synchronization is of major importance to guarantee an efficient use of the available resources.

- Second, the soft- and softer-handover mechanisms require the arrival of the radio frames at the UE received via different Node-Bs/sectors within a certain time interval to allow for a selection/combination of the received frames. If this synchronization requirement is not fulfilled, the quality

[6]The term downlink refers to the communication originated at the RNC with the UEs as final destination while uplink refers to the reverse direction.

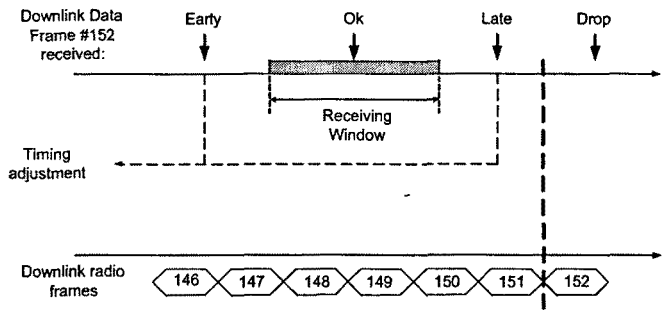

Figure 4.19: RNC to Node-B Synchronization

of service experienced for this connection will be degradated and the resources used in the wired and wireless part wasted. Figure 4.20 depicts the soft/softer-handover mechanism.

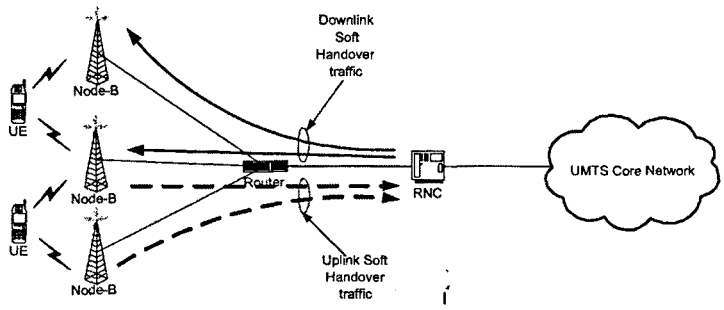

Figure 4.20: Soft handover synchronization requirements

Usually, last-mile links are low capacity links that in case of being congested could delay the arrival of the packets at the Node-B above their receiving window. In this case, packets would be discarded at the Node-B resulting in a waste of resources in the path between the RNC and the Node-B and in the air interface since the assigned resources for this packet would be lost. While this waste of resources could not happen in an UTRAN using ATM transport since the packets had delay guarantees, in the IP-based UTRAN case it could happen, if no mechanisms are implemented to avoid it, due to the IP best effort nature.

In practice, these two synchronization requirements result in all packets sent by the RNC to the Node-Bs having a common delay deadline to fulfill to meet at the same time both requirements. Therefore, *all* packets traversing the Iub interface in the downlink direction have to fulfill delay requirements.

Uplink

In the uplink case, the receiving window requirement does not apply between the Node-B and the RNC since there are no reserved resources at the RNC that have to be used within a certain delay deadline. However, the soft/softer-handover mechanisms can also be used in the uplink resulting in packets having to meet a delay deadline for the reception at the RNC. The current R'99 UMTS system does not provide the Node-B with means to differentiate between traffic with and without soft/softer-handover requirements. Therefore, since no differentiation is possible at the Node-B all the traffic in the uplink has to be handled as if it would have delay requirements regardless of whether the type of traffic requires it and whether it is soft/softer-handover traffic.

4.3.2 Standard Packet Scheduling Mechanisms

In the following section we briefly explain the reasons why the usage of standard scheduling mechanisms at the intermediate routers is not suited to deal with the synchronization requirements described in the previous section.

Strict Priority Scheduling

The simplest solution to provide lower delays to delay-sensitive packets than to delay-insensitive packets is to schedule packets with strict Priority Scheduling (PS). This scheduling consists in transmitting always the packets of the highest priority class available.

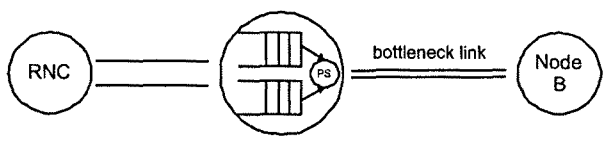

Figure 4.21: Priority scheduling at the router

Weighted Fair Queuing Scheduling

An alternative to Strict Priority scheduling that allows providing bandwidth guarantees to all packets is Weighted Fair Queuing (WFQ) also known in earlier literature as packet generalized processor sharing (PGPS) [87]. This scheduling

involves to continuosly recalculate the scheduling sequence so that the next queue to be serviced is the one that needs to be serviced to meet its long-term average bandwidth target. Provisioning a larger weight to high priority traffic we ensure that, in case of overload, low priority packets are dropped before higher priority ones. The advantage of this solution in comparison to strict priority is that it allows trading-off some non-critical additional delay for higher priority classes in order to provide a better QoS to lower priority classes.

Earliest-Deadline-First Scheduling

An Earliest-Deadline-First (EDF) scheduler [88] assigns each arriving packet a time stamp corresponding to its deadline, i.e., a packet from connection j with a deadline d^j that arrives at the scheduler at time t is assigned a time stamp of $t + d^j$. The EDF scheduler always selects the packet with the lowest deadline for transmission. In the case subject of study, this kind of scheduling has the advantage as compared to WFQ of being able to schedule explicitly based on the synchronization requirements which is the most stringent requirement that applies to the Iub interface.

All the standard scheduling solutions described suffer from the same major drawback: they do not take advantage of the relaxed delay requirements of low priority packets since, because of performing the differentiated scheduling once the Iub interface synchronization requirements apply, all packets have to fulfill exactly the same delay deadline and thus, it is no longer possible to delay some of them without risking their arrival on time at the Node-B. Therefore, these solutions do not perform well in our scenario since, under congestion, packets with low priority will very likely reach their destination with a delay larger than their deadline and will therefore be dropped, resulting in useless consumed bandwidth both in the bottleneck links and in the air interface.

4.3.3 Differentiated Packet Scheduling Design for UTRAN

In order to achieve the objectives stated at the beginning of this section of designnig a scheduling mechanism that takes into account both the Iub interface synchronization requirements and the application QoS needs to guarantee an efficient use of the UTRAN scarce resources we design the differentiated downlink packet scheduling described in the following.

We have previously seen that, in order to provide better QoS service to high

priority packets, standard differentiated scheduling methods at intermediate routers in the path from the RNC to the Node-Bs are not a good option due to several reasons. Our proposed alternative to overcome these problems is to schedule packets at the RNC according to their priorities as the receiving window constraint only starts counting once the sequence frame number has been assigned by the RNC. By delaying packets at the RNC instead of at the intermediate routers a differentiation based on the different QoS application requirements is possible without the cost of risking that due to this additional delay the packets will not fulfill the Iub synchronization deadline.

Based on the different standard packet scheduling mechanisms described in the previous section we consider EDF as the best suited method to provide the desired QoS differentiation in this case, while fulfilling the Iub synchronization requirements, since an explicit reference to the time deadlines to be fulfilled is possible. Note however that similar results could be obtained with WFQ with the single drawback of requiring a higher configuration effort due to the non-explicit relationship of the assigned weights to the resulting delay. Figure 4.22 depicts our scheduling proposal. Packets arriving to the RNC to be delivered to a Node-B are classified depending on their QoS class and buffered in their corresponding queue. A deadline is assigned to each packet based on their arrival time and the traffic category. The RNC schedules then the transmission of the packets to the Node-Bs based on the deadlines of the first packet of each queue using the EDF method. If a multiplexing scheme is used, for instance the one described in Section 4.2, the scheduling is applied to the multiplexed packets taking into account the deadline of the first packet inserted in the container of each traffic class. Note that the proposal relies in a proper admission control performed at the core network to guarantee that enough resources are available to fulfill the accepted services.

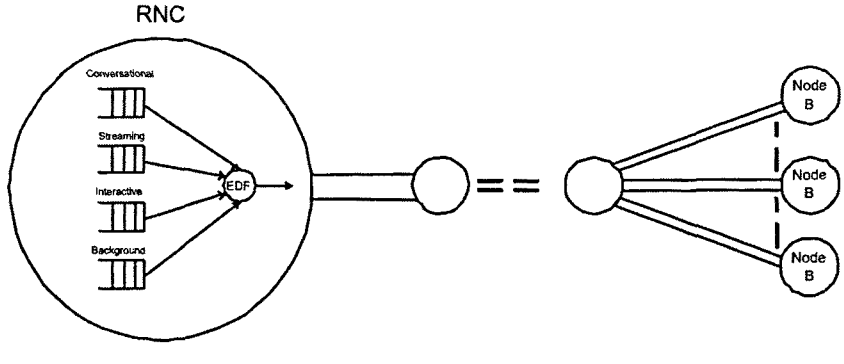

Figure 4.22: Differentiated Downlink Scheduling at the RNC

The proposed scheduling performed at the RNC achieves the following objectives:

- Maximize the efficiency of the usage of the potentially low capacity links between the RNC and the Node-Bs by only sending through these links the packets that will arrive on time (i.e., before the deadline associated to the receiving window).
- Maximize the efficiency of the air interface usage, by ensuring that all packets that leave the RNC and therefore have a sequence frame number assigned in the air interface, are not dropped but reach the Node-B with a delay lower than their deadline.
- Provide packets with a delay appropriate to their requirements (e.g., VoIP packets can be scheduled with a lower delay than Best Effort data packets).
- Protect high priority flows from lower priority ones.

Additionally, the intermediate routers do not need to support any kind of differentiated scheduling since it has been already performed at the RNC.

4.3.4 Performance Evaluation & Discussion

In this section, we evaluate via simulation the performance improvement that results from implementing our proposed EDF downlink packet scheduling at the RNC instead of using a standard QoS scheduling mechanism as WFQ or simple FIFO scheduling at the bottleneck router. The results have been obtained with the OPNET simulator in the scenario described below. The simulations required to modify the UMTS R'99 elements provided by OPNET in order to emulate the IP-RAN architecture described in Section 4, e.g., substitution of ATM transport by IP, and to implement our proposed scheduling mechanism at the RNC.

The scenario chosen for the simulations is the same as the one used in Section 4.2. It consists of a variable number of UEs uniformly distributed along the coverage area of a Node-B and of an RNC connected to the Node-B through a bottleneck link. The bottleneck link is emulated as one E1 link (2048 kbps capacity).

Since we are interested in evaluating the improvement in the performance when different QoS scheduling mechanisms are used we focus on the 'Mid-term' and 'Long-term' scenarios previously described (see Table 4.7) where UEs generating traffic with different QoS requirements are considered. In the 'Mid-term' scenario multimedia users represent 20% of the total number of users and the other 80% are VoIP users while in the 'Long-term' scenario the number of VoIP users and of other multimedia traffic are equal, i.e., 50% each group. In the rest

of the document we will refer to these two scenarios as '80-20 user mix case' and '50-50 user mix case' respectively.

To study the performance of our proposed EDF downlink packet scheduling at the RNC the four different types of traffic defined by 3GPP are considered (see Table 4.6). For generating Conversational, Streaming, Interactive and Background traffic we use the same applications already described in Section 4.2.

Based on the improvement in the performance observed in the results presented in Section 4.2 we consider for this study the case of using the described multiplexing scheme in the Iub interface and RoHC in the air interface.

The Transmission Time Interval (TTI) considered for this study is of 20ms and the maximum delay allowed after the TTI before discarding the packet is 5ms. These are common values in practice.

The configuration for the WFQ scheduler at the intermediate router has been obtained empirically through simulation, when the bottleneck link is no congested, with the single objective of providing a lower delay to the classes with a higher priority. The resulting configuration used for the 80-20 user mix case is a weight of 85 for Conversational, 14 for Streaming, 0.9 for Interactive and 0.1 for Background. In the 50-50 user mix case the configuration used is a weight of 60 for Conversational, 38 for Streaming, 1.5 for Interactive and 0.5 for Background.

The EDF scheduler has been configured with deadlines multiple of the TTI and different for each QoS class. The deadlines chosen based on the considerations provided in [89] and [85] are: 20ms for Conversational, 40ms for Streaming, 100ms for Interactive and 200ms for Background.

Iub Interface Delay

We investigate first the differences in the delay experienced by each QoS class when the three different scheduling mechanisms are used in the 80-20 user mix case. In Figure 4.23 we can observe that, as expected, while the FIFO scheduling provides a very similar delay for all classes the WFQ scheduling introduces differentiation between them based on the weights assigned. A small differentiation is observed though in the FIFO case due to the different frame generation rate of the applications that results in the QoS classes generating traffic less often observing a larger queue length than the ones generating more often. Even though by introducing WFQ scheduling in the intermediate router the QoS perfromance improves, the improvement is minor as compared to the case of performing EDF scheduling at the RNC. As commented before, the fact of performing the scheduling at the RNC instead of after leaving it allows to delay low priority packets when the Iub interface receiving window requirement does not apply yet. Additionally, since with our proposal the sequence frame number is set once the packet is ready

to be sent by the RNC, the Iub interface delay is lower because the multiplexing delay is excluded.

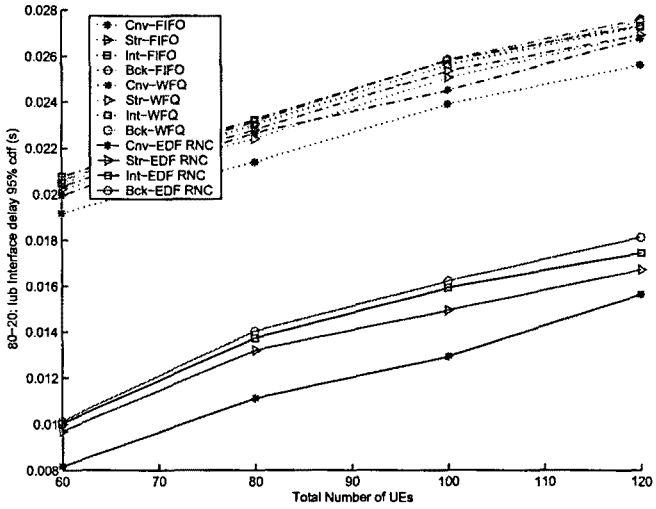

Figure 4.23: Impact of the number of UEs over the Iub Interface delay for each of the three different scheduling mechanisms in the 80-20 user mix case

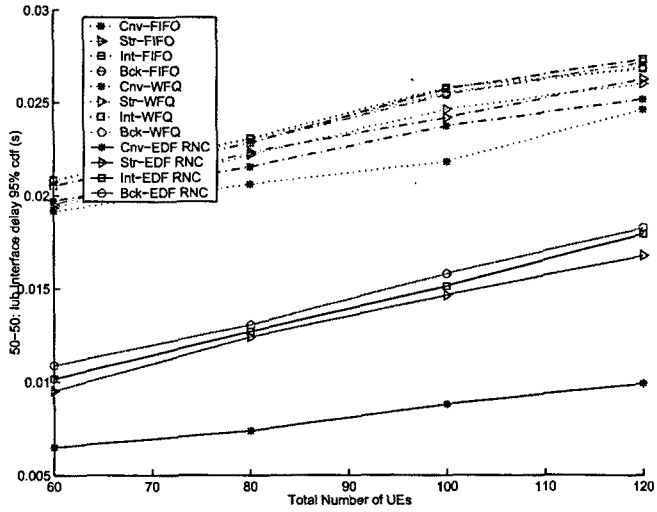

Figure 4.24: Impact of the number of UEs over the Iub Interface delay for each of the three different scheduling mechanisms in the 50-50 user mix case

Similar results are obtained in the 50-50 user mix case, as shown in Figure 4.24, where the main difference now is that, due to the larger amount of lower

priority traffic, a higher differentiation can be obtained by the WFQ and EDF scheduling schemes. A particular case can be observed in congestion conditions (100 and 120 UEs) for the FIFO scheduler where the the Interactive class experiences a slightly higher delay than the Background one. This is just due to our specific 50-50 user mix case (30% of Background users and 10% of Interactive ones) and application traffic characteristics which results in the Background traffic observing a queue length shorter than the Interactive traffic.

In the rest of the experiments we focus on the 100 UEs case as the most relevant one for our study since it is the first case where for both user mix cases some traffic classes experience a delay above the configured maximum of 25ms before the packets are discarded.

Iub Interface Packet Error Rate

Figures 4.25 and 4.25 provide details on the change in the delay distribution, cumulative distribution function (cdf), for the different QoS classes introduced by the two QoS scheduling mechanisms as compared to plain FIFO. As we can observe, in the 80-20 user mix case, WFQ manages to significantly improve the FIFO performance by trading-off some additional delay for the different classes. On the other hand, in the 50-50 user mix case the WFQ configuration chosen favours in excess the conversational class resulting in a poor performance with regard to the additional delay for the rest of the classes as compared to the FIFO case. Finally, the EDF scheduling at the RNC shows a clear improvement in the delay observed for both cases with respect to the other two scheduling methods with the additional advantage of improving the control of the jitter.

The results with respect to the packet error rate observed at the Iub interface, corresponding to the delay results previously presented, are shown in Figures 4.27 and 4.28. As expected, the results perfectly match the delay distribution ones where while the EDF scheduler manages to keep all the values below the dropping threshold at the Node-Bs, the WFQ scheduler improves mainly the packet losses for the Conversational class and depending on the configuration also for the rest of the classes. The particular case already observed in the delay graph for the 50-50 user mix case is reproduced here where due to the configure traffic mix for this case the losses for the interactive class are higher than for the background one.

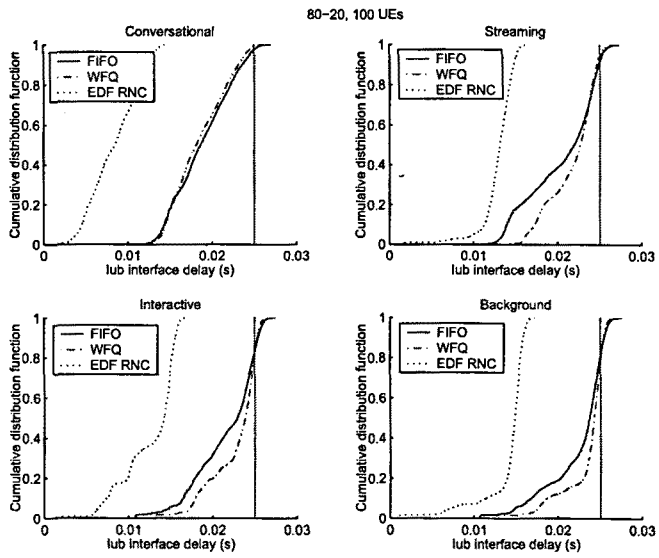

Figure 4.25: Impact of the number of UEs over the Iub Interface delay for each of the three different scheduling mechanisms in the 80-20 user mix case

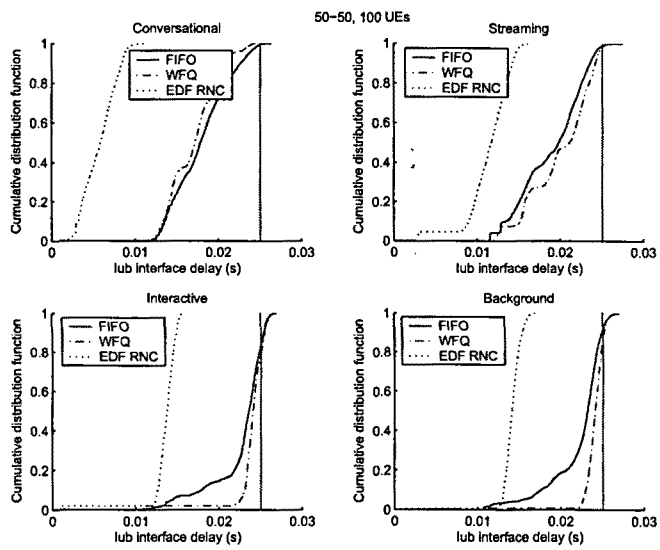

Figure 4.26: Impact of the number of UEs over the packet error rate for each of the three different scheduling mechanisms in the 80-20 user mix case

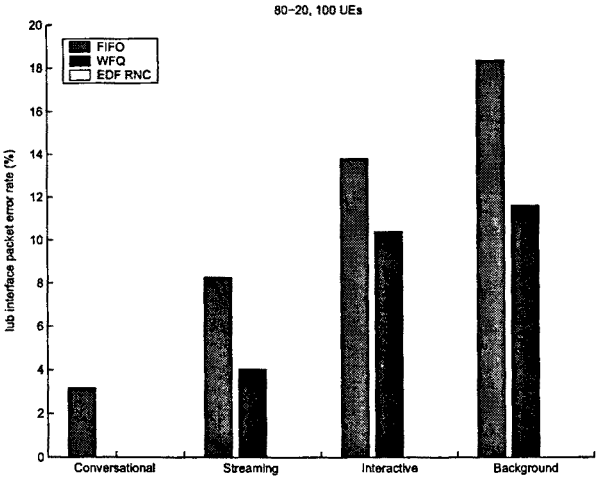

Figure 4.27: Impact of the number of UEs over the packet error rate for each of the three different scheduling mechanisms in the 80-20 user mix case

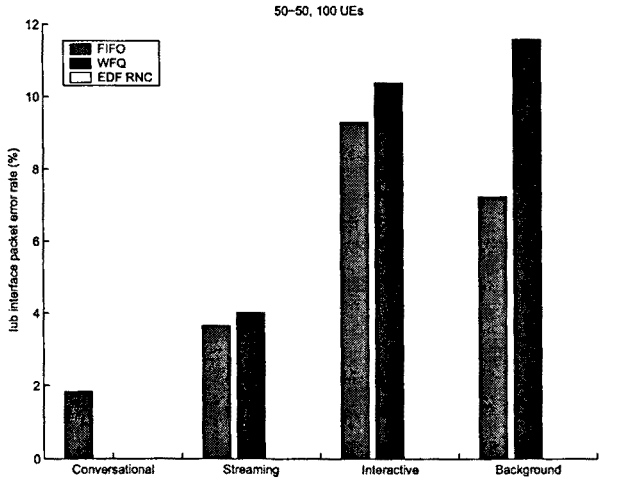

Figure 4.28: Impact of the number of UEs over the packet error rate for each of the three different scheduling mechanisms in the 50-50 user mix case

4.3.5 Summary

In this section we have analyzed the specific requirements of the UTRAN in order to evaluate whether standard packet scheduling mechanisms used at intermediate routers would provide the required QoS differentiation when the ATM transport is substituted by IP.

The main conclusion that can be drawn from our results is that, due to the specific synchronization requirements in the Iub interface, the appropriate place to perform the differentiated scheduling in the downlink is the RNC. Otherwise, since all packets have the same delay requirements once they have left the RNC, a differentiated scheduling at the intermediate routers results in a waste of the scarce UTRAN resources. Note that a similar method could be applied at the Node-Bs in the uplink case.

The main drawback of our proposal is the increase in the complexity at the RNC because of setting the sequence frame number to the radio frames at the instant when the regular IP packets or multiplexed ones have to be sent. However, the proposal has been discussed with actual RNC implementors which indicated that it is feasible and if significant performance improvements would be expected could be implemented.

We evaluated via simulation the performance improvement obtained when an EDF scheduler is used at the RNC as compared to the implementation of WFQ or simple FIFO at intermediate routers. The results have shown that because the proposed scheduling can delay low priority packets without interfering with the Iub synchronization requirements a significant performance improvement can be obtained with respect to the delay differentiation and the resulting packet error rate. We propose to use and EDF scheduler because it is easier to configure for the Iub interface requirements than WFQ where a explicit configuration of the priority considering the desired maximum delay is not possible. However, it is possible to tune WFQ to obtain similar results. Additionally, since EDF improves the jitter it is specially indicated for this case to reduce the buffer requirements at the Node-Bs.

4.4 Summary of Main Results

In this chapter several issues that arise when IP transport is introduced in the UTRAN have been addressed. The significant increase of the overhead requires of header compression and multiplexing methods to achieve at least a usage of the UTRAN resources similar to the one when ATM transport is used. Otherwise, the relevant increase in the network running costs due to capacity problems would threaten the actual deployment in the future of IP-based RANs. Additionally, the specific UTRAN transport requirements force the adaptation of the standard packet scheduling mechanisms to make an efficient use of the network resources while providing the required QoS.

The results presented in Section 4.1 and in [90] demonstrate that by using header compression schemes and by designing radio access bearers adapted to these schemes the resources required to transmit IP packets over the air interface can be significantly reduced. Specifically, we found the configuration for a VoIP radio access bearer when RoHC is used that reduces in about 50% the air interface resources required by the reference VoIP RAB defined by 3GPP.

In Section 4.2 and [91] a multiplexing scheme to reduce the overhead for the IP transport in the Iub interface is described and analyzed. The study covers three different scenarios where the number of users generating traffic different than VoIP increases gradually which concludes that by combining header compression and multiplexing methods the efficiency in the usage of the UTRAN resources can increase significantly (between 100% and 260% in our scenarios).

Finally, in Section 4.3 and [91] we propose a differentiated scheduling mechanism based on EDF that fulfills the Iub interface specific requirements while providing the QoS differentiation required by the applications. The method, which main novelty is to perform the scheduling at the RNC instead of at intermediate routers, allows to make use of the different QoS application needs without interfering with the UTRAN transport requirements resulting in a relevant improvement with respect to the Iub interface delay and the packet error rate. This proposal has resulted in a patent application [92].

Chapter 5

QoS for Wireless LANs

Future All-IP networks will have to provide QoS guarantees across heterogeneous networks, including Wireless LANs, which is currently one of the most popular access networks. Given that the QoS mechanisms provided by the 802.11 standard are expected to be insufficient to fulfill the QoS requirements of certain relevant applications, an intensive research activity has been conducted during the last years to enhance the 802.11 MAC layer QoS support. In parallel, the IEEE 802.11 standardization body recognized the need for this enhancement and created the 'Task Group E' in order to elaborate a standard that extends the 802.11 MAC layer functionality to include mechanisms that provide the required QoS guarantees.

The upcoming IEEE 802.11e standard represents a key element toward providing QoS guarantees across heterogeneous networks, however, 802.11e does not indicate how to actually deliver the required QoS guarantees but provides only the mechanisms, therefore, QoS algorithms need to be designed. Additionally, the introduction of Wireless LAN capabilities in mobile devices with severe battery limitations, e.g., cellular phones, raises new issues regarding the interaction of the 802.11e functionality in combination with available power saving mechanisms.

Different approaches can be considered for supporting QoS in Wireless LANs. [93] is based on the Integrated Services architecture proposed for the wireline Internet where the control over wireless resources is very strict, motivated by the argument that strict control, with complex and sophisticated mechanisms and protocols, is required to maintain good quality in the wireless environment.

Other approaches are based on the Differentiated Services architecture, which provides service differentiation using simpler mechanisms. There have been several proposals for service differentiation in wireless mainly differentiated by whether

the mechanisms rely on centralized control and polling of backlogged mobile hosts see e.g., [94] or a distributed control is considered see e.g., [95], [96] and [97]. Since the 802.11 DCF mechanism is implemented in all 802.11 WLAN cards while PCF is seldom implemented, most of the research has focused on the extension of DCF. These architectures are based on the idea of modifying the backoff time computation of the 802.11 standard to provide service differentiation. In [95] the backoff time computation is modified by assigning shorter CWs to real-time traffic. This approach however, does not decouple real-time traffic from non real-time and, as a consequence, the service quality of real-time traffic is sensitive to the changing conditions of data traffic. In addition, [95] does not provide different priorities for data traffic. [96] and [97] propose the use of different CWs and different backoff increase parameters, respectively, for different priorities of data traffic but no support for real-time traffic is provided. The fact that the parameters in [96] and [97] are statically set makes the level of differentiation uncertain due to its dependency with the load of the channel.

The Black Burst scheme in [98] introduced a distributed solution to support real-time sources over 802.11, by modifying the MAC for real-time sources to send short transmissions to gain priority. This method can offer bounded delay. The disadvantage of [98] is that it is optimized for isochronous sources, preferably with equal data rates, which can be a significant limitation for applications with variable data rates.

Regarding the interaction of 802.11e and 802.11 power save mode, to the best of our knowledge there is no published related work analyzing the resulting performance when used together. In the area of providing QoS in a Wireless LAN a lot of research has been done during the last several years as already indicated. With respect to the 802.11 power save mode, the independent mode for ad-hoc networks has been studied for instance in [99, 100] and the infrastucture mode in [101, 102].

In the following section we provide an overview of the 802.11 MAC layer, the QoS differentiation mechanisms being developed for 802.11e and the 802.11 power saving mode. Based on that, we describe our contributions in the research area of QoS for Wireless LANs. Regarding the enhancement of the DCF MAC layer three extensions are presented which address three possible QoS requirements: delay bounds, bandwidth guarantees and relative bandwidth requirements. Then, an analysis of the impact of the 802.11 power saving mode over the 802.11e functionality is provided followed by our proposal to minimize the impact of this interaction while keeping a low power consumption. Part of this work has been used for the development of the NEC 3G/WLAN mobile terminal N900iL.

5.1 802.11 MAC layer

The basic IEEE 802.11 Medium Access mechanism is called Distributed Coordination Function (DCF) and is based on the Carrier Sense Multiple Access with Collision Avoidance (CSMA/CA) protocol [16]. CSMA/CA was first investigated thoroughly in [103] and [104]. The MAC scheme used in IEEE 802.11 is an extended version of the FAMA protocol [105]. It is slotted, i.e. the access can happen only at specific instants. The 802.11 MAC protocol operation is shown in Figure 5.1.

In the DCF mode, a station must sense the medium before initiating the transmission of a packet. If the medium is sensed idle for a time interval greater than the DCF Inter Frame Space (DIFS), then the station transmits the packet. Otherwise, the transmission is deferred and a backoff process is started.

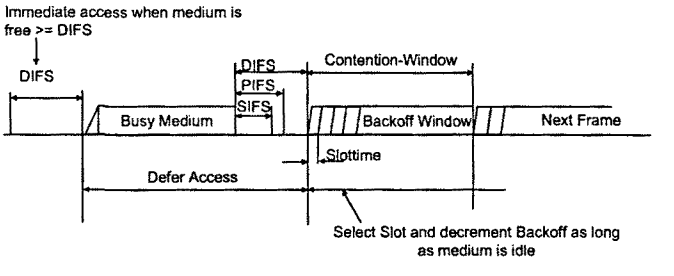

Figure 5.1: Basic 802.11 MAC protocol operation

Specifically, the station computes the backoff interval as an equally distributed random value taken from the range of 0 to the so-called Contention Window (CW), where the backoff time is measured in slot times. This backoff interval is then used to initialize the backoff timer. This timer is decreased only when the medium is idle and is frozen when it is sensed busy. Each time the medium becomes idle for a period longer than a DIFS, the backoff timer is periodically decremented, once every slot-time.

As soon as the backoff timer expires, the station starts to transmit. A collision occurs when two or more stations start transmission simultaneously in the same slot. To avoid collisions, a Request To Send (RTS) and a clear to send (CTS) can be exchanged between source and receiving station prior to the actual frame transmission. In addition, an Acknowledgement (Ack) is transmitted to the source after successful reception of the frame to detect collisions. The Ack scheme can additionally be used to control the retransmission of erroneous frames. The RTS/CTS scheme is also used for hidden node handling.

If a CTS or acknowledgment is not received by the source station, it assumes that the transmission attempt was not successful and re-enters the backoff process.

To reduce the probability of collisions, the CW is doubled after each unsuccessful transmission attempt until a predefined maximum (CW_{max}) is reached. After a successful frame transmission, if the station still has frames buffered for transmission, it must execute a new backoff process.

The second access mechanism specified in the IEEE standard is built on top of DCF and it is called Point Coordination Function (PCF). It is a centralized mechanism, where one central coordinator polls stations and allows them undisturbed, contention free access to the channel. In contention free access mechanism, collisions do not occur since the access to the channel is controlled by one entity.

The three Inter Frame Spaces (IFS) serve the purpose of defining different levels of access priorities. They define the minimal time that a station has to let pass after the end of a transmitted frame, before it may start transmitting a certain type of frame itself. After a SIFS (Short IFS), the shortest interframe space, only acknowledgements, CTS and data frames in response to poll by the PCF may be sent. The use of the DIFS and the PIFS has already been explained. This use of IFS allows the most important frames to be sent without additional delay and without having to compete for access with lower priority frames.

The basic access mechanism of 802.11, the DCF mode, does not guarantee anything else than Best Effort service. The second access mechanism specified in 802.11, the PCF mode, is intended to support real-time services by using a central polling mechanism. This mechanism, however, is not supported in most wireless cards, and it was shown in [106] that the cooperation between PCF and DCF modes leads to poor throughput performance. Therefore, the differentiation mechanisms available when using the standard 802.11 MAC layer are unfortunately not sufficient to provide the service guarantees required by future All-IP networks where e.g., bandwidth and delay guarantees might be requested.

The IEEE 802.11 Working Group identified the need for QoS enhancements, and created the Task Group E to enhance the current 802.11 MAC protocol to support applications with QoS requirements. These enhancements are currently under development and will lead to the 802.11e extension of the 802.11 standard.

5.2 802.11e QoS support mechanisms

The 802.11 Task Group E is currently completing the design of the 802.11 MAC enhancements which will lead to the 802.11e extension of the standard. 802.11e defines the Hybrid Coordination Function (HCF) to support QoS. Two channel access methods are defined: a contention-based channel access method called

the Enhanced Distributed Channel Access (EDCA) and a contention-free channel access referred to as HCF Controlled Channel Access (HCCA). Within a superframe two phases of operation are possible in 802.11e, contention period (CP) and contention-free period (CFP). HCCA can be used in both CP and CFP while EDCA can be used only during CP.

New mobile devices incorporating 802.11e functionality before the standard is completed are likely to include first the EDCA mechanisms and later HCCA. This can be seen for instance in the fact that the Wi-Fi Alliance [107] will start certifying the Wi-Fi Multimedia Extensions (WME) at the end of 2004 and the Wi-Fi Scheduled Multimedia (WSM) in the beginning of 2005. WME is based on EDCA while WSM is based on HCCA and includes EDCA. Additionally, HCCA still requires further work to solve some detected problems in the case of overlapping HCs due to loose of coordination as pointed out in [108]. Based on that, we focus our study on the interaction of EDCA with the 802.11 power save mode since it is the most probable configuration to be implemented in the short-term in 802.11e-capable mobile devices.

5.2.1 HCF contention-based channel access (EDCA)

802.11e introduces the concept of *transmission opportunity* (TXOP) which is the basic unit of allocation of the right to transmit onto the wireless medium. Each TXOP is defined by a starting time and a defined maximum duration advertised by the AP. The length of a TXOP is the duration during which the TXOP holder maintains uninterrupted control of the medium including the time required to transmit frames sent as an immediate response to the TXOP holder's transmissions.

Two modes of EDCA TXOP have been specified, the initiation and the continuation of an EDCA TXOP. An initiation of the TXOP occurs when the EDCA rules allow access to the medium while a TXOP continuation occurs when a channel access function retains the right to access the medium following the completion of a frame exchange sequence.

Traffic differentiation is based on *user priority* (UP) and is achieved through varying: the amount of time a station senses the channel to be idle before backoff or transmission, the length of the contention window (CW) to be used for the backoff and the duration a station may transmit after it acquires channel access. This is realized by the introduction of four *access categories* (AC) and multiple independent backoff entities. The four ACs are AC_VO, AC_VI, AC_BE and AC_BK. The labels correspond to the applications for which they are intended, i.e., voice, video, best effort and background. Figure 5.2 [108] depicts the parallel backoff entities functionality and the mapping to be performed from the eight priorities defined by 802.11D to the four ACs. Note that the backoff entities migth

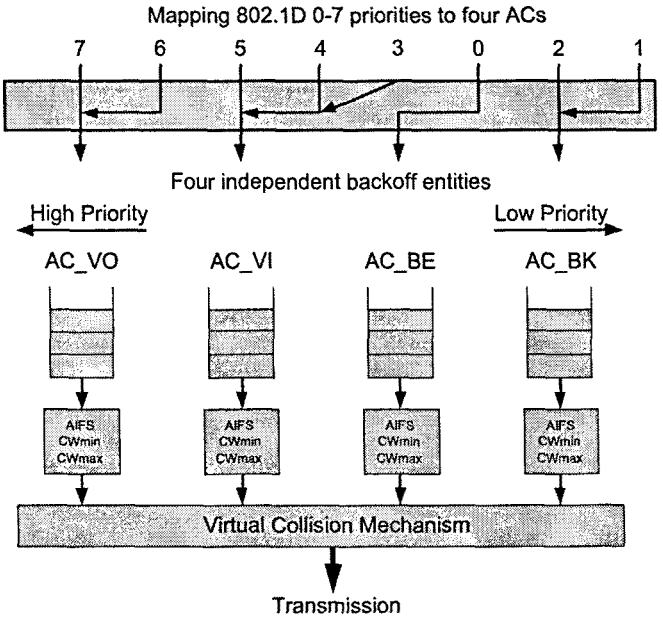

Figure 5.2: Backoff Entities within one station

be located in the same station or in different stations. A collision between backoff entities within the same station is defined in 802.11e as a *virtual collision.* Such a collision, instead of implying that both backoff entities invoke again the backoff procedure with a doubled CW, results in the lower priority station/s following the normal backoff procedure and the highest priority station transmitting undisturbed. In the following we describe the EDCA parameters that define the priority to access the wireless medium.

Obtention of an EDCA TXOP

The EDCA parameters for each AC to be used by the backoff entities to obtain a TXOP are distributed by the HC and can be modified over time via information fields included in the beacon frames. EDCA modifies the 802.11 transmission procedure of a backoff entity by introducing a new interframe space defined as *Arbitration Interframe Space* (AIFS). The AIFS enhances the function of the 802.11 DIFS allowing different values for each AC with a minimum value of DIFS for the 802.11e stations and of PIFS for the 802.11e AP. The duration of AIFS[AC] is calculated based on the *arbitration interframe space number* AIFSN[AC] as follows: $AIFS[AC] = SIFS + AIFSN[AC] \times aSlotTime$; where $aSlotTime$ refers to the duration of a slot.

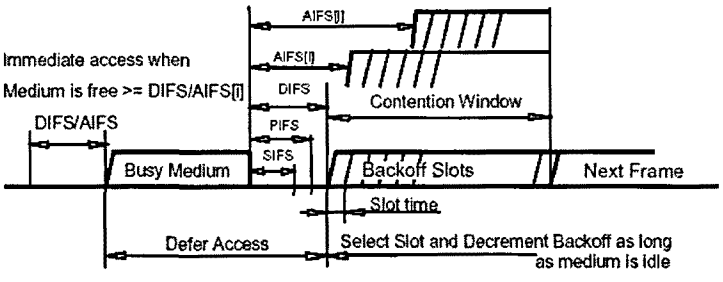

Figure 5.3: IFS relationships

A smaller AIFSN[AC] results in a higher priority when accessing the medium since the backoff counter starts decrementing after detecting the medium being idle for a duration equivalent to the AIFS[AC].

EDCA modifies the backoff procedure by requiring to the backoff instances to maintain a separate state variable for the contention window and by making the minimum (CWmin) and maximum (CWmax) size dependent on the AC. Taking into account that the CWmin value is used as the initial value to determine the random backoff period, the smaller the CWmin value is for a specific AC the higher the priority to access the medium. The same applies to the CWmax value which refers to the maximum CW value that can be reached by a certain AC, the smaller this value is the higher chances to win a contention with other stations when trying to gain access to the shared medium. Figure 5.3 illustrates the IFS and CW concepts.

Finally, the duration of a TXOP (TXOPlimit) is another AC dependent parameter that provides differentiation since the larger this value is the larger the duration of the continuous usage of the channel by a certain AC.

A brief overview of the QoS main differences introduced by EDCA as compared to the legacy DCF has been provided in this section. For a thorough overview of HCF please refer to [108].

5.3 802.11 Power Management

The IEEE 802.11 standard defines two independent power management mechanisms, depending on whether the infrastructure or ad hoc mode is used, that allow mobile stations to enter a power saving mode of operation where they turn off their receiver and transmitter to conserve power. In our study we focus on the infrastructure power management scheme during the contention period as the most

relevant case for 3G/WLAN devices. Note that currently most of the wireless LAN deployments use the infrastructure mode with the access arbitrated by the distributed coordination function (DCF).

Access Point operation

In infrastructure mode, the power management mechanism is centralized in the Access Point (AP). APs maintain a power management status for each currently associated station that indicates in which power management mode the station is currently operating. Stations changing power management mode inform the AP of this fact using the power management bits within the frame control field of transmitted frames.

The AP buffers unicast and multicast data frames destined to any of its associated stations that are in power save mode. If an AP has buffered frames for a station, it will indicate it in the traffic indication map (TIM) which is sent with each Beacon frame. During the association process every station is assigned by the AP an Association ID code (AID). The AID indicates with a single bit in the TIM whether frames are buffered for a specific station.

Stations request the delivery of their buffered frames at the AP by sending a Power Save Poll (PS-Poll). A *single* buffered frame for a station in power save mode is sent after a PS-Poll has been received from a station. Further PS-Poll frames from the same station are acknowledged and *ignored* until the frame is either successfully delivered, or presumed failed due to maximum number of retries being exceeded. This prevents a retried PS-Poll from being treated as a new request to deliver a buffered frame.

Finally, APs have an aging function that deletes buffered traffic when it has been buffered for an excessive period of time.

Station operation

A station may be in one of two different power states:

- *Awake*: station is fully powered.
- *Doze*: station is not able to transmit or receive and consumes very low power.

While being in power save mode a station listens to selected beacons based upon the listen interval parameter which refers to the number of beacon periods that the station will be in the doze state until it awakes at the expected time of a

beacon transmission. In short, a station awakes for listening a beacon once every n beacons, where n is an integer ≥ 1. The listen interval value used by a station is communicated to the AP in its association request.

Each station learns through the TIM in the beacon whether the AP buffered any frames destined to them while they were in the doze state. If a station sends a PS-Poll to retrieve a buffered frame, the AP can respond acknowledging (ACK) it or sending directly the data frame. In the event that neither an ACK nor a data frame is received from the AP in response to a PS-Poll frame, then the station retries the sequence, by transmitting another PS-Poll frame. If the AP sends a data frame in response to a PS-Poll, this frame is sent before other frames of stations not in power saving mode that might be waiting at the AP buffer to be transmitted. On the other hand, if the AP responds to a PS-Poll by transmitting an ACK frame, the data frame follows the normal procedure and is transferred in a subsequent frame exchange sequence initiated by the AP. In the rest of the document we assume that PS-Polls are acknowledged. We have chosen this option because of fairness reasons since otherwise data frames requested through a PS-Poll would have priority over the frames from stations not in power save mode.

In the frame control field of the frame sent in response to a PS-Poll, the AP sets a bit labeled More Data if there are further frames buffered for this station. The station is required to send a PS-Poll to the AP for each data frame it receives with the More Data bit set. This ensures that stations empty the buffer of the frames held for them at the AP.

Mobile stations should also awake at times determined by the AP, when broadcast/multicast frames are to be transmitted. This time is indicated in the Beacon frames as the delivery traffic indication map (DTIM) interval. The broadcast/multicast frames are sent by the AP before transmitting any unicast frame following the normal transmission rules. The actual number of DTIMs that can be skipped by a station if ReceiveDTIM is false depends on its configuration. If ReceiveDTIM is true a station must awake at every DTIM.

Note that the power save mode functionality does not imply that frames sent from the station to the AP are delayed until the next beacon is received, i.e., mobile nodes wake up whenever they have data to send and follow the normal 802.11 clear channel assessment procedure.

Example of the 802.11 Power Save Mode operation

Figure 5.4 illustrates the infrastructure power save mode procedure during the contention period assuming a listen interval for station 1 (STA 1) and STA 2 of 2 beacon intervals, and a DTIM period of 5 beacon intervals.

In the example, first the process for delivering broadcast (BC) and multicast

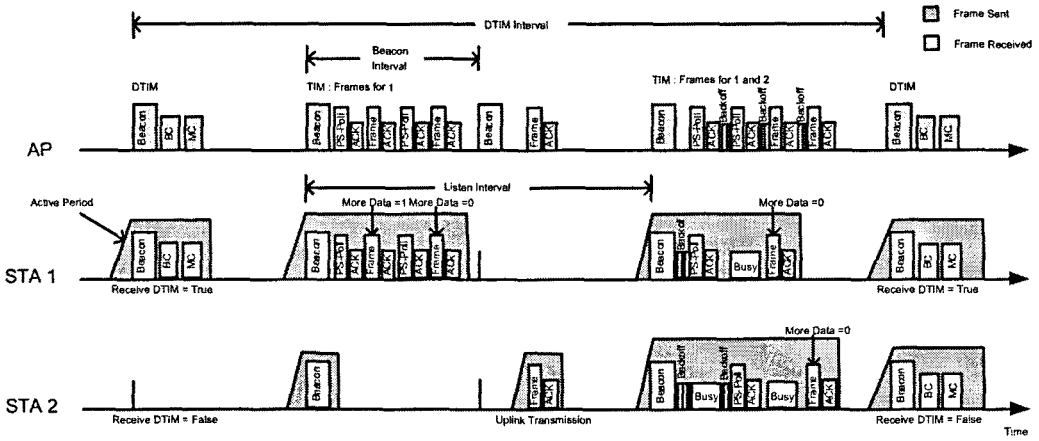

Figure 5.4: Sample of infrastructure power management operation

(MC) frames is shown. A beacon is sent by the AP containing the DTIM, STA 1 with ReceiveDTIM set to true powers-up its receiver for the reception of the broadcast and multicast packets while STA 2 does not because ReceiveDTIM is set to false. Next, both STAs awake, as required by their listen interval, to receive a beacon. STA 2 switches to the doze mode since no packets are buffered in the AP for that STA as indicated in the TIM for its AID. On the other hand, STA 1 sends a PS-Poll because its bit in the TIM is true. After receiving the corresponding data frame, since the More Data bit was set to true, a new PS-Poll is sent by the same station. In the next received frame the More Data bit is set to false so the station returns to the doze state.

In the following beacon the stations should not awake due to their listen interval but STA 2 awakes for sending a data frame to the AP. As mentioned before, the power save mode does not imply any restriction for awaking when a packet needs to be sent in the uplink. The next beacon, listened by both stations, results in both having to transmit a PS-Poll. Since they are aware of the fact that another station will also send a PS-Poll through checking the TIM, they perform the backoff procedure trying to avoid a collision. In this case, STA 1 has to wait for a shorter period and thus transmits first its PS-Poll and STA 2 defers. After receiving the PS-Poll and sending an ACK, the AP has to defer because of the transmission of the PS-Poll of STA 2. Finally, the AP transmits the frames for both STAs in the order they were requested. In the next beacon including DTIM, STA 2 wakes up for that beacon even if ReceiveDTIM is false since it has to awake for some of them.

For further details about the power save mode operation the reader is referred to [16].

5.4 Expedited Forwarding MAC Extension

The principle of the DIME-EF contention resolution scheme is shown in Figure 5.5. This scheme uses principles of the EY-NPMA MAC protocol described in [109], and, according to [110], has a residual collision rate almost independent from the number of contending stations. However, the parameters of the contention resolution (CR) scheme as used in [109] will be adapted to the requirements of the EF Scheme.

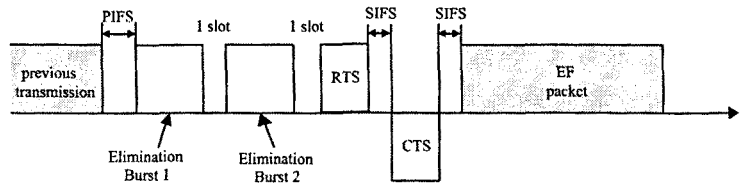

Figure 5.5: Contention resolution scheme for EF traffic.

A station with EF traffic starts its contention cycle when a PIFS has passed after the end of a previous transmission. DIME-EF uses two bursts for elimination, elimination burst EB1 and EB2. These bursts may consist of a random data or pseudo-noise pattern. Their only purpose is to occupy the channel such that stations not using the DIME-EF cannot sense the channel idle for longer than a PIFS duration and, hence, do not interfere a DIME-EF access attempt.

The duration of the EBs are multiples of the Slot Duration defined in the 802.11 standard. The duration of EB1 is calculated according to the following probability density:

$$P_{E1}(n) = \begin{cases} p_{E1}^{n-1}(1-p_{E1}) & ;1 \leq n < m_{E1} \\ p_{E1}^{m_{E1}-1} & ;n = m_{E1}, \end{cases} \tag{5.1}$$

where n is the number of slot durations EB1 shall last, p_{E1} is a probability parameter between 0 and 1 and m_{E1} is the maximum number of EB1 slots. Note that the above formula requires that EB1 lasts at least one slot. This is necessary in order to occupy the channel and keep terminals not using EF from making an access attempt.

The duration of EB2 shall be calculated according to the probability density

$$P_{E2}(n) = \frac{1}{m_{E2}} \quad \text{for } 1 \leq n\, m_{E2}, \tag{5.2}$$

i.e. it is taken from an equally distributed variable in the range between 1 and the maximum number of EB2 slots, m_{E2}. Note that here the duration is at least one slot for the same reasons as for EB1.

A station that makes an access attempt, first chooses the duration of EB1 and EB2. If it senses the channel free for at least a PIFS, it transmits its EB1. After this transmission, the station senses the channel for one slot duration. If the channel is sensed free, it continues to send its EB2 after the sensing slot. After the transmission of EB2, it senses the channel again. If it is free, it starts to transmit its RTS after a slot duration and the transmission continues as defined for the data transmission using the DCF. If, however, the station senses the channel busy after its transmission of EB1 or EB2, it withdraws its transmission attempt and defers until the channel has been free for at least a PIFS. Using this mechanism, the station which chooses the longest EB1 and EB2 among all contending stations wins the contention and is allowed to transmit.

If two stations happen to have the same EB1 and EB2 durations, they collide. However, due to the importance of the packets, we use the already defined mechanisms in 802.11 for collision detection, i.e. the RTS/CTS handshake and the transmission of an Ack after the packet reception. In fact, the Ack will be transmitted in any case if a packet is being transmitted from a station using the new scheme to a station using the old scheme and, hence, shall be kept for the sake of backwards compatibility.

The DIME-EF scheme will be analyzed mathematically in the following clause. It will be shown that the performance of the scheme depends on the values of p_{E1}, m_{E1} and m_{E2}, but also on the number of stations entering a contention cycle. The goal of the mathematical analysis is to parameterize the DIME-EF scheme appropriately for the application in the IEEE 802.11 extension. It will also be a basis to justify the selection of this specific scheme, even if there might have been other possible candidates.

5.4.1 Mathematical Analysis

The idea for the analysis has been taken from [110], although the results differ significantly.

Assume that N_1 stations enter the EB1 period of a specific DIME-EF contention resolution cycle where the duration of the EB1 of each station is given according to Equation 5.1. Then, the probability that the EB1 period ends after i

slots and exactly k stations survive, is given by:

$$P_{E1,i,k}(i,k) =$$

$$\begin{cases} (1-p_{E1})^k & ;i=1;\ k=N_1 \\ \binom{N_1}{k}\left[p_{E1}^{i-1}(1-p_{E1})\right]^k \cdot \left(1-p_{E1}^{i-1}\right)^{N_1-k} & ;1<i<m_{E1} \\ \binom{N_1}{k}\left(p_{E1}^{i-1}\right)^k \cdot \left(1-p_{E1}^{i-1}\right)^{N_1-k} & ;i=m_{E1} \end{cases} \tag{5.3}$$

Consequently, the probability that exactly k stations survive EB1, can be represented as:

$$P_{E1,k}(k) = \begin{cases} \sum_{i=2}^{m_{E1}} P_{E1,i,k}(i,k) & ;1 \le k < N_1 \\ \sum_{i=1}^{m_{E1}} P_{E1,i,k}(i,k) & ;k=N_1 \end{cases} \tag{5.4}$$

These k stations are the ones that enter the EB2 period. The average duration $\bar{T}_{E1}$ of EB1 can be calculated as:

$$\bar{T}_{E1} = \mathrm{E}\left(P_{E1,i}(i)\right) \cdot T_{slot} = T_{slot} \cdot \sum_{j=1}^{m_{E1}} j \cdot P_{E1,i}(j) \tag{5.5}$$

where $\mathrm{E}(\cdot)$ denotes the expected value, T_{slot} a slot duration in IEEE 802.11 and

$$P_{E1,i}(i) = \begin{cases} (1-p_{E1})^{N_1} & ;i=1 \\ \sum_{k=1}^{N_1} P_{E1,i,k}(i) & ;1<i\le m_{E1} \end{cases} \tag{5.6}$$

is the probability that the EB1 period ends after i slots.

The same calculation is now being performed for the EB2 cycle. Let N_2 denote the number of stations entering the EB2 cycle. Then, the probability that EB2 ends

after i slots with k stations left, is given by:

$$P_{E2,i,k}(i,k,N_2) = \begin{cases} \left(\frac{1}{m_{E2}}\right)^k & ;i=1;\ k=N_2 \\ \binom{N_2}{k}\frac{(i-1)^{N_2-k}}{m_{E2}^{N_2}} & ;1<i\leq m_{E2} \end{cases} \tag{5.7}$$

The expected duration of an EB2 cycle depends on the outcome of the EB1 cycle in terms of numbers of surviving stations and can be represented as:

$$\begin{aligned} \bar{T}_{E2}(N_2) &= T_{slot}\cdot\sum_{N_2=1}^{N_1} P_{E_1,k}(N_2)\cdot \mathrm{E}\left(P_{E_2,i}(i,N_2)\right) \\ &= T_{slot}\cdot\sum_{N_2=1}^{N_1}\left[P_{ES,k}(N_2)\cdot\sum_{i=1}^{m_{E2}}\cdot P_{E2,i}(i,N_2)\right] \end{aligned} \tag{5.8}$$

where

$$P_{E2,i}(i,N_2) = \begin{cases} \left(\frac{1}{m_{E2}}\right)^k & ;i=1;\ k=N_2 \\ \sum_{k=1}^{N_2} P_{E2,i,k}(i,k,N_2) & ;1<i\leq m_{E2} \end{cases} \tag{5.9}$$

denotes the probability that the EB2 cycle ends after i slots. The overall collision probability P_c is the situation where more than one station survive the EB2 cycle and can be calculated as:

$$P_c = \sum_{N_2=2}^{N_1}\left(1-P_{E_2,k}(1,N_2)\right)\cdot P_{E1,k}(N_2) \tag{5.10}$$

with

$$P_{E_2,k}(k,N_2) = \begin{cases} \sum_{i=2}^{m_{E2}}\binom{N_2}{k}\frac{(i-1)^{N_2-k}}{m_{E2}^{N_2}} & ;1\leq k<N_2 \\ \left(\frac{1}{m_{E2}}\right)^{N_2}+\sum_{i=2}^{m_{E2}}\binom{N_2}{k}\frac{(i-1)^{N_2-k}}{m_{E2}^{N_2}} & ;k=N_2 \end{cases} \tag{5.11}$$

as the probability that k out of N_2 stations survive the EB2 cycle.

The overhead O_1 of a single access attempt depends on three main values:

- The expected duration $T_{DIME-EF}$ of a successful DIME-EF cycle, i.e. a cycle which finishes without a collision. This is given by the sum of $\bar{T}_{E1}$, see Equation 5.5, $\bar{T}_{E2}$, see Equation 5.8, and $2 \cdot T_{slot}$ for the carrier sensing slots after EB1 and EB2.
- The time it takes to detect a collision of the DIME-EF scheme, T_{coll}. A collision will be detected if the RTS of the sender is not answered by a CTS of the receiver. The medium can be accessed again by a EF station after a PIFS following the RTS. This time is denoted by T_{RTS}, and $T_{coll} = T_{DIME-EF} + T_{RTS}$.
- The collision probability P_c according to Equation 5.10.

The overhead for a single access attempt in terms of average duration of the DIME-EF scheme, then, is calculated as:

$$O_1(m_{E1}, p_{E1}, m_{E2}, N_1) = P_c \cdot T_{coll} + (1 - P_c) \cdot \bar{T}_{DIME-EF} \tag{5.12}$$

Iterating this overhead of a single access cycle for subsequent access cycles, weighted with the residual collision probability for a single attempt, yields the average overhead O:

$$O(m_{E1}, p_{E1}, m_{E2}, N_1) = O_1 \cdot \frac{1}{1 - P_c} \tag{5.13}$$

The overhead O can be interpreted as a function that weighs the overhead of the collision avoidance scheme against the additional overhead that needs to be spent if collisions occur. It is clear that, the more overhead is spent for the collision avoidance, the smaller the collision probability. On the other hand, each collision adds a certain well-known amount of overhead because it can be detected due to the RTS/CTS scheme used. Note that O depends on the parameters given in Equation 5.13. The optimum parameter set for m_{E1}, p_{E1} and m_{E2} is found when the overhead O reaches its minimum for a given N_1, i.e. we seek $\min(O(m_{E1}, p_{E1}, m_{E2}, N_1)$. The function O has been computed and has the following properties:

- There is always a dedicated minimum for a given value of N_1.
- The minimum is very stable for values of m_{E1} and m_{E2} bigger than the ones for the minimum.

- The value of p_{E1} can be chosen from a big range around the optimum value without significant impact on the overhead.
- The bigger N_1, the bigger the value of the optimum value for p_{E1}. The optimum values for m_{E1} and p_{E1} remain almost unchanged.
- The residual collision probability P_c decreases with increasing values of m_{E1}, p_{E1} and m_{E2}. The increase of m_{E2} has the biggest impact.

The selection of N_1 depends on the usage scenario. For the optimization of the DIME-EF scheme, it was assumed that 10 EF stations almost completely occupy the available data rate of the Basic Service Set. This scenario was assumed to be the worst case for the 2 Mbit/s DS modus of IEEE 802.11 and was chosen as the reference scenario. By iteratively performing simulations and adapting m_{E1}, p_{E1} and m_{E2}, it was found that in this scenario, on average approximately seven stations enter each DIME-EF cycle. Therefore, $N_1 = 7$ was chosen. The resulting optimum values for m_{E1}, p_{E1}, m_{E2}, the resulting overhead O and the residual collision probability P_c are:

$$\begin{aligned} p_{E1} &= 0.43 \\ m_{E1} &= 5 \\ m_{E2} &= 4 \\ O &= 218.69\mu s \\ P_c &= 10.4\% \end{aligned} \tag{5.14}$$

All simulations presented in Section 5.7.4 have been performed using this parameter set.

5.4.2 Rationale for choosing the DIME-EF scheme

The DIME-EF scheme can be compared to other schemes with only one elimination phase. The bursting is necessary because of the carrier sensing of legacy stations that may interrupt a DIME-EF cycle. Assume the following very simple scheme with similar overall overhead as the DIME-EF scheme with the parameters according to Equation 5.14: Each station chooses a random number of slots for its elimination burst duration out of 9 possible slots. After the bursting, the stations sense the channel for 1 slot. If it is free, they immediately continue with the transmission of an RTS, otherwise they withdraw their access attempt. Assuming an equal distribution according to Equation 5.2, the overhead can be calculated according to the equations given above for the EB2 cycle. The overhead O for the reference scenario, then, has a value of approx. $226\mu s$ at a residual collision

rate of $P_c = 34.6\%$. It is immediately obvious that the overhead is bigger and the number of access attempts for a single packet to be transmitted is higher than with the DIME-EF scheme. A similar calculation with similar results can be performed for a geometric distribution.

It is the combination of the two EB cycles with the probability distributions according to Equations 5.1 and 5.2 which makes the DIME-EF scheme very efficient. The EB1 cycle has the property that the probability for a low number of surviving stations entering the EB2 cycle, is high, almost independent from the number N_1 of contending stations. The EB2 cycle, then, is well suited to sort out a single station out of a low number N_2 of remaining stations.

5.4.3 Hidden Node Algorithm

Hidden stations are a severe problem in distributed Wireless LAN systems. In the above explanation of the DIME-EF proposal we did not consider this problem. The Hidden Node Algorithm (HNA) proposed in the context of HIPERLAN [111] could also be used to handle hidden stations in DIME-EF. With this solution, the performance of non-hidden stations is preserved, and only the hidden nodes see their performance significantly affected.

5.4.4 Performance Evaluation & Discussion

To test the performance of the DIME architecture presented in this document, we have simulated it on a network consisting of a number of wireless terminals in a 2 Mbps Wireless LAN communicating with a fixed node. These simulations have been performed in ns-2 [42].

For the purpose of simulating the contention resolution scheme described in Section 5.4, the existing implementation of the 802.11 MAC protocol in ns-2 has been extended by the functions necessary for the DIME-EF. In all simulations, stations using the normal 802.11 MAC protocol (i.e. Best Effort in our architecture) coexist with stations using EF, in such a way that each station uses either EF or Best Effort. The Best Effort stations always have something to transmit. The packet length of the Best Effort stations is set to 500 bytes for all simulations. No packet dropping is applied for EF stations. The traffic of the EF stations is of UDP type, since UDP is usually applied in conjunction with EF.

As a quality criterion, we set a maximum delay of 25 ms. This limit shall not be exceeded by 3% or more of the packets. Therefore, the emphasis of all simulations is on delay. The total number of stations in all simulations is 20, i.e. the number of stations using Best Effort is 20 minus the number of EF stations.

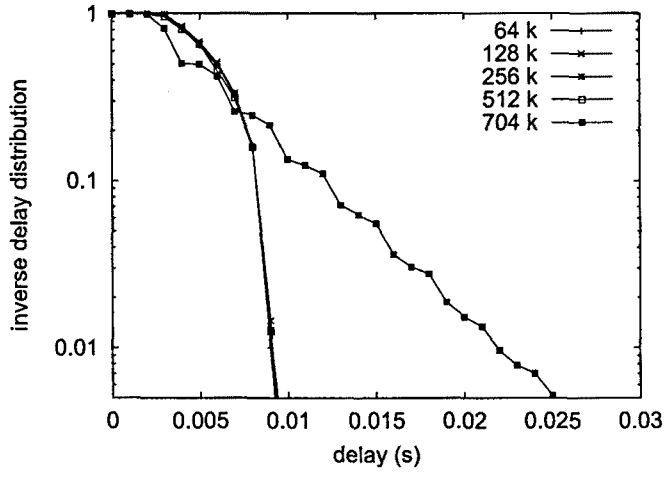

Figure 5.6: Inverse delay distribution for 2 EF stations, CBR, 500 byte packet length

The stations are located such that they are all within communication distance of each other.

Simulation results for constant bit rate (CBR) sources with 500 bytes packet length are shown in Figures 5.6 and 5.7. The simulation results in Figure 5.8 are obtained for 100 bytes packet length. Each of them shows an inverse distribution of the delay in seconds for a given number of EF stations with the data rate of a single station as parameter. The interpretation of the graphs is as follows: If one is interested to know how many percent of the packets have a delay higher than the one selected, one must pick the time on the x-axis and read the corresponding number on the y-axis. A number of 0.1 on the y-axis means that 10% of the packets were later than the selected time.

The simulations show that the air interface can bear a EF saturation throughput of about 1300 Kbps for 500 bytes packet length and of below 700 Kbps for a packet length of 100 bytes. In general, the saturation throughput decreases with decreasing packet length because each packet carries a certain, more or less constant overhead. However, it is likely that some real-time applications, such as voice over IP, use short packet lengths and, hence, the performance of the DIME-EF scheme for short packets is important.

As long as the required total data rate of the EF stations remains below the saturation throughput, the actual throughput of each EF station corresponds to its required data rate. The data rate left is being used by the Best Effort stations and is shared almost equally between them. If the required data rate of the EF stations exceeds the saturation throughput, the EF stations share the maximum data rate

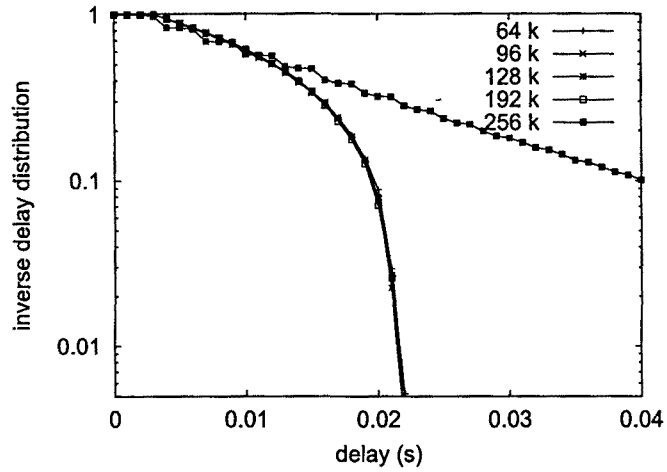

Figure 5.7: Inverse delay distribution for 6 EF stations, CBR, 500 byte packet length

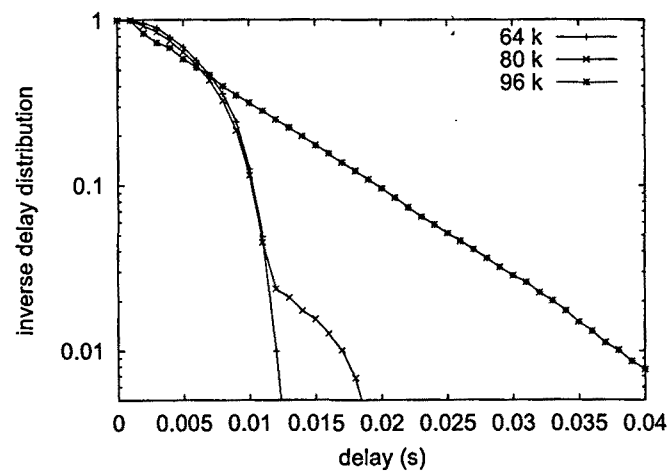

Figure 5.8: Inverse delay distribution for 6 EF stations, CBR, 100 byte packet length

equally, whereas the Best Effort stations get no throughput at all.

Figure 5.6 shows the results for two stations using EF. The data rates range from 64 Kbps up to 704 Kbps per EF station. As can be seen, the delay for all data rates up to 512 Kbps remains below 10 ms in all cases. The data rates achieved by the EF stations corresponds to the data rate delivered by the traffic sources, i.e. they can deliver all offered packets to the destination. The delay increases at a data rate of 704 Kbps but still remains below the allowed limit. In this case, however, the throughput of the EF stations is limited to approximately 650 Kbps, i.e. half of the saturation throughput for each station. The Best Effort stations could not deliver any packet during this simulation run.

The curves depicted in Figure 5.7 show a similar situation. The delays are higher than with two stations but still remain in the allowed region. If each station uses 256 Kbps, the saturation throughput is exceeded and the delays increase significantly. The same scenario with a packet length of 100 bytes per EF station is shown in Figure 5.8. The quality criterion can be met for 6 stations with 64 Kbps each but the saturation throughput is already reached with a data rate of 96 Kbps per EF station.

The fact that the delay distribution is almost independent from the data rate of each terminal is quite in line with the results obtained in [110]. An interpretation of the results is that, as long as the EF stations do not always have something to transmit, they do almost not interfere with each other and the transmission delay of the packets plus the waiting time for the end of an onging transmission is decisive. Since the packet length is constant for all EF and Best Effort stations, all have to wait equally long on average. Furthermore, the delay depends on the number of Best Effort stations contending for the channel. The dependence of the transmission delay on the packet length and on the number of Best Effort stations is a subject for further study in this project.

The graphs in Figure 5.9 show the delay distributions for a data rate of 64 Kbps per station at a packet length of 500 bytes and varying numbers of stations. The same situation for a packet length of 100 bytes is depicted in Figure 5.10. It can be seen from the graphs that the quality criterion is met for 6 EF stations. For 8 EF stations and more, the quality criterion can not be met. Whereas the curve for 6 stations with 500 bytes packet length decreases very rapidly, the curve for 100 byte packets has a longer tail.

The graph in Figure 5.11 shows the inverse delay distribution for ON/OFF traffic for 6 EF stations with a data rate of 64 Kbps and 100 and 500 bytes packet lengths. The ON/OFF sources have exponentially distributed burst and idle times. The curves denoted with "long" have an average burst time of 2 s and idle time of 8 s, whereas the curves with "short" have average burst and idle times of 500 ms. The data rate is the average data rate of the EF stations, i.e. the peak data rate is higher than the average rate. The curves for 500 bytes packet length are rather

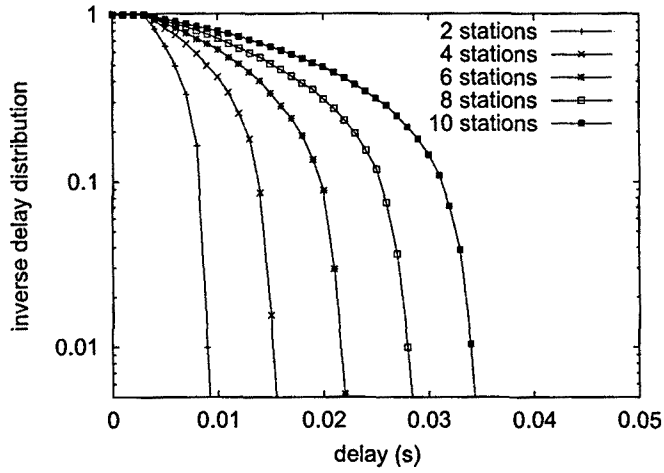

Figure 5.9: Inverse delay distribution 64 Kbps with varying numbers of EF stations, CBR , 500 bytes packet length

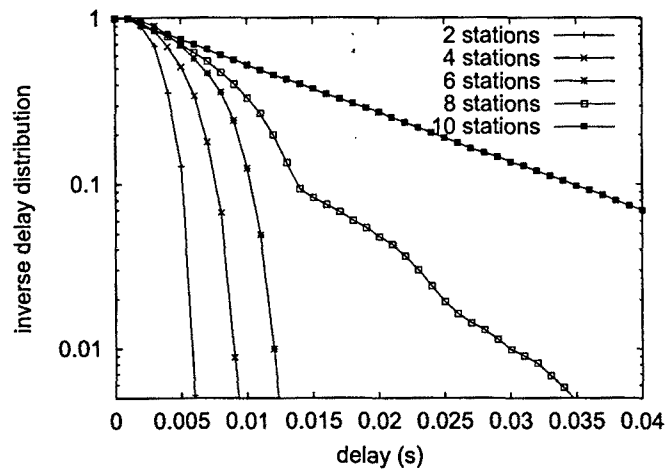

Figure 5.10: Inverse delay distribution 64 Kbps with varying numbers of EF stations, CBR , 100 bytes packet length

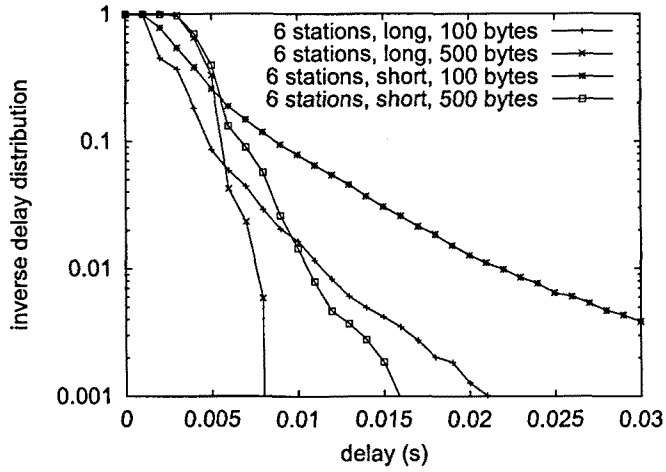

Figure 5.11: Inverse delay distribution 64 Kbps for 6 EF stations, ON/OFF traffic, 100 and 500 bytes packet lengths

	data rate (kbps)				
stations	32	64	128	256	512
2	x	x	x	x	x
4	x	x	x	x	
6	x	x			
8	x				
10					

Table 5.1: Overview which configurations meet the quality criterion

steep, whereas the 100 bytes curves have a rather long tail. All scenarios meet the quality criterion.

Table 5.1 shows which combinations of numbers of EF stations and data rate per EF station meet the quality criterion for all possible scenarios, i.e. for 500 and 100 bytes packet lengths as well as for CBR and ON/OFF traffic. A cross in the table entry means that the criterion is met. As a rule of thumb, an admission control derived from this table would allow not more than six stations and not more than a data rate of 64 Kbps per station to use EF. As can be seen from the delay graphs above, a more sophisticated admission control scheme would have to consider additional criteria, such as the packet length and burstiness of EF applications.

It can be seen from the simulation results that the contention resolution scheme described in Section 5.4 can meet the quality criterion reliably for at least 6 EF stations with data rates up to 64 Kbps per station for CBR and ON/OFF traffic

with packet lengths of 100 and 500 bytes. If the available bandwidth is used by EF stations up to or close to the saturation throughput, however, the EF stations use most or all of the available bandwidth and the service quality of Best Effort stations drops dramatically.

5.5 Assured Forwarding MAC Extension (ARME)

DiffServ is based on simple mechanisms with minimal control and signaling, and does not require to keep per-flow state at core nodes. ARME, the Assured Rate MAC Extension we propose, follows the same principles: it is based on distributed control, minimizing thus the signaling overhead at the MAC layer, and does not require to keep per-flow state at the MAC level.

Also like DiffServ, the ARME architecture provides a soft kind of QoS, i.e. statistical QoS guarantees are given to traffic aggregates, but an individual packet does not receive any kind of guarantee. Note that this fits well the type of QoS that can be achieved with a distributed and connectionless MAC.

In ARME we distinguish two types of service: the Assured Rate Service and Best Effort. An Assured Rate station in ARME is a station that has contracted a service with a certain assured rate, while a Best Effort station has not contracted any rate.

In the DCF approach, the throughput received by a station depends on its CW: the smaller the CW, the higher the throughput. In ARME, the Assured Rate Service is supported by the DCF function of the current standard with minor changes in the computation of the CW in order to give to each station the expected throughput according to the service contracted by the station. Thus, both the Assured Rate station and the Best Effort access the channel with the DCF mode but with different CWs. In Section 5.5.1 we present in detail the algorithm for computing the CW for Assured Rate stations.

The protocol operation of ARME is shown in the example of Figure 5.12, in which, after the end of a previous transmission, there are two stations with a packet to transmit, one Assured Rate station and one Best Effort station. In the example, the Assured Rate station, which is competing with a smaller CW, accesses the channel first. The Best Effort station uses the CW calculated according to the current IEEE 802.11 standard and accesses the channel afterwards. Note that with this choice of the CW for Best Effort, 802.11 terminals behave as Best Effort terminals in the ARME architecture, providing thus backward compatibility.

According to the above explanation of ARME, Best Effort and Assured Rate packets use the same IFS but compete with each other with different CWs. This can be compared to the RIO buffer management in DiffServ [112], in which *in-*

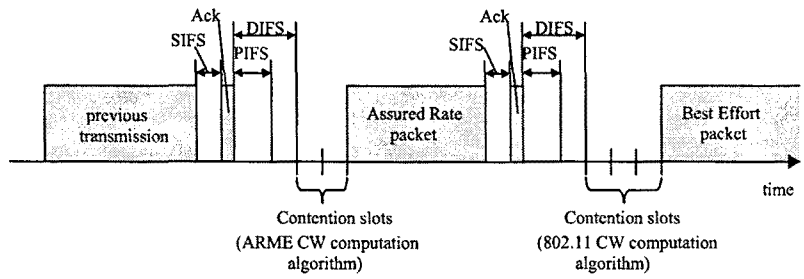

Figure 5.12: Protocol Operation.

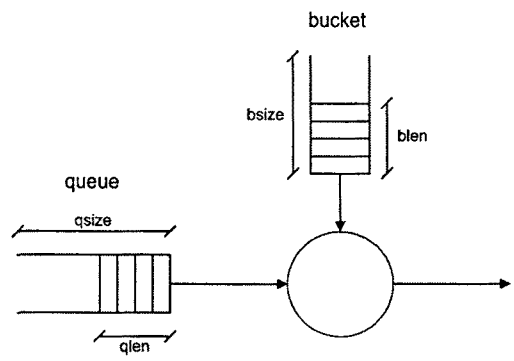

Figure 5.13: Token bucket algorithm for AS.

profile and *out-of-profile* packets share the same buffer but are dropped with different probabilities as a function of the buffer occupancy. The difference is that ARME, in contrast to RIO, has to work on a distributed basis.

The CW of Best Effort traffic cannot be arbitrarily increased for backward compatibility reasons. Also, the CW of Assured Rate traffic cannot be arbitrarily decreased, since this would lead to an unstable situation with permanent collisions. The consequence of these limitations in the CWs make it impossible to totally control the capacity given to each service. Therefore a certain level of impact of Best Effort to Assured Rate is unavoidable. This impact has been studied in the simulations (see Section 5.7.4).

Our approach requires admission control to ensure that the sum of the throughputs committed to the Assured Rate Service is not larger than the total throughput available in the Wireless LAN. This admission control in the wireless access should be considered as an integral part of the admission control defined in the DiffServ architecture.

5.5.1 Contention Window Computation for ARME

In the DCF mode of the 802.11 standard, the size of the CW determines the probability for a station to win the contention. The smaller the CW is, the higher the probability of getting access to the channel. As a consequence, there is a direct relationship between the CW assigned to a station and the bandwidth that this station will receive in a specific scenario. An Assured Rate Service can therefore be provided by assigning to a station the CW corresponding to the bandwidth requested by this station.

The difficulty of this approach, however, relies in determining the CW that will lead to the specified bandwidth. Note that this value depends on the number of stations that compete for accessing the channel and their CWs, which is a changing condition.

The approach we have chosen for the calculation of the CW in ARME is a dynamic one: each station monitors the bandwidth experienced and modifies its CW in order to achieve the desired throughput. For each packet transmitted, we estimate the sending rate of the terminal; in the case that the estimated rate is smaller than the desired one, we slightly decrease the CW, while in the opposite case, we increase it slightly.

The above explanation describes the basics of the algorithm. However, in the adjustment of the CW, there are additional aspects that have to be taken into account:

- We do not want the CW to increase above the values used by the Best Effort terminals, since this would lead to a worse performance than Best Effort. On the other hand, as explained in Section 5.5, for backward compatibility reasons, the CW for Best Effort should be the one defined by the 802.11 standard.
- If the low sending rate of the application is the reason for transmitting below the desired rate, then the CW should obviously not be decreased.
- When estimating the sending rate, it would be desirable to control the allowed burstiness of the source.
- CWs should not be allowed to decrease in such a way that they negatively influence the overall performance of the network.

Considering all the above issues, we have designed an algorithm for the computation of the CW, which is inspired in the token bucket algorithm. In our scheme, we use the number of bytes in the bucket (bucket length) and the occupancy of the transmission buffer (queue length) as input parameters in the algorithm (see Figure 5.13). This is further explained in the following points:

- The token bucket gets filled at the desired transmission rate. For each successful transmission, the length of the transmitted packet in bytes is subtracted from the bucket. Thus the bucket length (*blen*) represents the resources that the user has for transmitting packets.
- The user has resources to transmit a packet only if the bucket has enough bytes in it (we have taken a certain limit *blim* to represent the minimum needed).
- The bucket size (*bsize*) determines the accepted burstiness of the source; the maximum length allowed to a burst is equal to $bsize - blim$.
- The queue length (*qlen*) expresses the willingness of a station to transmit packets. The CW is only decreased if the queue is not empty (if the queue is empty, the user is not filling it, which means that the current CW satisfies the sending needs of the user).
- When increasing the CW, the value assigned to it can never exceed the size of the CW used for Best Effort.
- If the channel is detected to be below its optimum limit of throughput due to too small values for the CWs (i.e. overload), the CW is increased. This aspect is discussed in detail in the following clause.

The above considerations lead to the following algorithm. This algorithm computes a value p which is used to scale the CW values defined in 802.11. Note that, besides this scaling of the CW, the backoff time computation algorithm is left as defined in the 802.11 standard (i.e. the Contention Window is doubled after each unsuccessful transmission attempt for a given number of times).

$$\begin{aligned} \texttt{if } (qlen = 0) \texttt{ then } p &= (1 + \Delta_1)p \\ \texttt{else if } (blen < blim) \texttt{ then } p &= (1 + \Delta_2)p \\ \texttt{else } p &= (1 - \Delta_3)p \\ p &= min\{p, 1\} \\ CW &= p \cdot CW_{802.11} \end{aligned} \tag{5.15}$$

where Δ_1 is a constant and Δ_2 and Δ_3 are calculated in the following way

$$\Delta_2 = \frac{blim - blen}{blim}\Delta_1 \quad (5.16)$$

$$\Delta_3 = \frac{blen - blim}{bsize - blim}\Delta_1 \quad (5.17)$$

The presented algorithm depends on the number of parameters, namely *blim*, *bsize* and Δ_1. Simulations have shown that the tuning of these constants is not critical for the performance of the protocol as long as they have reasonable values. In the simulations results presented in Section 5.7.4 we have taken *blim* equal to $token\_size$, *bsize* equal to $5 * token\_size$, $token\_size$ equal to 1072 bytes and Δ_1 equal to 0.025.

5.5.2 Performance evaluation & discussion

To test the performance of the ARME scheme presented in this section, we simulated it on a network consisting of a number of wireless terminals in a 2 Mbps Wireless LAN communicating with a fixed node. These simulations were performed with ns-2. For this purpose, the CW computation algorithm previously described was inserted into the existing implementation of the 802.11 MAC DCF protocol in ns-2. In the simulations performed, stations using the normal 802.11 MAC protocol (i.e. Best Effort in our architecture) coexisted with stations using the Assured Rate Service, in such a way that each station used either the Assured Rate Service or Best Effort. The packet length was set to 1000 bytes for all simulations.

We chose to use the RTS/CTS mechanism in all cases. This mechanism, optional in the 802.11 standard, increases bandwidth efficiency in case of many collisions, since with this mechanism collisions occur with the relative small control packets rather than with long data packets. Since our architecture may lead to larger number of collisions than the normal 802.11 MAC DCF, this mechanism can be especially beneficial in our case.

Bandwidth Assurance

In ARME, the assurance of the requested bandwidth for Assured Rate is done adjusting adaptively the CW of Assured Rate stations according to the measured throughput. Figure 5.14 shows this dynamic adjustment; the simulation corresponds to a scenario with a total number of 10 stations, 8 of which are Best Effort

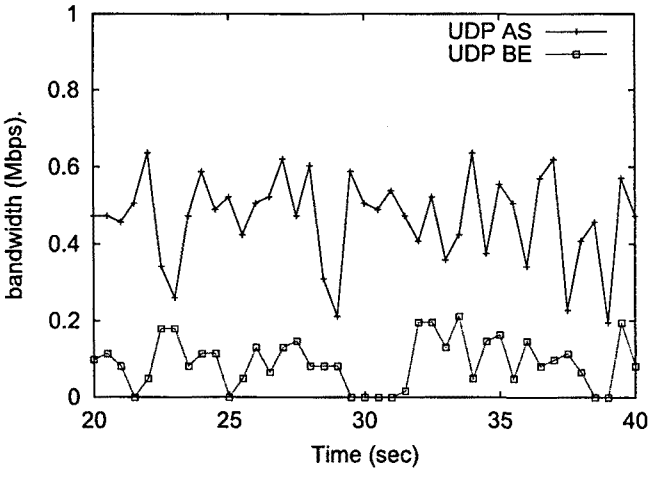

Figure 5.14: Instantaneous Bandwidth of 1 AS station vs. 1 Best Effort station.

and 2 Assured Rate with a rate assurance of 500 Kbps each. All stations are sending UDP CBR traffic at a rate of 500 Kbps. It can be seen that the instantaneous bandwidth of Assured Rate stations (referred as AS in the graph) oscillates around the desired value (500 Kbps), while Best Effort stations (referred as BE) receive a much lower throughput.

Impact of Best Effort terminals

In Section 5.5 we have argued that it is impossible to avoid a certain level of impact of Best Effort stations on the Assured Rate Service. This impact is studied in the simulation results shown in Figure 5.15. This figure shows the variation of the throughput received by Assured Rate stations in different scenarios when the number of Best Effort stations increases. In these simulations, Assured Rate stations receive a bandwidth assurance such that a total amount of 1 Mbps is assigned to Assured Rate (i.e. in the case of 1 Assured Rate station, this station receives a bandwidth assurance of 1 Mbps; in the case of 2, each receives a bandwidth assurance of 500 Kbps; in the case of 4, 250 Kbps; and in the case of 8, 125 Kbps).

It can be seen that the total bandwidth received by the Assured Rate Service (ideally 1 Mbps shared among the Assured Rate stations) decreases with the number of Best Effort stations. When the total number of stations is 50, the bandwidth received by Assured Rate stations is about half of the committed rate (i.e. 500 Kbps). Note that the total bandwidth received by Assured Rate decreases with the total number of stations almost independently of the number of Assured Rate

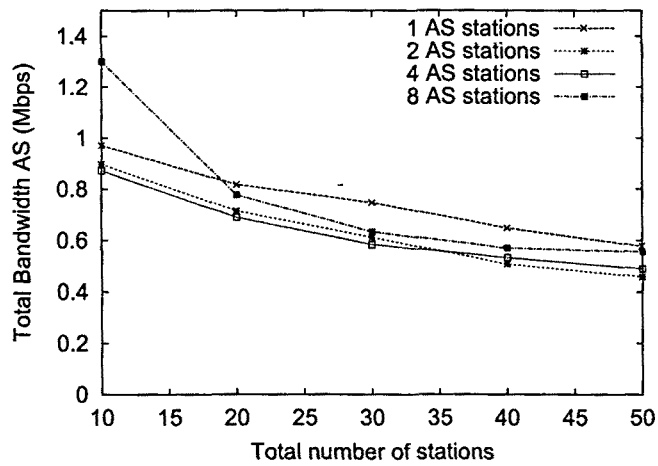

Figure 5.15: Impact of Best Effort to the bandwidth for Assured Service.

stations.

In the point corresponding to 8 Assured Rate stations and 2 Best Effort, Assured Rate receives a throughput much higher than the one committed (1.3 Mbps). Note, however, that if only the committed 1 Mbps was given to Assured Rate, the 2 Best Effort stations would experience each a higher throughput than an Assured Rate station, since they would share the remaining 1 Mbps. The nature of the mechanism we have proposed in ARME for the CW computation ensures that this undesirable situation does not occur: with our algorithm, the leftover bandwidth is equally shared between Assured Rate and Best Effort stations such that a Best Effort station never receives a better treatment than an Assured Rate one.

Figure 5.16 shows the bandwidth received by an Assured Rate station and the one received by a Best Effort station in the case of 2 Assured Rate stations and varying the total number of stations. It can be seen that it is not only Assured Rate stations but also Best Effort which see their bandwidth decreased when the total number of stations increases. Note that even though with 50 stations Assured Rate stations get about half of the committed bandwidth (250 Kbps each), they still get a throughput 10 times higher than Best Effort stations, which get about 25 Kbps each. This result could be interpreted as a good tradeoff between differentiation (Assured Rate stations get a much higher throughput) and fairness (Best Effort stations do not starve).

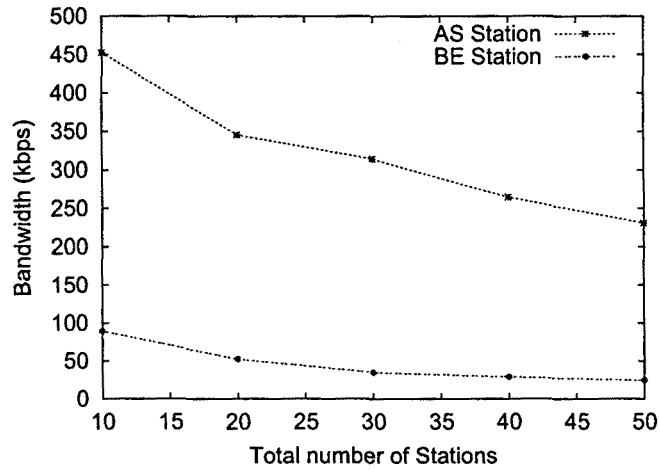

Figure 5.16: Assured Service vs. Best Effort.

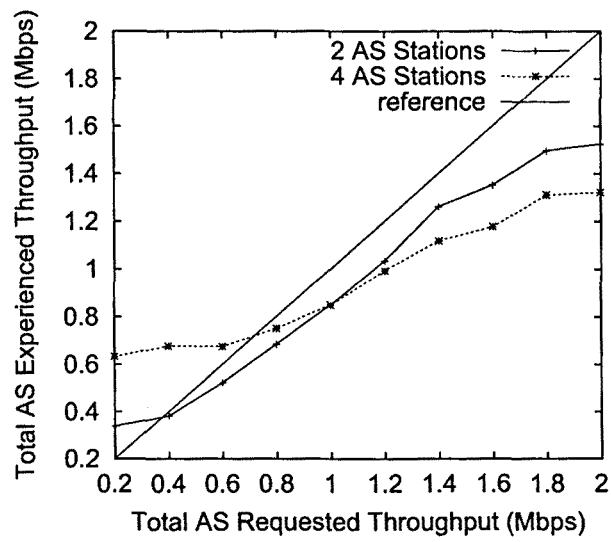

Figure 5.17: Over and undercommitment.

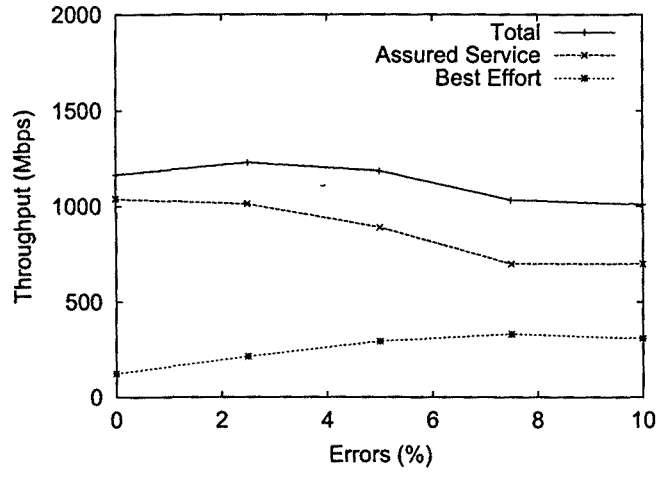

Figure 5.18: Level of differentiation as a function of the error rate.

Over and undercommitment

The network is undercommitted when the Assured Rate Service is given a much lower bandwidth than the throughput available, and overcommitted when it is given a higher bandwidth than the available throughput.

A situation of undercommitment can occur when most of the Assured Rate stations are not active. In this case, it would be desirable that Assured Rate stations could use the leftover bandwidth, therefore receiving a higher throughput than the one requested.

On the other hand, a situation of overcommitment can easily occur when Assured Rate stations are configured statically. With static configuration it is desirable to be able to commit a higher bandwidth than the one available in the channel, assuming that it is highly improbable that all Assured Rate stations will be active at the same time. However, such configuration can lead to a situation of overcommitment with a certain probability. In such situation, it will be impossible for Assured Rate stations to receive the requested throughput. This situation, however, should not lead to unstability; instead, it would be desirable that Assured Rate stations shared the available overall data rate.

In Figure 5.17 it can be seen that the behavior with under and overcommitment is the desired. This simulation has been done for a scenario with a total number of 10 stations, of which 2 (first case) or 4 (second case) are Assured Rate stations and the rest are Best Effort stations. In the following clause a situation of extreme overcommitment has been simulated, showing that the behavior in that case is also the desired.

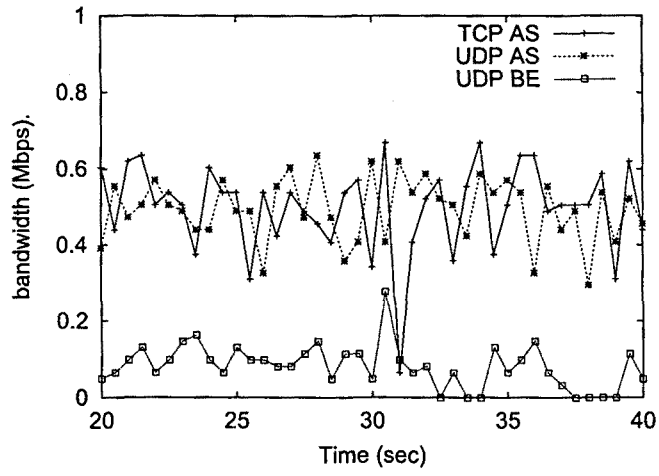

Figure 5.19: TCP vs. UDP.

Impact of Errors

If we consider a non-ideal channel, the lack of an Ack can be due to a collision but also due to an error in the channel; in this case, the lack of an Ack would be falsely interpreted by an Assured Rate station as an indication of overload. As a reaction, the AS station would increase its CW more aggressively than it should, and, as a consequence, the achieved level of differentiation between AS and Best Effort would be lower than the desired.

Figure 5.18 shows the total throughput, the throughput of Assured Rate and the throughput of Best Effort as a function of the percentage of errors in the channel, for the a extreme scenario of 100 stations half of them Assured Rate and the other half Best Effort. It can be seen that the level of differentiation (ratio between Assured Rate and Best Effort throughputs) decreases with the error rate, as expected. However, even at very high error rates (10%) in such a extreme scenario, the level of differentiation (i.e., the ratio between the throughput received by Assured Rate and Best Effort stations) still keeps reasonably high.

TCP vs. UDP

When TCP and UDP flows compete with each other, the bandwidth distribution tends to favor UDP. This is because, in case of congestion, TCP backs off because of its congestion control mechanism, and UDP, without any kind of congestion control and therefore more aggressive, consumes the bandwidth left by TCP. A QoS architecture with bandwidth assurance should overcome this dif-

ferent level of aggressiveness of the sources and provide all sources with their committed throughput independent of the congestion control algorithm they use. This requirement, however, is difficult to meet, and most QoS architectures do not achieve the desired level of fairness between TCP and UDP (see e.g. [113] for the Differentiated Services architecture).

To study the level of fairness between TCP and UDP achieved by ARME, we performed the following experiment: two Assured Rate stations, one endless TCP and the other UDP CBR, had a committed throughput of 500 Kbps, while the remaining 8 stations were Best Effort stations sending UDP CBR traffic. The UDP Assured Rate station sends at a rate of 500 Kbps, the Best Effort ones at a rate of 1 Mbps. Figure 5.36 shows the instantaneous bandwidth achieved by the TCP Assured Rate source, the UDP Assured Rate source and one UDP Best Effort source. It can be seen that the result is the desired: both Assured Rate stations oscillate around their committed throughput, while Best Effort stations receive the bandwidth left over by Assured Rate.

From this experiment we conclude that ARME provides TCP with a fair treatment with respect to UDP. This is because the ARME algorithm adapts the CW to the aggressiveness of the source: a less aggressive source, like TCP, will see its CW reduced until it receives the committed throughput, while a more aggressive source, like UDP, will achieve its committed throughput with a larger CW.

5.6 Summary

We have proposed the DIME architecture for providing QoS in Wireless LAN. Since Wireless LAN may be considered as just one hop in the communications path, the goal of DIME is to provide for Wireless LAN the same Per-Hop Behaviors that have been standardized for DiffServ: Expedited Forwarding and Assured Forwarding.

The DiffServ architecture for wired links is based on simple mechanisms with minimal control and signaling, and does not require to keep per-flow state at core nodes. The design of DIME has been done following the same principles: it is based on distributed control, minimizing thus the signaling overhead at the MAC layer, and it does not require to keep per-flow state at the MAC level.

Also like DiffServ, the DIME architecture provides a soft kind of QoS, i.e. statistical QoS guarantees are given to traffic aggregates, but an individual packet does not receive any kind of guarantee. Note that this fits well the type of QoS that can be achieved with a distributed and connectionless MAC.

DIME consists of two extensions to the IEEE 802.11 standard: DIME-EF and ARME. The fact that these extensions have been designed as independent modules

gives the manufacturer the option to omit one of them if either EF or AF are not needed, simplifying thus the migration effort from the existing standard.

DIME-EF reuses the PIFS of the 802.11 standard in a distributed manner. We show that distributed control can meet the requirements of real-time services. Simulations have proved that with proper admission control the proposed extension satisfies the user's requirements for low delay.

ARME modifies the CW computation of the DCF mode of the standard. The algorithm for the computation of the CW has been designed in such a way that 802.11 terminals behave as Best Effort terminals in the proposed architecture. The simulations performed show that this extension provides bandwidth assurance to AF terminals in normal circumstances, while the leftover bandwidth is shared equally between Best Effort and AF. Furthermore, starving Best Effort terminals is avoided in case of overload by trading off the bandwidth assurance of AF.

5.7 Distributed Weighted Fair Queuing

With weighted fair queuing, the bandwidth experienced by a flow i, r_i, is proportional to the *weight* that this flow has been assigned, W_i:

$$\frac{r_j}{s_j} = \frac{r_i}{s_i} \quad \forall i, \forall j \tag{5.18}$$

In the DCF approach, the bandwidth received by a flow depends on its CW: the smaller the CW, the higher the throughput. In DWFQ, weighted fair queuing in Wireless LAN is supported by the DCF function of the current standard with minor changes in the computation of the CW in order to give to each flow a bandwidth proportional to its *weight*.

According to the above explanation, terminals conforming to the IEEE 802.11 standard and DWFQ terminals compete with each other with different CW. In order to allow backward compatibility, the stations conforming to the IEEE 802.11 standard should behave as DWFQ stations with the default *weight*. In this study we take the default *weight* equal to 1. This value corresponds to the basic service; *weights* smaller than 1 are not allowed, and any larger *weight* means "better than average" kind of treatment.

In the discussion and simulations of this study, we will assume that all packets at a node belong to a single flow. The proposed approach, however, could be easily extended when multiple queues are maintained at each node, as discussed in Section 5.7.3.